NASA CONTRACTOR REPORT

NASA CR-1096

STUDY ON A TECHNIQUE FOR DETECTING PHOTONS IN THE 100 - 1000Å WAVELENGTH REGION

by O. P. Rustgi

Prepared by
NORTHROP CORPORATE LABORATORIES
Hawthorne, Calif.
for Electronics Research Center

NATIONAL AERONAUTICS AND SPACE ADMINISTRATION • WASHINGTON, D. C. • JUNE 1968

NASA CR-1096

STUDY ON A TECHNIQUE FOR DETECTING PHOTONS IN THE 100 - 1000 Å WAVELENGTH REGION

By O. P. Rustgi

Prepared under Contract No. NAS 12-3 by
NORTHROP CORPORATE LABORATORIES
Hawthorne, Calif.

for Electronics Research Center

NATIONAL AERONAUTICS AND SPACE ADMINISTRATION

For sale by the Clearinghouse for Federal Scientific and Technical Information
Springfield, Virginia 22151 – CFSTI price $3.00

TABLE OF CONTENTS

LIST OF TABLES

LIST OF FIGURES

LIST OF FIGURES (CONTINUED)

LIST OF FIGURES (CONTINUED)

LIST OF FIGURES (CONTINUED)

LIST OF FIGURES (CONTINUED)

LIST OF FIGURES (CONTINUED)

SUMMARY

This report is submitted in fulfillment of the final phase of Contract No. NAS 12-3 between the Northrop Corporation and the National Aeronautics and Space Administration, Electronics Research Center. It represents the work done during the period beginning 15 April 1965 and ending 15 October 1967 and describes in detail the research and development culminating in a series of selective detectors for the vacuum ultraviolet region between 1000 and 100Å.

A general survey of the various modes of interaction of electromagnetic radiation in the 100 - 1000Å region with matter has been conducted. These interactions have been analysed in terms of photon efficiency, wavelength cut-off, minimum photon flux required for detection of these effects, ease of wavelength resolution through selective detection, and ease of fabrication and calibration of resultant detectors.

Based on this analysis, the transmittance of thin films and photoionization in gases are selected as the possible interactions resulting in selective detectors. Thin films of aluminum, bismuth, indium, titanium, and tin are prepared and supported on mosaic glass obtained from Permionics Corporation. Techniques are developed to seal the mosaic glass with a film to the metallic plate. This plate is then used as a filter as well as a window for a rare gas ion chamber to form the resultant selective detector. Spectral response characteristics of selective detectors using (1) bismuth film with neon, argon, and krypton; (2) indium film with argon, krypton, and xenon; and (3) titanium film with argon, neon, and helium are presented with emphasis on selectivity of response. The long wavelength response is limited either by the photoionization onset of

the filling gas or by the onset of optical transmission in a thin film whereas the short wavelength response is limited by the transmission cut-off in thin films. These results were presented at the joint meeting of the American Physical Society, Sociedad Mexicana De Fisica, and the Canadian Association of Physicists held on 21 - 23 June 1967, at Toronto, Canada, under the heading of "Use of Thin Films in Selective Detection of Extreme Ultraviolet Radiation Between 100 - 1000Å," by Om P. Rustgi which appeared in the Bulletin of the American Physical Society, Vol. 12, p. 640 (1967). Following is the abstract of this paper:

> We have prepared ion chamber detectors which utilize the transmittance property of thin metallic films and the ionization property of rare gases in the wavelength region between 1000 and 100Å. Thin films of Bi, In, and other metals have been used as windows for the detectors containing Kr, A, and other rare gases. Spectral response has been measured by collecting the positive ions produced in the ion chamber. For a combination of Bi film and Kr, A, or Ne gas, the output signal is limited to 850 - 510Å, 787 - 510Å, and 580 - 510Å wavelength intervals, respectively. The technique of supporting thin films will be described.

In order to narrow down still further the spectral region in which these detectors are sensitive, composite films of Al and Sn are prepared and transmittance measured. Transmittance of thin parylene pellic type C are also reported for potential use as a support for metallic films. Preliminary results are reported on the photon-induced fluorescence in air but are not utilized to narrow down the spectral range of selective detectors.

The capillary spark discharge light source is successfully operated in the pulse-burst mode and intensity measurements made by means of a Reeder thermocouple and an ultraviolet photodiode. Preliminary results on the photoelectric yield of elkonite 10W3 alloy are reported using the new spherical photoelectric cell.

SECTION I

INTRODUCTION

The application of vacuum ultraviolet techniques to observation and interpretation of basic physical phenomena in the laboratory and in space has assumed a new significant role due to increasing aerospace experiment mission requirements. During the past decade, there has been an increasing demand for the development of new detectors in the vacuum ultraviolet region of the spectrum. Various space sciences involve the derivation of astrophysical and geophysical quantities from photon fluxes obtained by means of detectors sensitive to various regions of the vacuum ultraviolet spectrum.

Satellite and rocket spectroscopy has led to the measurement and identification of solar radiation below the cut-off limit of the earth's atmosphere. The emission of short wavelength radiation, including X-rays, from the Sun is associated with sun-spot activity and solar flares.[1] These radiations interact strongly with the gases and vapors present in the upper atmosphere and cause dissociation, excitation, and ionization. The expected ionospheric characteristics are derived as directly as possible from the vacuum ultraviolet observation and then compared with the well-known D-, E-, and F-layer formation. The comparison leads to (1) a high ionosphere recombination coefficient decreasing rapidly with height, (2) contributions to the E-layer from both UV and X-rays, and (3) very little difference in the solar cycle variations from the D-, E-, and F-layers although intensity variations are greater from high than low ions. In order to construct planetary model atmospheres of earth and other planets, one takes recourse to the measurement of solar vacuum ultraviolet radiation as a function of altitude. Knowing the total absorption coefficient of various gases

and vapors as a function of wavelength, it is possible to build planetary model atmospheres.[2,3] Rocket spectroscopy detected the presence and distribution of ozone up to 70 km by measuring the atmospheric attenuation of UV radiation of 2550Å with altitude. Molecular oxygen has been traced to 170 km by the absorption of 1500Å radiation, the maximum of the Schumann - Runge dissociation continuum and the total atmospheric density has been measured to 160 km by X-rays between 44 and 60Å. The decrease in intensity of Lyman-α is a gauge of the O_2 concentration in the D-region and may also provide a means of determining H_2O at these altitudes. The absence of Lyman-γ at 200 km indicates the presence of molecular nitrogen, which has a strong absorption band exactly at the wavelength of Lyman-γ.

The measurement of vacuum ultraviolet radiation is of great significance in the study of the Sun in terms of giving information on the number of ions in the solar atmosphere.[4] This makes it possible to derive (1) the amount of solar material in each temperature range, (2) the chemical abundancies, and (3) the physical differences between the quiet solar atmosphere, center of activity, and flares. A program of interest to solar physics has been outlined by Goldberg.[5] The important parameters of study are (1) a systematic study of the solar spectrum of all wavelengths shorter than 3000Å, (ii) X-rays, (iii) line profiles and (iv) UV spectro-heliograms. The region below 1700Å is of particular interest to the study of the chromosphere and the corona where more energetic events take place. This requires continuous monitoring over periods of time on the order of an hour, only possible through the use of highly stabilized satellite observatories. Fast scanning of transient solar phenomenon will greatly enhance our knowledge of the physical problems associated with plages, flares, etc. Observations of the ultraviolet tail of the solar energy curve and parallel measurements of limb darkening would provide an important check on present models of the solar photosphere, especially within the highest layers. Continuous monitoring might also reveal significant short-term variations in the solar energy output.

The first experiments dealing with the observations of ultraviolet radiation from the Sun carried out by Tousey and his group[6] at NRL employed a grating spectrograph using a photographic film as a detector. Highly resolved spectra have since been obtained by further flight experiments, and some of the intense lines have been identified. Monitoring of intensities at these short wavelengths require the use of electronic radiation detectors in satellite-based experiments.[7,8] There also remain some unresolved inconsistencies in solar ultraviolet intensity measurements made with film and with photocathode surfaces in the wavelength region below 1000Å. Since this particular field of investigation of the vacuum ultraviolet is of relatively recent origin when compared to, for instance, the visible region of the spectrum, it is clear that much detection development must be done before this art will have achieved the sophistication required of modern experimentation.

SECTION II

LITERATURE SURVEY

In order to improve on the detection techniques for the electromagnetic radiation between 100 - 1000 Å, it is important to consider the various modes of interaction of this radiation with matter.

Various Modes of Interaction

The three main effects which have been used for detection of vacuum ultraviolet radiation can be classified as follows:

The first effect is based on the most elementary property of any form of energy, namely, its ability to heat a body in which it is absorbed. Detectors based on this effect are classified as thermocouples, bolometers, thermopiles, or similar instruments. In order to determine the absolute intensity of radiation in the vacuum ultraviolet region below 1000Å, this detector requires its calibration at a wavelength in the visible or near ultraviolet region which is far removed from the region under consideration. Also, an assumption has to be made that these detectors have a flat response to all wavelengths; i.e., its quantum efficiency is constant. The gold black, with which the receiving surface of these detectors is coated, is assumed to be completely black. This requires that the coating of the detector surface have negligible reflectance (true of almost all surfaces in the VUV) and that the number of photoelectrons ejected from the detector surface be very small. A substantial photoelectric yield will imply loss of photons for the production of heat and hence an error in the absolute photon flux.

The second mode of interaction is where a chemical change is produced in the receiver. Photographic techniques are included in this

category. Schumann first introduced special photo-emulsions which were poor in gelatin.[9] In recent years the Eastman SWR short wavelength radiation film and the Kodak Pathe film have been the types generally used and studied for solar ultraviolet radiation measurements. The English product Ilford 2 is similar to SWR and the Kodak Pathe supplies high sensitive emulsions of the Schumann type, SC-4, SC-5, SC-7, DC-3, and SWR-C. Emulsions with SC suffix are gelatin free and are useful for $\lambda > 50$A.

The third mode of interaction concerns itself with the absorption of photons in solids and gases by electrons in which the energy of a single quantum of radiation is imparted to an electron. This electron, then, either gets ejected from its bound state to become a free electron leaving the absorbing atom or molecule in the ionized ground, excited, or dissociated state or gets to a higher energy level leaving the atom or molecule in the excited or dissociated state. One can also consider other processes where the incident photon gets scattered without change in energy, the most important of these being the resonance scattering. The excited neutral molecule or ion resulting from the absorption of a vacuum ultraviolet photon may decay to the ground state by the emission of a long wavelength photon. Such a process is termed photon induced fluorescence. The cross section for total photo absorption, photo ionization, and fluorescence are large enough to be considered in selecting these modes of interaction in gases in the construction of a selective detector for use in the wavelength region below 1000A. We shall discuss the interaction with gases and solids separately.

Interaction with Gases

In order to deal with the interaction of a photon beam with a gas, one takes recourse to the Lambert's law, which relates the change in intensity $\Delta I(\lambda)$ of a photon beam of intensity $I(\lambda)$, when passing through an absorption thickness Δx, by the relation

$$\Delta I(\lambda) = -\mu I(\lambda)\Delta x \qquad (1)$$

where μ is a constant of proportionality and is a property of the medium called the absorption coefficient and is measured in units of cm^{-1} if Δx is measured in cm. Integrating over the cell length (L') one gets

$$I(\lambda) = I_o(\lambda)e^{-\mu(\lambda)L'} \tag{2}$$

where $I(\lambda)$ is the intensity of the beam at the exit end of the gas cell and $I_o(\lambda)$, the incident intensity. The length of the cell (L')reduced to normal temperature (273^oK) and pressure (760mm) is given by

$$L' = L\left(\frac{P}{760}\right)\left(\frac{273}{T}\right)$$

Therefore,

$$\mu(\lambda) = \frac{\ln\left(\frac{I_o(\lambda)}{I(\lambda)}\right)}{L\left(\frac{P}{760}\right)\left(\frac{273}{T}\right)} \tag{3}$$

If Beer's law, which states that the amount of light absorbed is proportional to the number of absorbing molecules through which the light passes, is obeyed, then the absorption coefficient can be written as

$$\mu = n_o\sigma \tag{4}$$

where n_o is the Loschmidt's number = 2.687×10^{19} molecules/cm^3 and σ is known as the total absorption cross section, which one molecule presents with respect to the incident radiation and has the dimensions of cm^2. Hence the total absorption cross section for a monochromatic beam can be written as

$$\sigma(\lambda) = \frac{\ln\left(\frac{I_o(\lambda)}{I(\lambda)}\right)}{n_oL\left(\frac{P}{760}\right)\left(\frac{273}{T}\right)} \tag{5}$$

Here no assumption as to the mechanism by which this may occur is involved.

The various mechanisms by which absorption may take place are (i) photoionization (removal of an electron); (ii) photodissociation of a molecule associated with ionization; (iii) fluorescence produced by the decay of excited or ionized molecules.

In rare gases, where the absorption is mainly due to ionization, one can measure the total number of ion-pairs produced in an ion chamber by dividing the current produced with the electronic charge, e. The cross section for photoionization, σ_i, is related to the total absorption cross section σ, by the relation

$$\sigma_i = \eta \sigma \tag{6}$$

where η is the photoionization efficiency. This quantity has been found to be equal to unity for all rare gases, He, Ne, A, Kr, Xe.[10] Hence $\sigma_i = \sigma$. In most other cases $\sigma_i < \sigma$.

Using a many lined spectrum obtained from a high voltage condensed spark discharge in a gas filled capillary tube, Weissler and coworkers[11] have measured σ and σ_i on the short wavelength side of the first ionization threshold. Since then there has been a tremendous improvement in the light sources and measuring techniques. More refined observations have since been made by Vodar and coworkers[12] in N_2, CO_2, C_6H_6, and CH_3OH. Huffman et al,[13] developed a helium and other rare gas continuum light sources for photoelectric scanning in the vacuum ultraviolet. Utilizing the continuum light source, they measured absorption coefficients of nitrogen,[14] xenon and argon,[15] carbon monoxide,[16] Oxygen,[17] activated nitrogen,[18] and krypton[19] in the 580 - 1100Å region.

Using the above mentioned helium continuum light source, Cook et al, measured the total photo absorption and photoionization cross sections, namely, σ and σ_i, for N_2, H_2, and H_2O,[20] H_2 and D_2,[21] CO,[22] and O_2 and N_2.[23] Metzger et al, using the same techniques, measured both σ and σ_i

for NO,[24] and supplemented the fluorescence intensity measurements for H_2O, NH_3, CH_4, C_2H_2, C_2H_4, and C_2H_6.[25] These and previously mentioned authors revealed very clearly the autoionization levels between $2P_{1/2}$ and $2P_{3/2}$ ionization limits in all the rare gases. All these measurements were limited between 580Å and 1100Å. Watanabe[26] et al, have measured ionization potentials of some molecules by the photoionization method in the photon energy range from 800 - 1600Å. Identity of the most loosely bound electrons, the effect of alkyl substitution, and the relationship between ionization continua and absorption bands are suggested for some molecules.

Very recently, photoionization and photo absorption cross section measurements of all the rare gases and few of the atmospheric gases have been made by Samson in the wavelength region below 1000Å. Using a high voltage condensed spark discharge in argon to produce a many lined spectrum, he has measured the total photoionization cross section from threshold down to 280Å in argon,[27] xenon,[28] helium,[29] and observed new autoionized energy levels in krypton, argon, and xenon.[30] Results in Ne were extended down to 200Å.[31] Samson and Cairns observed the photoionization cross sections in O_2 and N_2 at most intense solar emission lines[32] and measured the total absorption cross sections in H_2, O_2 and N_2 [33] and in CO and CO_2 [34] between 550 and 200Å. Cairns and Samson[35] also used the microwave discharge in a mixture of He and O_2 to obtain atomic oxygen and measured its absorption cross section between 900 and 500Å. The absorption cross section measurements were measured below the ionization threshold limit in krypton and xenon down to 170Å by Rustgi et al.[36] These results were utilized in the calculations of the oscillator strengths which agree well with earlier calculations. Rustgi also measured the total absorption cross section for argon and methane[37] and found that in methane the cross section did not become negligible around 500Å but had a value of about 6 Mb below 200Å. Between 80 and 600Å, photoionization cross sections of Ne, He, and Xe have been measured by Ederer and Tomboulian[38,39] and by Lowry et al.[40] Madden and

Codling, using continuum radiation from the 180 Mev electron synchrontron, have observed new autoionizing states in He, Ne, A;[41] and Kr and Xe[42] in the wavelength region from 600Å down to 120Å. They have also observed the inner shell electron excitation in neutral Kr and Xe as a function of wavelength.[43] Tables 1 through 7 list the values of absorption coefficients for He, Ne, A, Kr, Xe, O_2, N_2, and H_2 as a function of wavelength. Figure 1 shows the variation of σ_i as a function of photon energy for xenon, krypton, argon, neon, and helium.

Weissler et al,[44] utilizing a mass spectrometer in conjunction with a vacuum ultraviolet monochromator, measured (by mass analyses) the products formed as a result of photon impact and the consequent dissociative ionization of molecules. These results have been very valuable in ascertaining the importance of their relative cross sections. Absorption, ionization, and ion fragmentation cross sections of hydrocarbon vapors including ethane, propane, cyclopropane, ethylene, and acetylene were obtained by Schoen[45] in the wavelength range from 1400 down to 500Å. The ionization cross sections attained peaks near 16 ev in alkanes and near 17.5 ev in olefins. Beyond the peaks the ionization efficiency was almost 100%.

The peaks and valleys in the mass analysis of photoionization products of O_2 have been associated with excited states of the particular ion. To what extent the absorption of a photon results in fluorescence can be estimated by looking at the gas cell at right angles to the incident beam. The equation describing such a phenomenon is given by $O_2 + h\upsilon\ (20\ ev) \rightarrow O_2^{+*} + e^-\ (1\ ev)$. If this holds, then the decay from the excited state of the ion, O_2^{+*}, to the ground state of the same ion O_2^+, should be detectable as fluorescence in the visible region of the spectrum. Such fluorescence has been observed in a number of gases like N_2, O_2.[46] In contrast to observations in argon, where no fluorescence was observed, both N_2 and O_2 showed fluorescence. In N_2, the fluorescent intensity recorded by the photomultiplier shows the same time variation as the light source pulse of the exciting radiation (no delay), and in O_2, where the fluorescent intensity pulse shows considerable delay in

TABLE 1. HELIUM ABSORPTION COEFFICIENTS FROM 100 Å TO THRESHOLD

SHELL	λ(Å)	$\mu(cm^{-1})$	λ(Å)	$\mu(cm^{-1})$	λ(Å)	$\mu(cm^{-1})$
K	100.90	12.9	171.09	24.4	297.9	69
	104.81	11.6	173.01	24.7	308.4	80
	107.00	9.8	177.75	25.6	317.7	84
	110.48	9.8	181.21	26.0	323.2	85
	115.82	9.6	182.40	28.4	329.3	91
	116.38	9.9	184.04	31.6	338.1	95
	117.85	11.0	185.74	30.2	352.2	103
	118.97	11.2	188.44	32.1	357.5	108
	122.25	12.2	192.82	29.2	364.0	113
	124.58	12.8	195.95	32.7	368.4	117
	125.23	14.9	198.03	31.9	375.7	120
	126.06	13.4	200.68	32.1	382.1	124
	128.26	13.4	202.32	32.9	390.6	132
	129.83	13.3	203.86	32.7	394.0	133
	131.80	13.9	207.24	41.9	397.1	133
	132.28	14.2	207.79	40.2	400.3	134
	132.84	14.2	209.28	38.1	405.7	140
	133.35	14.4	213.09	37.8	410.6	143
	135.52	15.1	214.25	38.3	416.6	148
	138.07	15.4	215.20	39.4	423.3	156
	139.02	16.0	216.02	38.3	425.5	157
	140.07	17.4	220.35	40.5	429.7	157
	144.82	19.6	221.65	36.5	436.5	160
	147.27	19.0	222.77	35.4	442.8	163
	151.51	19.0	223.78	36.5	448.8	166
	153.94	22.6	225.20	38.6	452.0	167
	156.18	22.1	227.53	42.1	464.4	174
	159.36	22.5	231.20	42.7	473.6	180
	160.10	21.9	233.52	42.1	478.0	184
	162.47	22.3	246.20	44.8	482.0	185
	164.60	23.5	247.60	44.8	489.3	191
	166.17	22.3	262.1	43	494.3	195
	168.08	23.8	283.1	60	498.4	196
	170.21	24.0	294.1	58	503.0	198
					504.26	---

TABLE 2. NEON ABSORPTION COEFFICIENTS FROM .01 TO 44.6 Å

SHELL	λ(Å)	Experimental[a] $\mu(cm^{-1})$	Semiempirical $\mu(cm^{-1})$
K	.01	---	$.051 \times 10^{-3}$ ref. b
	.02	---	.071 " "
	.03	---	.084 " "
	.05	---	.102 " "
	.08	---	.121 " "
	.098	$.133 \times 10^{-3}$	---
	.100	---	.131 " "
	.130	.143 "	---
	.175	.166 "	---
	.200	.189 "	---
	.260	.243 "	---
	.417	.522 "	---
	.497	.837 "	---
	.631	1.62 "	---
	.710	2.25 "	---
	.880	4.09 "	---
	1.00	5.85 "	---
	1.235	11.16 "	---
	1.389	15.3 "	---
	1.54	21.6 "	---
	1.934	44.1 "	---
	2.500	90 "	---
	3.57	247 "	---
	4.36	430 "	---
	5.17	687 "	---
	6.97	1554 "	---
	8.32	2475 "	2487.000×10^{-3} ref. c
	9.87	3879 "	---
	13.37	7350 "	7416 " "
	14.298	---	---
L	17.6	---	971 " "
	21.7	---	1677 " "
	23.7	---	2141 " "
	27.4	---	3218 " "
	31.6	---	4725 " "
	36.3	---	6876 " "
	44.6	11790 "	11860 " "

[a] Determined from the mass absorption coefficients compiled by S. J. M. Allen in A. H. Compton and S. K. Allison, X-Rays in Theory and Experiment, (D. VanNostrand Co., Inc., N. Y., 1935), p. 799.

[b] J. A. Victoreen, J. Appl. Phys. 20, 1141 (1949).

[c] B. L. Henke, J. Appl. Phys. 28, 98 (1957).

TABLE 2. NEON ABSORPTION COEFFICIENTS FROM 80 Å TO THRESHOLD (Continued)

SHELL	λ(Å)	$\mu(cm^{-1})$	λ(Å)	$\mu(cm^{-1})$
L	80.57	67.2	260.45	236.0
	83.50	68.0	263.45	237.6
	85.32	74.3	266.95	230.0
	90.40	81.3	267.50	212.0
	96.58	71.3	277.30	206.6
	99.60	77.8	283.50	216.0
	104.81	91.3	282.32	215.7
	110.48	100.4	283.1	224
	115.82	99.9	297.9	228
	117.85	102.3	329.3	236
	118.97	104.8	338.1	238
	129.83	118.8	352.2	241
	133.45	127.2	364.0	245
	135.52	129.1	368.4	243
	138.07	133.7	375.7	243
	150.01	152.6	382.1	242
	151.50	151.7	390.6	242
	159.36	160.9	394.0	241
	162.47	164.4	397.1	241
	164.60	164.2	400.2	243
	166.17	168.2	405.7	243
	168.08	170.1	410.6	243
	172.16	177.7	416.6	242
	173.01	183.1	423.3	242
	184.04	182.5	425.5	243
	185 ±5	187.0	429.7	242
	185.74	191.7	436.5	239
	192.82	191.2	442.8	240
	194.59	182.8	448.8	240
	195.95	195.8	452.0	239
	202.32	203.3	464.4	234
	203.86	200.1	473.6	231
	207.24	206.3	478.0	230
	209.28	204.7	482.0	228
	214.25	209.0	489.3	225
	215.20	207.6	494.3	223
	218.50	207.0	498.4	221
	220.35	217.6	503.0	218
	227.52	220.9	511.0	214
	228.00	213.0	516.1	212
	231.20	221.7	521.6	209
	233.52	221.4	528.7	202
	238.47	222.2	541.4	198
	241.50	212.0	546.9	193
	243.02	220.0	553.5	188
	246.20	231.9	558.0	186
	247.60	230.9	561.6	185
	248.60	240.0	567.5	182
	251.50	225.0	573.5	168
	256.31	230.0	574.93	---

TABLE 3. ARGON ABSORPTION COEFFICIENTS FROM .01 TO 44.6 Å.

SHELL	λ(Å)	Experimental[a] $\mu(cm^{-1})$	Semiempirical $\mu(cm^{-1})$
K	.01	---	$.092 \times 10^{-3}$ ref. b
	.02	---	.128 " "
	.03	---	.153 " "
	.05	---	.190 " "
	.08	---	.247 " "
	.098	$.328 \times 10^{-3}$	---
	.100	---	.293 " "
	.130	.437 "	---
	.175	.714 "	---
	.200	.794 "	---
	.260	1.510 "	---
	.417	5.260 "	---
	.497	8.93 "	---
	.631	17.45 "	---
	.710	23.2 "	---
	.880	42.9 "	---
	1.000	62.5 "	---
	1.235	111.0 "	---
	1.389	153.0 "	---
	1.540	211.0 "	---
	1.934	420.0 "	---
	2.500	846.0 "	---
	3.570	2160.0 "	---
	3.870	2610.0 "	---
L	3.870	263.0 "	---
	4.360	360.0 "	---
	5.170	578.0 "	---
	6.970	1335.0 "	---
	8.320	2070.0 "	2076.000×10^{-3} ref. c
	9.870	3320.0 "	---
	11.90	5860.0 "	---
	13.3	---	6760 " "
	17.6	---	12680 " "
	21.7	---	19720 " "
	23.7	---	24150 " "
	27.4	---	33700 " "
	31.6	---	45800 " "
	36.3	---	61950 " "
	44.6	81600.0 "	---
	50.6	---	---

[a] Determined from the mass absorption coefficients compiled by S. J. M. Allen in A. H. Compton and S. K. Allison, X-Rays in Theory and Experiment, (D. VanNostrand Co., Inc., N. Y., 1935), p. 799.

[b] J. A. Victoreen, J. Appl. Phys. 20, 1141 (1949).

[c] B. L. Henke, J. Appl. Phys. 28, 98 (1957).

TABLE 3. ARGON ABSORPTION COEFFICIENTS FROM THRESHOLD TO 280 Å. (Continued)

λ(Å)	$\mu(cm^{-1})$	λ(Å)	$\mu(cm^{-1})$	λ(Å)	$\mu(cm^{-1})$	λ(Å)	$\mu(cm^{-1})$
230	5.9	436.5	766	470.1	897	616.7	783
264	33.5	436.7	770	470.8	900	618.8	981
282.8	23	436.9	768	471.3	900	625.2	978
297.8	47	437.5	770	474.0	912	629.8	973
308.0	72	438.1	796	475.7	909	634.0	978
317.3	98	438.8	794	479.4	900	637.0	964
323.0	115	439.4	780	484.2	912	641.0	971
329.0	143	440.0	768	486.8	912	644.1	971
337.6	167	440.7	763	487.9	915	649.0	971
351.0	233	441.3	757	492.5	915	651.0	973
357.6	253	441.9	731	496.5	924	660.0	952
363.8	285	442.1	712	499.4	926	662.7	971
375.2	360	442.6	695	501.3	924	664.8	968
381.6	382	443.2	673	505.8	936	668.3	956
389.9	434	443.8	720	509.3	936	670.2	960
393.3	426	444.2	773	512.1	945	675.2	924
396.5	454	444.5	778	514.3	945	677.1	936
399.3	466	445.1	796	517.5	952	680.5	945
405.2	535	445.7	796	519.5	945	683.0	945
405.7	520	446.4	796	521.9	964	684.8	945
410.0	558	447.9	788	524.2	964	688.4	950
411.5	562	449.8	787	526.7	964	692.8	940
416.9	709	450.2	790	529.3	991	694.9	945
417.6	734	450.8	808	532.0	978	700.0	915
418.2	750	451.4	800	536.0	985	703.0	945
418.8	769	452.1	808	539.3	971	705.4	934
419.4	781	452.7	798	541.8	999	709.2	915
420.0	790	453.3	817	544.9	973	713.7	912
420.7	800	453.9	810	549.3	973	715.5	920
421.3	767	454.5	810	551.4	985	718.4	940
421.8	760	455.2	800	555.1	985	721.0	915
422.4	738	455.8	790	558.8	985	724.8	900
425.2	762	457.0	783	562.1	995	727.2	900
425.8	767	457.6	780	564.6	981	735.6	883
426.4	767	459.8	778	567.9	981	737.0	887
427.0	790	462.2	768	570.4	981	739.9	906
427.7	712	462.5	768	573.7	971	742.4	905
428.3	764	463.1	780	577.0	978	744.6	890
428.9	760	463.7	723	580.0	964	747.5	865
429.5	752	464.4	669	583.0	978	751.1	845
430.1	773	465.0	579	585.5	973	755.1	866
430.9	798	465.6	492	588.9	990	760.6	856
431.5	789	466.3	536	594.1	978	765.3	876
432.2	787	466.6	619	596.7	978	767.3	830
432.9	804	466.9	695	599.5	991	772.4	860
433.7	782	467.6	822	603.4	991	774.6	852
434.2	747	468.2	882	608.5	964	776.8	845
434.5	692	468.7	900	610.0	973	779.7	627
435.0	703	468.8	897	613.0	998	783.2	671
436.0	742	469.5	900	614.8	991	787.6	364

TABLE 4. KRYPTON ABSORPTION COEFFICIENTS FROM .01 - .8 and at 44.6 Å

SHELL	λ(Å)	Experimental[a] $\mu(cm^{-1})$	Empirical[b] $\mu(cm^{-1})$
K	.010	---	$.183 \times 10^{-3}$
	.012	---	.201 "
	.015	---	.227 "
	.020	---	.263 "
	.025	---	.298 "
	.030	---	.334 "
	.040	---	.414 "
	.050	---	.514 "
	.060	---	.649 "
	.080	---	1.037 "
	.098	2.08×10^{-3}	---
	.100	---	1.64 "
	.120	---	2.50 "
	.150	---	4.40 "
	.200	10.8 "	9.56 "
	.260	21 "	---
	.417	77 "	---
	.497	129 "	---
	.631	238 "	---
	.710	338 "	---
	.800	408 "	---
	.866	---	---
L	---	---	---
M	44.6	118000. "	---

[a] Determined from the mass absorption coefficients compiled by S. J. M. Allen in A. H. Compton and S. K. Allison, X-Rays in Theory and Experiment, (D. Van Nostrand Company, Inc., New York, 1935), p. 799

[b] J. A. Victoreen, J. Appl. Phys. 20, 1141 (1949).

TABLE 4. KRYPTON ABSORPTION COEFFICIENTS FROM THRESHOLD TO 280 Å. (Continued)

λ(Å)	$\mu(cm^{-1})$	λ(Å)	$\mu(cm^{-1})$	λ(Å)	$\mu(cm^{-1})$	λ(Å)	$\mu(cm^{-1})$
170	7.6	405.7	435	555.1	904	736.8	1118
230	17.3	410.6	438	564.6	923	745.1	1116
247	47.5	416.6	428	570.6	948	748.1	1107
265	65.3	423.3	439	586.0	972	755.1	1154
283.7	73	425.5	435	596.6	993	760.4	1151
294.7	112	429.7	532	609.8	1028	766.1	1169
298.5	106	436.5	498	618.9	1041	772.7	1180
309.0	160	442.8	527	625.6	1049	779.4	1157
318.2	169	447.3	549	630.2	1053	783.1	1176
323.7	244	450.6	570	636.6	1057	789.1	1164
327.0	202	462.8	591	640.8	1077	795.6	1162
329.8	193	471.4	562	644.6	1070	800.8	1161
338.5	193	474.4	634	649.7	1086	814.6	1091
349.5	201	479.4	675	660.6	1078	821.5	1116
352.6	291	487.2	695	663.6	1096	827.4	1153
358.0	278	492.2	699	671.1	1104	834.8	1140
364.4	256	496.3	483	675.6	1037	840.1	1167
368.7	325	500.8	727	685.0	1121	844.6	1147
376.0	305	508.8	785	694.6	1136	850.4	878
380.0	340	514.6	303	700.6	1122	857.6	891
382.4	333	519.6	815	709.1	1146	870.3	812
390.7	376	526.7	835	714.1	1136	878.6	1276
394.0	374	539.6	877	721.2	1163	883.6	488
397.2	400	545.4	888	725.6	1132		
400.3	449						

TABLE 5. XENON ABSORPTION COEFFICIENTS FROM .01-.3 Å AND AT 44.6 Å

Shell	λ(Å)	Experimental[a] $\mu(cm^{-1})$	Empirical[b] $\mu(cm^{-1})$
K	.010	---	$.287 \times 10^{-3}$
	.012	---	.318 "
	.015	---	.366 "
	.020	---	.444 "
	.025	---	.536 "
	.030	---	.646 "
	.040	---	0.946 "
	.050	---	1.39 "
	.060	---	2.02 "
	.080	---	3.94 "
	.098	8.2×10^{-3}	---
	.100	---	6.96 "
	.120	---	11.30 "
	.150	---	20.65 "
	.175	31.3 "	---
	.200	---	44.90 "
	.250	---	81.40 "
	.300	---	129.50 "
	.359	---	---
L	---	---	---
M	---	---	---
N	44.6	39500 "	---

[a] Determined from the mass absorption coefficients compiled by S. J. M. Allen in A. H. Compton and S. K. Allison, X-Rays in Theory and Experiment, (D. Van Nostrand Company, Inc., New York, 1935), p. 799.

[b] J. A. Victoreen, J. Appl. Phys. 20, 1141 (1949).

TABLE 5. XENON ABSORPTION COEFFICIENTS FROM 80 - 202 Å. (Continued)

λ(Å)	$\mu(cm^{-1})$	λ(Å)	$\mu(cm^{-1})$
80.0	61	164.4	216
83.6	68	166.3	203
85.4	89	168.3	200
90.3	175	171.1	152
91.4	182	172.3	141
96.6	252	173.5	129
97.3	253	178.0	127
99.5	269	181.1	120
101.0	403	182.0	114
105.0	460	182.6	114
106.7	460	184.0	95
110.0	568	185.8	93
116.5	730	192.9	61
138.0	676	194.9	60
139.2	622	195.9	60
140.3	527	200.8	60
145.0	483	202.3	58
145.3	416	203.9	59
147.5	446	207.9	53
149.8	412	209.0	58
151.5	410	213.0	67
154.0	294	214.2	55
156.2	329	215.1	52
158.9	294	220.0	66
162.4	273		

TABLE 5. XENON ABSORPTION COEFFICIENTS FROM THRESHOLD TO 280 Å. (Continued)

λ(Å)	$\mu(cm^{-1})$	λ(Å)	$\mu(cm^{-1})$	λ(Å)	$\mu(cm^{-1})$	λ(Å)	$\mu(cm^{-1})$
284.0	78	416.6	194	515.4	486	638.6	971
294.9	114	423.4	214	521.0	514	642.8	994
298.7	96	425.8	219	528.1	537	646.1	1006
309.0	149	429.9	236	534.2	558	650.8	1025
318.7	153	436.6	253	540.7	594	661.8	1055
324.1	129	442.8	246	546.3	640	665.9	1099
330.2	98	447.5	260	552.9	661	672.6	1109
338.7	94	451.2	270	557.1	667	677.2	1090
352.8	124	461.3	294	560.4	620	686.3	1150
358.3	181	463.6	299	566.3	684	696.2	1201
364.5	147	466.6	302	572.4	627	701.7	1189
369.0	189	473.1	336	588.0	818	710.4	1238
376.1	150	477.4	351	590.4	759	715.6	1250
382.6	178	482.0	365	595.6	283	722.1	1279
390.7	185	488.9	359	595.7	800	726.3	1277
394.2	217	493.8	394	597.8	819	738.5	1296
397.5	202	497.8	367	611.5	890	746.8	1298
200.5	198	502.7	434	620.5	921	756.4	1371
405.7	169	506.8	443	626.8	932	762.2	1385
410.6	185	510.3	463	631.7	945	769.1	1395

TABLE 5. XENON ABSORPTION COEFFICIENTS FROM THRESHOLD TO 280 A. (Continued)

λ(Å)	$\mu(cm^{-1})$	λ(Å)	$\mu(cm^{-1})$	λ(Å)	$\mu(cm^{-1})$	λ(Å)	$\mu(cm^{-1})$
776.3	1415	858.7	1614	928.8	1129	975.0	650
781.6	1387	865.2	1607	935.2	1622	979.5	1121
784.9	1474	870.1	1633	938.5	1695	983.1	1466
796.4	1462	880.3	1664	941.6	1326	988.1	2240
802.3	1482	888.0	1661	943.5	1929	991.6	2495
805.1	1488	902.5	1656	946.9	883	996.1	3370
823.0	1463	906.3	1671	951.9	2466	1003.5	413
828.5	1530	911.6	1674	955.9	629	1008.5	420
836.0	1525	920.6	1684	959.6	1318	1015.6	782
845.7	1540	924.3	1443	964.4	2416	1018.5	937
851.5	1561	924.9	1392	969.5	1966		

TABLE 6. ABSORPTION COEFFICIENTS AND PHOTOIONIZATION YIELDS OF O_2 and N_2.**

Source Line λ(A)		Oxygen $\mu(cm^{-1})$	Oxygen $\eta(\%)$	$\mu(cm^{-1})$	$\eta(\%)$
303.781 He	II	446*	100	326*	100
429.918 0	II				
430.041 0	II	480*	100	564*	100
430.177 0	II				
434.975 0	III	561	100	637	100
498.431 0	VI	619	100	652	100
507.391 0	III	622	97	654	100
507.683 0	III				
508.182 0	III	638	97	598	100
519.610 0	VI	678	100	693	98
522.208 He	I	561	99	635	97
525.795 0	III	659	97	703	98
537.024 He	I	571	98	678	97
553.328 0	IV	705	93	669	96
554.074 0	IV	685	97	680	93
554.514 0	IV	709	97	660	93
555.262 0	IV	698	97	666	95
584.331 He	I	625	98	620	100
597.818 0	III	774	92	629	97
599.598 0	III	765	97	629	95
608.395 0	IV	648	94	630	100
609.705 0	III				
609.829 0	IV	714	94	636	100
610.043 0	III				
610.746 0	III	764	96	626	99
610.850 0	III				
616.933 0	IV				
617.033 0	IV	655	97	637	98
617.051 0	II				
624.617 0	IV	681	93	645	97
625.130 0	IV	661	96	642	97
625.852 0	IV	814	96	644	98

*Estimated error ± 10%

**J.A.R. Samson and R.B. Cairns, J. Geophy. Res. 69, 4583 (1964).

TABLE 6. ABSORPTION COEFFICIENTS AND PHOTOIONIZATION YEILDS OF O_2 AND N_2. ** (Continued)

Source Line λ(A)		Oxygen $\mu(cm^{-1})$	Oxygen $\eta(\%)$	$\mu(cm^{-1})$	$\eta(\%)$
629.732 0	V	801	97	652	97
684.996 N	III	709	100	653	95
685.513 N	III	496	100	670	95
685.816 N	III				
686.335 N	III	594	100	648	95
758.677 0	V	493	57	643	75
759.440 0	V	463	53	313	86
760.229 0	V	498	49	531	57
760.445 0	V				
761.130 0	V	547	51	1077	55
762.001 0	V	545	50	747	46
763.340 N	III	604	58	734	80
764.357 N	III	479	60	364*	69
765.140 N	IV	615	54	2295	77
774.522 0	V	382	63	914	40
779.821 0	IV	733	33	344	65
779.905 0	IV				
787.710 0	IV	644	54	226	89
790.103 0	IV	744	37	610	45
790.203 0	IV				
832.754 0	II	707*	38	Variable See Text	0
832.927 0	III				
833.326 0	II				
833.742 0	III	350*	39	Variable See Text	0
834.462 0	II	285*	38		0
835.096 0	III	267	37		0
835.292 0	III				
921.982 N	IV	148	79		0
922.507 N	IV	171	84		0
923.045 N	IV	272	88		0
923.211 N	IV				
923.669 N	IV	246	90		0
924.274 N	IV	480	83		0
972.537 H	I	860	83		0
977.026 C	III	107	62	2.2	0
989.790 N	III	37	69	4.5	0
991.514 N	III	47	69	2.0	0
991.579 N	III				
1025.722 H	I	41	64	0.027	0
1031.912 0	VI	28	1†	<0.02	0
1037.613 0	VI	21	0.1†	<0.02	0

*Estimated error ±10%

†Estimated error ± 50%

TABLE 7.

Absorption Cross Section of H_2, O_2 and N_2

Wavelength Å	Absorption Cross Section (10^{-18} cm^2)		
	H_2	O_2	N_2
209.3	0.266	9.04	6.46
225.2	-	10.6	
234.2	0.402	10.6	-
239.6	0.439	11.9	-
247.2	0.494	12.3	9.75
260.5	0.579	-	-
266.3	0.638	14.0	10.5
283.5	0.790	15.2	10.9
297.6	0.949	-	11.5
303.1	1.02	16.3	11.6
314.9	1.12	16.4	12.4
323.6	1.22	16.7	13.1
335.1	1.36	16.8	14.0
345.1	1.51	17.0	14.8
358.5	1.75	-	15.7
362.9	1.84	17.5	16.1
374.4	2.04	17.9	17.3
387.4	2.26	18.5	18.6
428.2	2.88	19.4	22.1
434.3	3.02	19.6	22.4
452.2	3.37	-	22.6
463.7	-	-	22.6
508.2	-	23.7	22.8
512.1	-	-	23.2
519.6	-	25.2	25.8
522.2	-	20.9	23.6
525.8	-	24.5	26.2
537.0	-	21.2	25.2

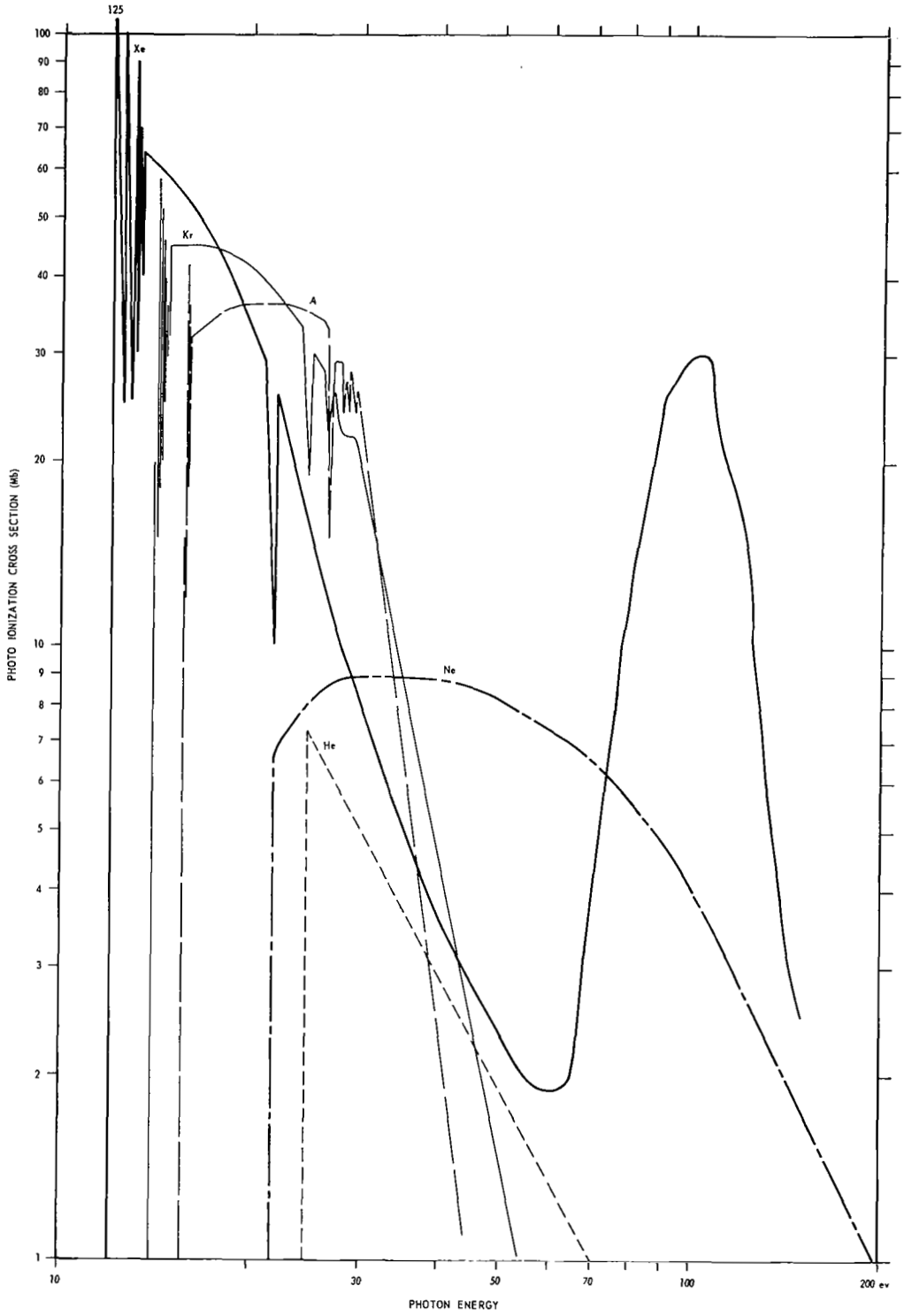

Figure 1 Variation of σ_i for He, Ne, A, Kr and Xe as a Function of Photon Energy

comparison with the exciting light source pulse. This delay of fluorescent emission may be connected with the lifetime of the excited state of the ion. The threshold of the observed fluorescence could be correlated with known excited states of the corresponding ions. As illustrated in Figure 2, the fluorescent efficiency in N_2 appears to be essentially constant with photon energy at wavelengths below the threshold down to the lowest available wavelength of 580Å.[47]

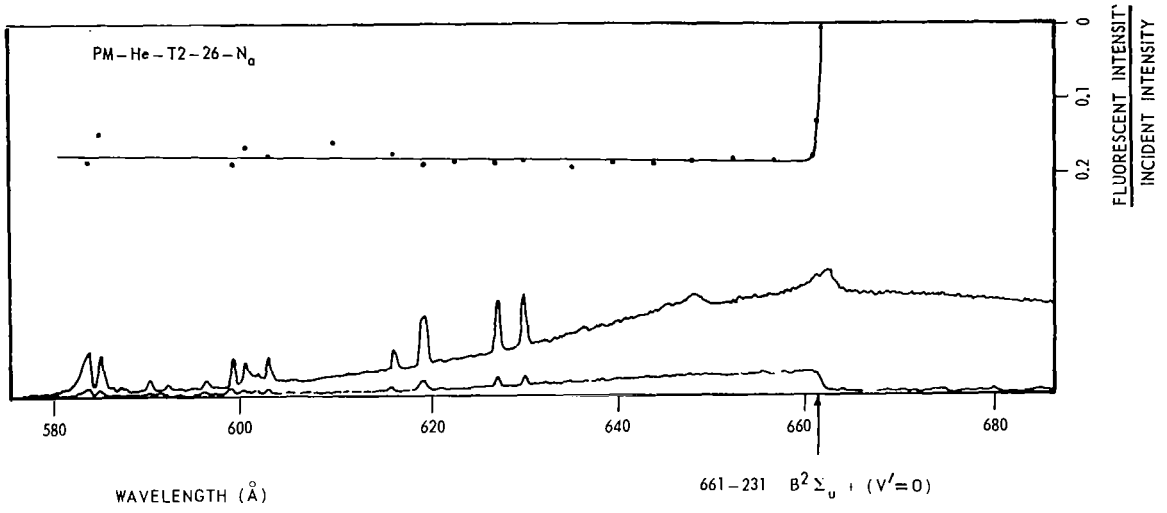

Figure 2 Photo Electric Scanning Record of Nitrogen Absorption at Relatively High Pressure. Sudden Decrease of Absorption Beginning at About 661 A Indicates Fluorescence of N_2^+.

Interaction with Solids

The interaction of short wavelength electromagnetic radiation with solids is best analysed by considering the optical and photoelectric properties of thin films and single crystals. If R denotes the fraction of this radiation reflected from a solid and T denotes the fraction transmitted by it, then the radiation absorbed, A, is related to both R and T by the equation

$$A = 1 - (R + T).$$

Because of the high energy of the photons associated with the electromagnetic radiation of wavelengths shorter than 1000Å, the interaction is not only confined with conduction electrons, which are relatively free, but ejection and excitation of inner electrons is possible. On the basis of free electron theory of solids, one derives the conclusion that most of the solids change from a totally reflecting medium to a perfectly transmitting medium.[48] Hence it would be profitable to examine the optical properties, namely, reflectance and transmittance of thin films in the wavelength region below 1000Å.

The first significant measurements of reflectance of a large number of materials were made by Sabine.[49] The samples were prepared in the form of films by thermal evaporation in vacuum. Reflectance measurements on Al, Sb, Be, Bi, Cd, Cr, Cu, Au, Fe, Pb, Mg, Mo, Ni, Pd, Pt, Ag, Te, Ti, Zn, and Zr films were made after the films had been exposed to air between preparation and measurement.

Reflectance measurements on thin films of Al, Sn, In, Bi, Au, Ag, and Cd were made by Walker et al[50], in the wavelength region between 1600 and 450Å. The films were prepared in the experimental chamber and, hence, were not exposed to air between preparation and measurement. The reflectance values were found to be higher than the earlier measurements. Rustgi et al[51], collected the reflectance measurements for Sb, Te, and Ti over the same wavelength interval. Other measurements include those of Cox et al[52], on zinc between 2200Å and 450Å; Hass and Tousey[53] on Al, Pt, and Rh indicating that the reduced reflectance of Al is due to oxidation. Important studies of the reflectance of evaporated layers and single crystals of Ge, Si, Se, and Te have been carried out by Robin-Kandare.[54] Multilayer coatings of magnesium fluoride and lithium fluoride on aluminum have been prepared and used for obtaining higher reflectance near 1200Å by Berning[55] and Angel et al.[56] Hunter[57] carried out a systematic study of the degradation of high reflectance multiple coatings with time in humid environments and showed that the Al + MgF_2 coatings are unaffected whereas the Al + LiF coating decreased

by about 25% in a few days. A detailed study of reflectance of few materials has been made by Madden.[58] The use of reflectance measurements in the calculation of optical constants has been amply demonstrated by Hunter et al,[59] Rustgi et al,[60] and Ehrenreigh et al.[61] Since the reflectance is very much dependent on the duration of evaporation of the film and the pressure at which evaporation takes place, it is not possible to present all the available data in a graphical form. Moreover it has not been possible to prepare films having high reflectance in the wavelength region below 1000Å.

Looking at the transmittance of various optical materials, it is found that all those materials which are useful as filters in the visible region of the spectrum become opaque in the near and far ultraviolet region of the spectrum. Table 8 shows the transmission limit of a large number of materials.

TABLE 8. FILTERS FOR NEAR AND VACUUM ULTRAVIOLET

Short Wavelength Limit of Transmission Å	Material
3050	Window glass
1900	Quartz
1780	Corning glass 9741
1700	Quartz
1600	Crystalline quartz
1600	Gypsum
1550	Quartz glass
1420	Sapphire
1415	Synthetic sapphire
1400	Barium fluoride
1270	Strontium fluoride
1220	Calcium fluoride
1050	Lithium fluoride

It is clear that LiF is the only material which is capable of transmitting down to 1050Å. In metals, the plasma frequency at which a solid changes from a perfectly reflecting medium to a transmitting medium, corresponds to wavelengths in the region below 1000Å. Thin unbacked films have been prepared and transmittance measurements made on some

films. Walker et al[50] observed the transmission in thin films of Al, Sn, In, and Bi while Rustgi et al[51] measured the transmission onset in Te, Ti, and Sb. These measurements were extended towards shorter wavelengths to observe new absorption edges in Te, Ti, Sh, and onset of optical transmission in Be by Rustgi.[62] Other materials studied for transmission so far include: Pb by Walker;[63] C by Samson[64]; Cr by Axelrod and Givens;[65] Mg by Kroger and Tomboulian;[66] and laser-deposited Ir by Samson.[67] Tomboulian et al[68] measured absorption coefficients in a large number of solids on the high energy side of the $M_{2,3}$ absorption edge. Table 9 gives the limits of transmission of all materials examined so far. The transmittance characteristics in the wavelength region below 1000Å for most of these materials are shown in Figures 3 and 4 while Figure 5 summarizes the transmission region for all materials as a function of photon energy. Table 10 shows the transmittance of various filter materials in the soft x-ray region.

The photoelectric yield of a large number of solids is known to be very low, 10^{-4} -10^{-5} electrons/photon incident, in the visible and near ultraviolet region of the spectrum. However, relatively few measurements existed before 1950 in the vacuum ultraviolet region of the spectrum. A systematic study on a few solids, Ni, Pt, and W was carried out by Hinteregger[70] over the wavelength region from 2500 down to 850Å. More comprehensive studies were reported by Walker et al[71], on (Ni, Cu, Pt, Au, W, Mo, Ag, and Pd) over the wavelength region between 1400 and 473Å. The samples were heat treated before and during measurement. These and other results were summarized by Weissler[11] in a comprehensive article. The substance of these studies indicates that near 1500Å, the photoelectric yield suddenly increases by as much as three orders of a magnitude from that in the near UV, indicating an onset of volume photoelectric effect, attaining a peak value near 900-800Å and then showed a slight decrease at shorter wavelengths. Subsequently, data on photoelectric emission were obtained in the same wavelength region on freshly evaporated films with and without backing.[50] These films were prepared in a vacuum of 5 x 10^{-5}mm Hg pressure. Recently, Heroux et al[72]

TABLE 9. REGION OF TRANSPARENCY IN THE VACUUM UV

Be	650 Å > λ > 110 Å
C	560 Å > λ > 44 Å
Mg	1100 Å > λ > 250 Å
Al	840 Å > λ > 170 Å
Si	700 Å > λ > 130 Å
Ti	690 Å > λ > 325 Å
Cr	500 Å > λ > 280 Å
Fe	900 Å > λ > 220 Å
Co	900 Å > λ > 190 Å
Ge	750 Å > λ > 400 Å and 380 Å > λ > 150 Å
In	1120 Å > λ > 35 Å
Sn	900 Å > λ > 510 Å
Sb	825 Å > λ > 375 Å and 335 Å > λ > 300 Å
Te	880 Å > λ > 310 Å
Pb	880 Å > λ > 700 Å
Bi	855 Å > λ > 525 Å 500 Å > λ > 450 Å and 450 Å > λ > 250 Å

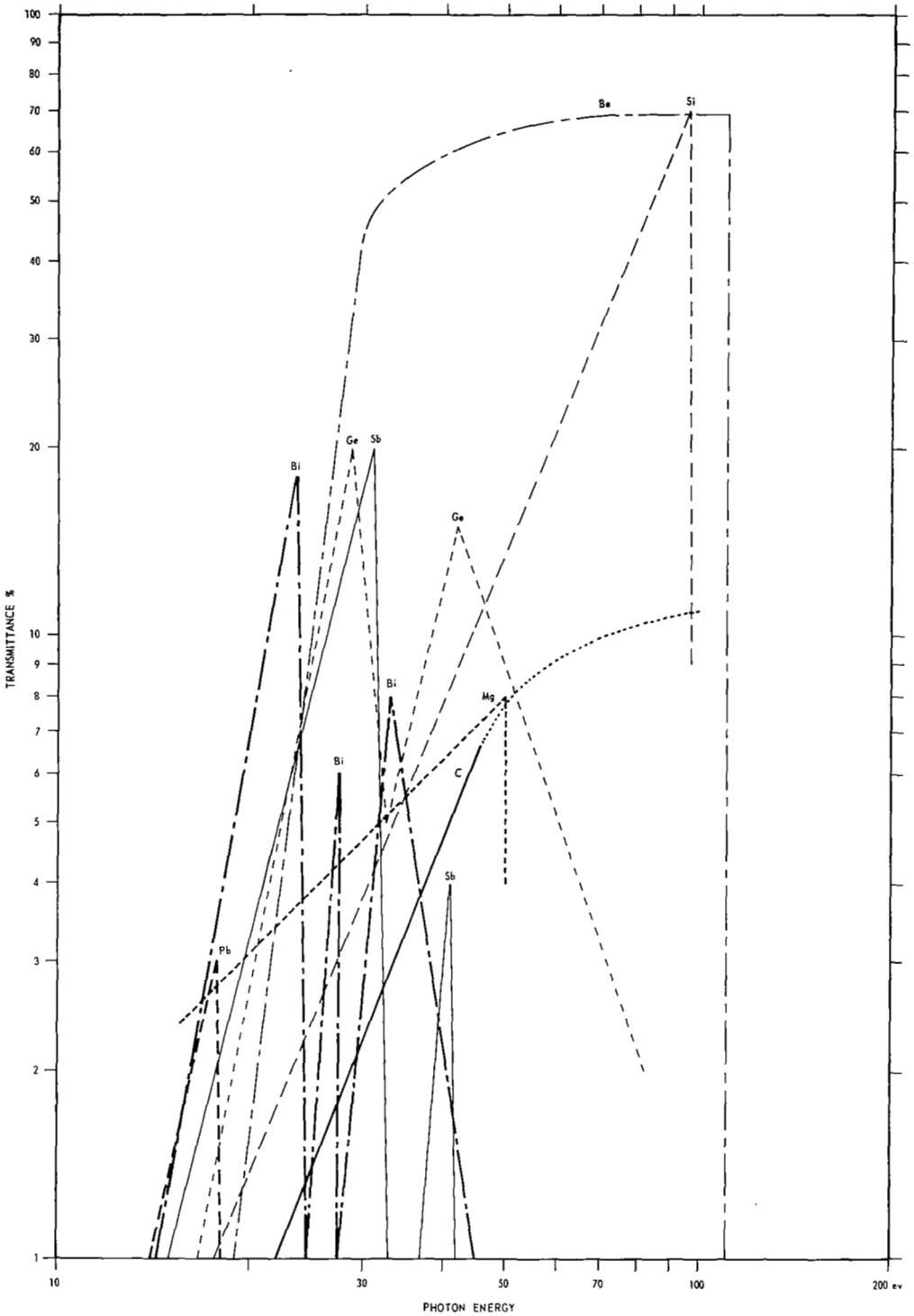

Figure 3 Transmittance Characteristics of Bi, Pb, Ge, Sb, C, Mg, Be and Si as a Function of Photon Energy

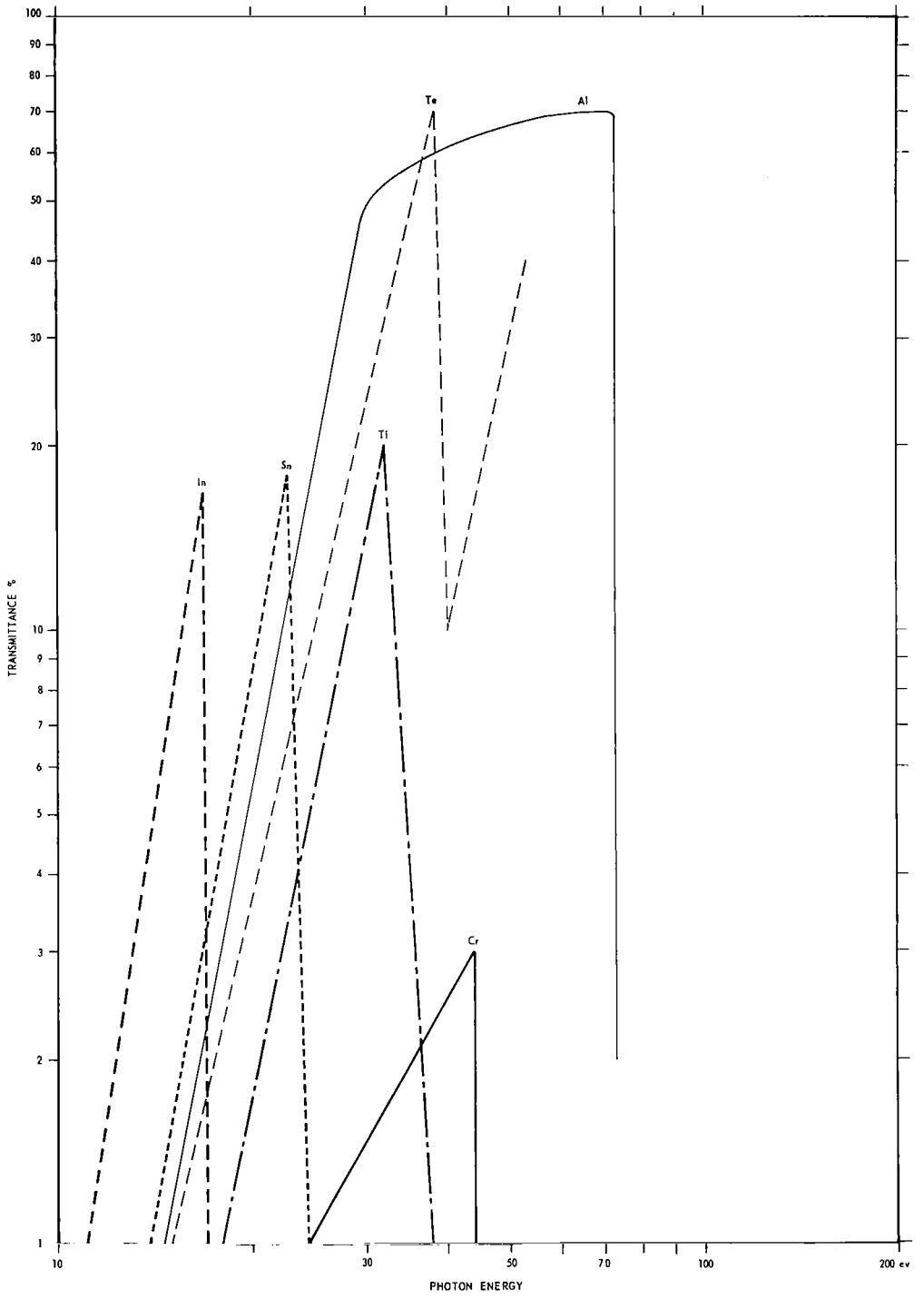

Figure 4 Transmittance Characteristics of In, Sn, Ti, Te, Cr and Al as a Function of Photon Energy

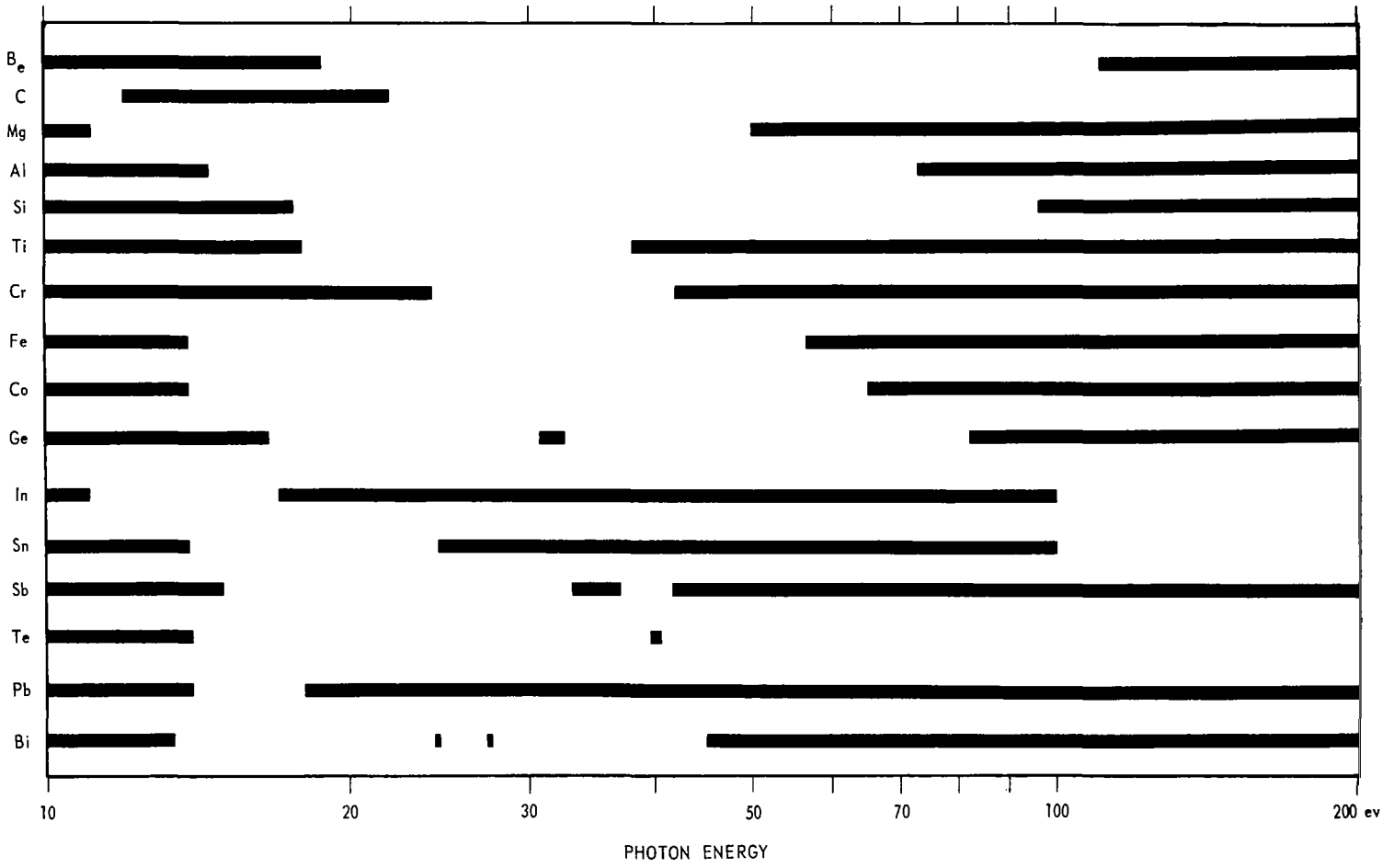

Figure 5 Summary Diagram of Transmission Limits of Various Materials. Solid Line Denotes Opacity.

TABLE 10. FILTERS FOR SOFT X-RAYS*

Transmission (%) at				Material	Thickness
5 Å	10 Å	15 Å	20 Å		
65	20			Zapon lacquer	5 μ
83	30			Cellophane	5 μ
83	30			Mylar	5 μ
90	40			Nylon	5 μ
89	40			Formvar	5 μ
92	50			Polystyrene	5 μ
92	50			Beryllium	10 μ
85	25			Polystyrene	10 μ
80	18			Formvar	10 μ
	70	30	10	Aluminum	2.5 μ
	32	5		Aluminum	7.5 μ
80	18			Beryllium	25 μ
	10			Parlodian	6 μ
	50			Parlodian	2 μ
	at 36 Å		>10%	Parlodian	1.3 μ

*U. Mayer, Space Sci Rev. 3, 781 (1964).

have reported photoelectric yields of solids and the electron energy distribution of the photo-emitted electrons using a planar analyser over the wavelength range between 1200 and 250Å . Samson[73] has extended the photoelectric emission data on aluminum and indicated its dependence on angle of incidence, polarization of the incident photon beam. Duckett and Metzger[74] and Newburgh[75] have carried out photoelectric emission studies on alkali halides over the wavelength range corresponding to the photon energies between 6 and 22 ev, the latter using retarding potential techniques. Yields as high as 70% were reported in these materials. Except for Lukirskii et al,[76] practically no data on photoelectric emission from solids exists for wavelengths less than 200Å. Cairns and Samson[77] have recently measured the photoelectric yield of Al films both in the forward direction and in the back direction and have shown that the interference effects account for the detailed shape of both the yield and transmittance curves of thin films.

Based on the above survey of various modes of interaction of vacuum ultraviolet radiation with gases and solids, it seems proper to describe the various existing detectors over the wavelength range below 1600Å and analyze the possibility of extending their use below 1000Å.

Review of Existing Vacuum UV Detection Technology

The most convenient radiation detector used in the vacuum UV region employs an ordinary enclosed photomultiplier in conjunction with a radiation converter, such as sodium salicylate ($Na\ C_7\ H_5\ O_3$).[78] In such cases, the primary radiation is causing the sodium salicylate to fluoresce, producing longer wavelength radiation centered around 4100Å which can be seen through the glass envelope of an ordinary photomultiplier tube.

Sealed photomultipliers may also be used in a way where photoelectrons originating at a vacuum UV photocathode may be accelerated to sufficiently high energies to produce a large burst of longer wavelength fluorescence photons from a suitable scintillator.[79] This scintillator can be viewed through the envelope of a sealed phototube.

At the Goddard Space Flight Center, Dunkelman[80] was successful in obtaining photomultiplier tubes with various window materials and photocathodes of higher work function. These tubes utilized the volume photoelectric effect, sensitive to radiation below 3000Å, and hence were insensitive to visible radiation. ASCOP, a subsidiary of Electro-Mechanical Research, Inc., and RCA developed these solar-blind tubes using CsTe, CsI for the photocathode material.

Hinteregger,[81] working with the volume photoelectric emission from solids, developed open structure photomultipliers sensitive to radiation below the cut-off of LiF, namely 1050Å. Most solids have a threshold of volume photoelectric emission near 1500Å, attaining a maximum value of roughly 10-20% near 800Å.

Another type of detector for use below 1000Å is the Bendix resistance strip magnetic photomultiplier which was developed by Goodrich and Wiley,[82] first suggested and used by Hinteregger. These detectors were reported to be very quiet, relatively noise-free, and readily adapted for space applications. Another design in window-less small photomultipliers developed by Goodrich and Wiley[83] is the continuous channel photomultiplier. This is in the form of a hollow glass tube with a highly resistive inner surface. It has an internal bore diameter of several tenths of a millimeter and a length to bore diameter ratio of ~ 50. A potential difference of 1000-2000 volts is maintained between the ends causing a current on the inner surface. Thus, an axial electric field is established down the length of the tube. The initial electron produced by a UV photon cascades down the length of the tube producing a gain of 10^5.

Another series of detectors, utilizing the photoionization of gases and vapors and transmission cut-off of optical filters, were developed. The first series of photon counters operative in the Geiger region utilized the photoelectric emission characteristics of the cathode material. Chubb and Friedman[84] and later Watanabe[85] used these counters for detection of UV radiation between 1050Å and 2500Å. Electro-negative

gases increase the cathode work function and greatly reduce by negative ion formation the probability that a photo-electron will initiate a count. In the Geiger mode of operation, each output pulse corresponds to an incoming photon, the amplification taking place near the anode due to electron multiplication in the high electric field. This mode of operation is very useful for weak light signals. At NRL and NASA, use of these counters were extended to include measurements of radiation below 100Å by replacing the optical window material with thin metallic foils. These metallic foils have transmittance at the atomic absorption edges.

Watanabe extended the Geiger type mode of operation to the proportional region where the output signal was directly proportional to the intensity of the radiation. The optical filters for short wavelength cut-off were chosen from LiF, CaF_2, BaF_2, sapphire, and quartz.

Another type of counter utilizing photoionization in gases and no gas multiplication was developed at the Goddard Space Flight Center.[86] Here the positive ions are collected by keeping the central wire at ground potential and the chamber body at a positive potential ranging from 20-100 volts. The total number of ion pairs formed are collected, giving a current proportional to the number of photons. These counters have since been commercially produced by Geophysics Corporation of America. The most desirable features of these counters are (i) high spectral selectivity, (ii) high quantum efficiency, (iii) compactness, and (iv) low electrical leakage. These counters were limited in their use only by the transmission limit of the filter and hence could not be used below the cut-off limit of LiF, namely 1050Å. A list of gas filled detectors with sealed optical filters is presented in Table 11.

Recently silicon p-n junction photodiodes have been exposed to radiation below 1000Å and found to have a flat response down to 584Å, when operated in the zero-bias photovoltaic mode.

TABLE 11. GAS FILLED DETECTORS USING OPTICAL FILTERS

Wave Length Range Å	Filling Gas	Press. (torr)	Window
1350-1480	$(C_2H_5)_2S$	5	BaF_2
1230-1350	NO	20	CaF_2
1100-1345	NO		LiF
1050-1350	NO	20	LiF
1230-1290	CH_3COCH_3	4.5	CaF_2
1050-1240	CS_2	15	LiF
1050-1180	$(CH_2)_2O$	4.5	LiF
44-60	N_2	400	Mylar (0.841 mg/cm^2)
44-55	N_2	400	Mylar + Al (0.00625 mm + 0.2μ)
8-20	Ne + ethylformate		Al (1.5 mg/cm^2)
8-16	N_2	760°	Al (2.8 mg/cm^2)
8-14	N_2	760	Al (4 mg/cm^2)
2-8	A	760	Be (21 mg/cm^2)
2-8	Ne + ethylformate		Be (24.4 mg/cm^2)
2-8	Xe	775	Be (0.13 mm)
2-20 kev (Proportional counter)	Ne + CO_2		Be (24.4 mg/cm^2)

SECTION III

ANALYSIS OF VARIOUS MODES OF INTERACTIONS

Having described the various modes of interaction of vacuum ultraviolet radiation with matter and the various types of detectors currently available, we must now consider the conditions under which they may be modified and used, their limitations and the relative merits of various alternatives.

The various parameters to be considered are:

(1) highest sensitivity
(2) high speed of response
(3) linearity of response over a large signal range
(4) rejection of long wavelength radiation or insensitivity to longer wavelengths

Taking each mode at a time, one notices that the use of thermocouples or thermopiles as a detector is not suitable because its response is very slow and shows no rejection for long wavelength radiation. Even though these detectors are presumed to have a flat spectral response over a wide range, their calibration in the vacuum ultraviolet is not very easy to perform. The photon flux output of various light sources in the vacuum ultraviolet region is low and hence causes a low signal output from the detector only observed by special electronic instrumentation.

The photographic emulsion techniques, although sensitive in the vacuum ultraviolet region, also suffer from the fact that the absorption coefficient of the emulsion is a function of the wavelength and hence makes it very difficult for calibration. It has also been noticed that

the choice of developer and the duration of the exposure of the film give a broad basis for selecting a combination to suit the experimentalist's needs, making it all the more difficult the process of extracting the intensity distribution. This technique has no rejection to long wavelength radiation.

In gases, one finds very sharp ionization thresholds, the cross sections rising to high values within an angstrom (as shown in Figure 1). The long wavelength rejection is very large. Since each gas has a different threshold, a detector based on the photoionization process could be very discriminative. Since the photoionization efficiency is one in most of the gases for $\lambda < 1000\text{Å}$, the minimum flux required for detection will depend upon the ability to read low currents and photoionization cross section values. Since σ_i decreases as λ decreases for all gases, except for Xe where it shows a peak near 120Å, there is a good rejection for $\lambda < 100\text{Å}$ at moderate pressures.

Photon induced fluorescence efficiency is small (of the order of a few percent), but its detection in the visible and near UV region should not be a problem. Not much experimental information is available at this time for this phenomenon. It seems worth-while to explore this phenomenon a little more.

Among the photon-solid interaction, the reflectance of most materials, being less than 5%, is not amenable for use in radiation detection. Moreover, reflectance increases at longer wavelengths and hence, can not provide any discrimination for $\lambda > 1000\text{Å}$.

The transmittance of thin films provides strong rejection for long wavelength radiation and increases as λ decreases below 1000Å. The threshold of optical transmission ($T > 0.1\%$) is very sharp in most cases followed by sharp cut-off limits at much shorter wavelengths. High transmittance films can be prepared and used as filters rather than windows as part of a detection system. Because of the inherent presence of pin holes in these films, strong rejection of the long

wavelength radiation is not possible especially when one is looking in the solar direction using sensitized photomultiplier tubes. However, a combination of thin film and Bendix photomultiplier should prove quite useful.

Volume photoelectric emission from solids has thresholds in the vacuum ultraviolet region near 1500Å. Since these surfaces can be used as photocathodes in a photomultiplier tube where a gain of 10^6 is easily obtainable, very low light level signals can be measured.

Currents of the order of 10^{-13} - 10^{-14} amps are easily measurable. Hence, the minimum photon flux required for detection lies in the neighborhood of 100 - 1000 photons/sec per sensitive area. The threshold of a thin film as filter and metallic photocathode in a photomultiplier could be set at about 10^3 - 10^4 photons/sec.

Because of the nature of interaction at this short wavelength radiation with gases and solids, the response of the detectors, described in the following section, would be faster than 1 m-second. Real time measurements of photons between 1000Å and 100Å would be possible.

SECTION IV

SELECTION OF THE MOST PROMISING INTERACTIONS

From the analysis presented in the previous section, it is clear that in order to select the most promising interactions for measuring photon fluxes in the 100 - 1000Å region amenable to wavelength resolution via a selective band detection technique, one must choose a combination of a thin film filter and rare gas ion chamber. In addition, the use of a thin film as a filter be explored in conjunction with open photomultiplier tubes using metallic photocathodes. Finally, examination of fluorescent radiation as a function of incident photon flux of various spectral distributions should be made as a possible means for selective detection.

In order to describe the proposed detector based on the above mentioned most promising interactions, we shall start with the following example. An argon filled continuous flow chamber will be capable of converting each photon between 787Å and 200Å into an ion-electron pair and acting in this fashion as a broadband detector. A thin film of indium has a transmittance which begins at 1120Å (0.1% transmission for a 1000Å thick film) and cuts off rather sharply at the $N_{4,5}$ - edge near 740Å and no transmittance below 740Å down to 100Å. If these rare gas continuous flow ion chambers were to be combined with thin film filters, the detector's wavelength range can be compressed into a very narrow region.

In general, the long wavelength limit of the detector will be determined either by the photoionization threshold of the filling gas or by the onset of transmittance of the filter material, while its short wavelength limit will depend again on either the photoionization cross-section of the filling gas or the filter transmission cut-off. In

the example mentioned above, the effective band-pass reduces to a bandwidth of 47Å between 740Å and 787Å. Table 12 lists a set of combinations of thin films and gases to be used in constructing such detectors resulting in well defined wavelength ranges over which measurement of photon fluxes are possible.

A knowledge of the transmittance of the filter is essential in determining the photon flux impinging from outside. The photon flux entering the ion chamber is calculated from the ion current measured in the ion chamber under conditions of saturation where it is assumed that all photons are completely absorbed and converted into ion electron pairs. This is only possible if the gas pressure in the chamber is high enough to absorb all photons in a small path length.

It is also possible to use two ion chamber-filter combinations in a bridge circuit in order to obtain narrower bandpass detectors. Specifically, a (neon-aluminum) and a (helium-aluminum) chamber have both the same short wavelength cut-off at 170Å, determined by the Al film. However, their long wavelength limit is, in the case of neon-filling, 578Å, and in the case of helium, 504Å. By careful adjustment of all parameters, a detector between 578Å and 504Å should be possible.

A further refinement of such a detector can be achieved by making use of the fluorescence caused by vacuum ultraviolet light impinging on gases. If an ion chamber, filled with O_2, is combined with a thin film aluminum filter, transmitting between 840Å and 170Å, then a "broad" band detector active over this entire wavelength region has been achieved. In order to narrow this region, one can make use of the known fluorescence properties of O_2, as reported by Judge et al.[87] Even though O_2 photoionizes over the entire region, its fluorescence occurs at sharply defined thresholds of the incident vacuum ultraviolet radiation, with a first maximum at 700Å and a second one at 650Å. In addition, the wavelength analysis of this fluorescence[87] has revealed that the fluorescence is essentially in the region between 4000Å and 3000Å due to transitions $O_2^+ \; a \longrightarrow O_2^+ \; X$, when the primary, exciting

TABLE 12. SOME THIN FILMS - GAS COMBINATIONS AS VACUUM ULTRAVIOLET DETECTORS

	Combination	Bandwith	Range
xenon	(1022 Å) + In (1120 Å-740 Å)	280 Å	1020 Å-740 Å
CO_2	(900 Å) + In (1120 Å-740 Å)	160 Å	900 Å-740 Å
Kr	(887 Å) + In (1120 Å-740 Å)	147 Å	887 Å-740 Å
CO	(885 Å) + In (1120 Å-740 Å)	145 Å	885 Å-740 Å
A	(787 Å) + In (1120 Å-740 Å)	47 Å	787 Å-740 Å
A	(787 Å) + Sn (911 Å-510 Å)	277 Å	787 Å-510 Å
A	(787 Å) + Bi (855 Å-510 Å)	277 Å	787 Å-510 Å
A	(787 Å) + Al (840 Å-170 Å) + In (1120 Å-740 Å)	100 Å	840 Å-740 Å
A	(787 Å) + Ge (747 Å-520 Å) + Sn (911 Å-510 Å)	237 Å	747 Å-510 Å
A	(787 Å) + Ge (747 Å-420 Å) + Bi (855 Å-510 Å)		
A	(787 Å) + Ti (690 Å-325 Å) + Sn (911 Å-510 Å)	180 Å	690 Å-510 Å
A	(787 Å) + Ti (690 Å-325 Å) + Bi (855 Å-510 Å)		
Ne	(578 Å) + Sn (911 Å-510 Å)	68 Å	578 Å-510 Å
Ne	(578 Å) + Bi (855 Å-510 Å)		
He	(504 Å) + Al (840 Å-170 Å)	337 Å	507 Å-170 Å

radiation is 703Å. In contrast, when the primary radiation is 630Å, the fluorescence occurs in two distinct and separate wavelength regions, between 4000Å and 3000Å, as before, and between 5000Å and 5800Å. These two fluorescence regions can be easily separated by filters and observed by a photomultiplier. Since the fluorescence efficiency is of the order of several percent, its detection with a photomultiplier, plus filter combinations, presents no serious instrumentation problem. Thus, the observation of fluorescence signals in conjunction with gas-filled ion chambers represents another alternative in the development of rugged, and reliable narrow-band far-ultraviolet detectors.

SECTION V

APPARATUS AND EXPERIMENTAL PROCEDURE

The experimental arrangement, as shown in Figure 6, consisted of a Seya-Namioka type vacuum monochromator, employing a 1-meter radius of curvature concave grating with 30,000 lines per inch. A pulse of light from an electric spark in the light source passed through the primary slit, S_1, 0.1 mm wide, and traveled through the arm of the monochromator to the grating G. There the beam was dispersed and consecutive component wavelength, $h\upsilon$, passed through the exit slit, S_2, also 0.1 mm wide, by rotating with an external motor, M, the grating about a vertical axis passing through the surface of the grating. The vacuum ultraviolet radiation with a bandwidth of about 1Å was then available for use in transmittance measurements of thin films and spectral response characteristics of selective detectors. In order to monitor the intensity, a sodium salicylate coated glass window was placed at the other end of the ionization chamber. The fluorescence radiation produced at this window was then measured by means of an EMI 9514-S photomultiplier tube.

The thermocouple radiation detector, Reeder (RUV-5VC) was housed in the exit slit assembly of the monochromator where it could be pulled into and out of the radiation by adjustable X-Y micrometer screws and provide photon fluxes at the exit slit of the monochromator.

The light source, shown in Figure 7, consisted of a capillary tube 55 mm long and 4 mm in diameter drilled into one end of a boron nitride rod. The other end of this rod was drilled to hold the high voltage electrode. The over-all dimensions of the rod were 9" long and 1.5" in diameter. The anode was made out of a copper-tungsten alloy, Elkonite 10W3, and was 12 mm in diameter while the cathode, made out of the

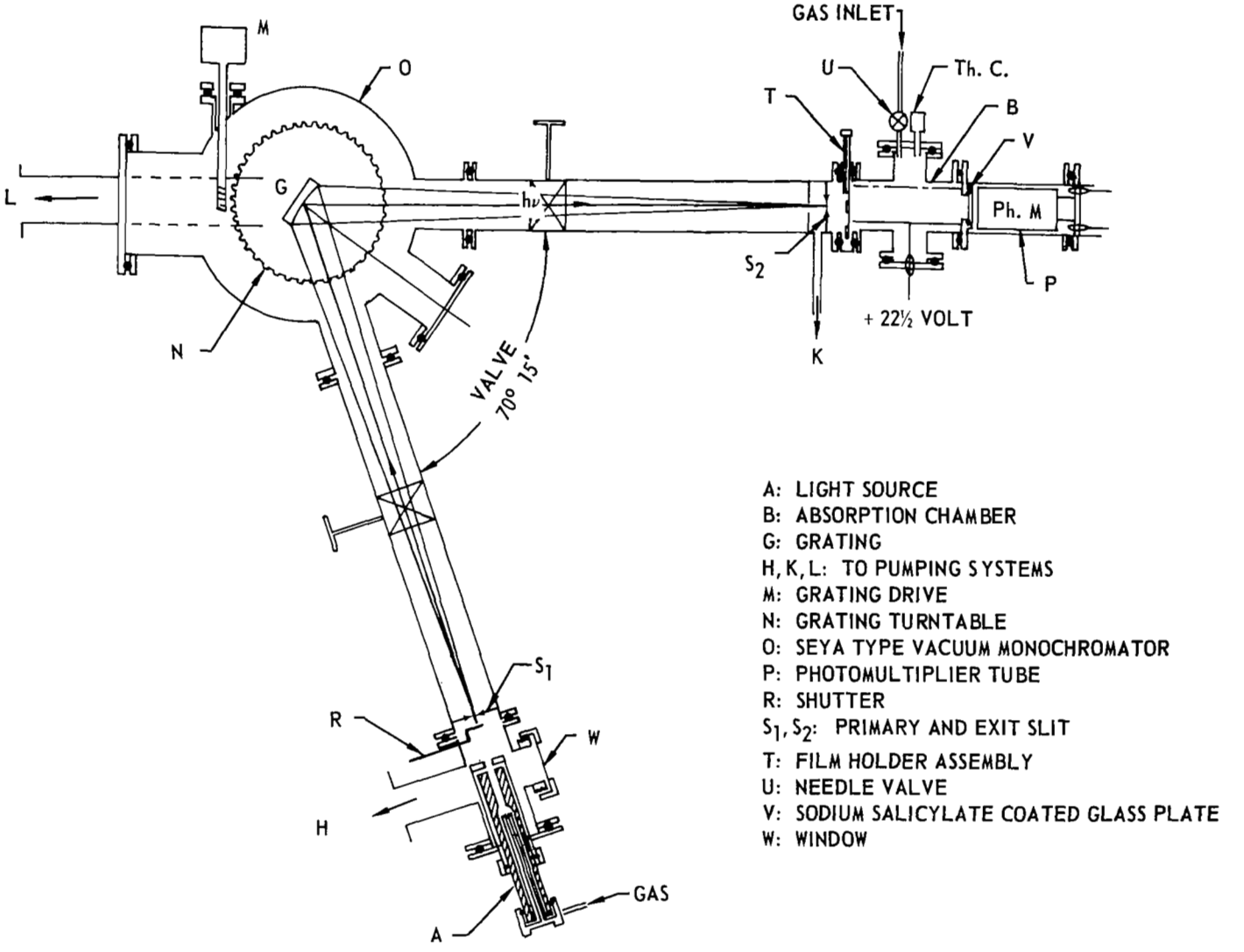

Figure 6. Schematic Diagram of a One-Meter Seya-Type Vacuum Monochromator.

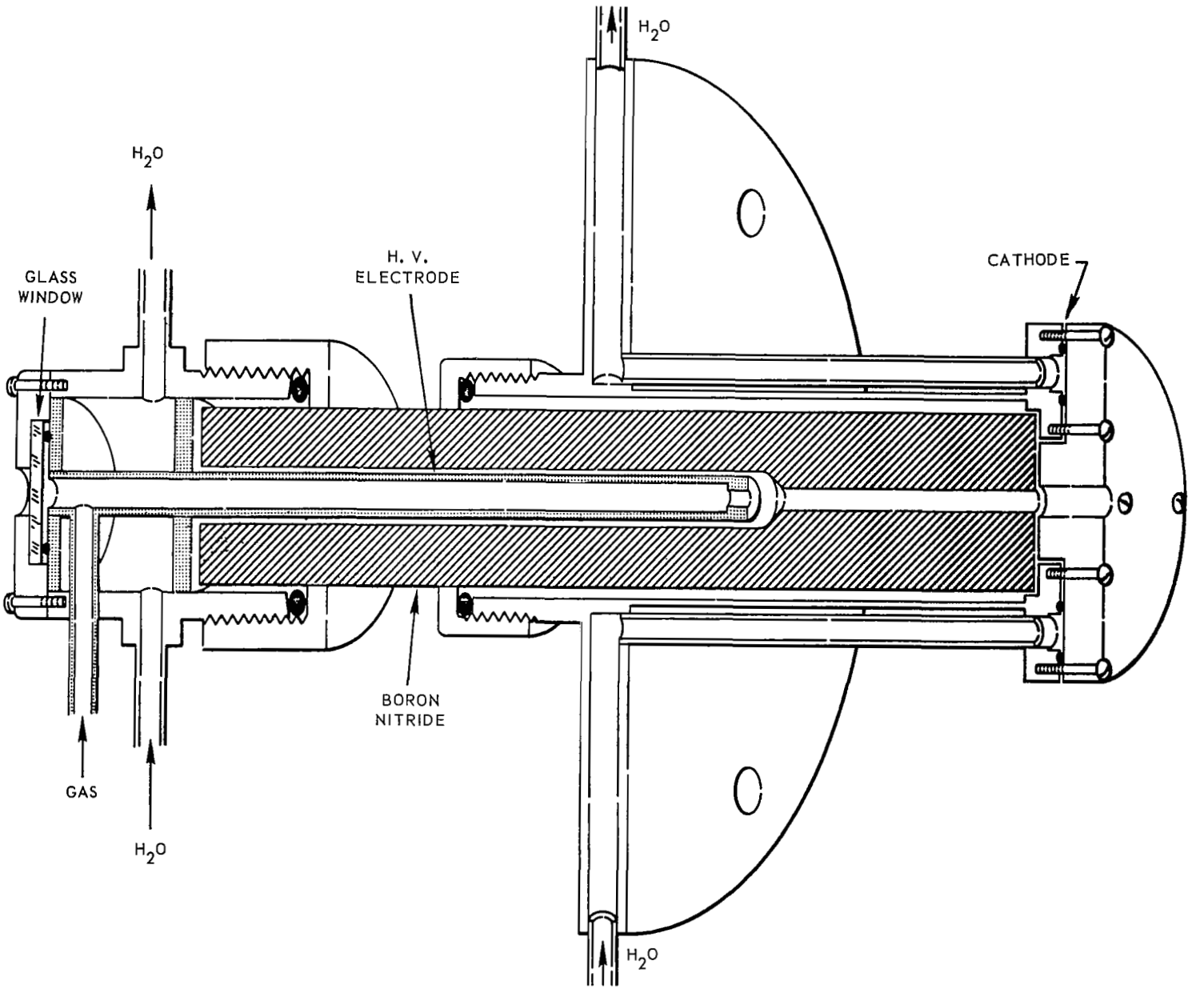

Figure 7. Capillary Spark Discharge Light Source in Cross Section.

same alloy, and placed close to the primary slit was made in the form of a circular disc having a hole in the center. Both the anode and cathode were water cooled and oriented along the optic axis. To prevent gases from the light source from entering the main grating chamber, a differential pumping system was used between the source and the primary slit.

To produce radiation shorter than 1000Å, the capillary tube was filled with either nitrogen or argon at a low pressure of approximately 75 micron. A low inductance capacitor of about 0.1μ F capacity was charged to a potential of 17,000 volts from a high voltage D.C. power supply and discharged 44 times per second by means of a WL 7703 ignitron switch. The value of 44 cylces per second was chosen so as not to interfere with the 60 cycle line frequency or any of its multiple. Each spark produced in the capillary tube resulted in a line spectrum of considerable intensity. One such spectrum using nitrogen gas is reproduced in Figure 8.

Preparation of Thin Films

Thin films of various materials were prepared by making use of the Speedivac Coating Unit Model 19E6/181 manufactured by Edwards High Vacuum Ltd. The 2" x 2" glass slides, used as substrate, were cleaned and coated with a thin layer of water-soluble sugar-aerosol solution.[88] After the solution was dried, the slide was supported in a rotating work-holder ring which in turn is supported by three equispaced ball races and is prevented from having side play by three more equispaced ball spaces. This workholder ring had a height adjustment and was placed 16" above the base plate. The thermal evaporation system consisted of a six-position vapor source turret constructed in copper permitting current loadings up to 400 amps. Heavy low voltage and grounding brushes were in permanent contact with the rims of the turret L.T. and ground plate to promote smooth operation, free from arcing. The turret, which was supported on a sturdy plate and positioned 4" above the base plate, was rotated by an external handwheel. Evaporation was carried out from a vapor source positioned vertically below the periphery of the workholder ring. Each

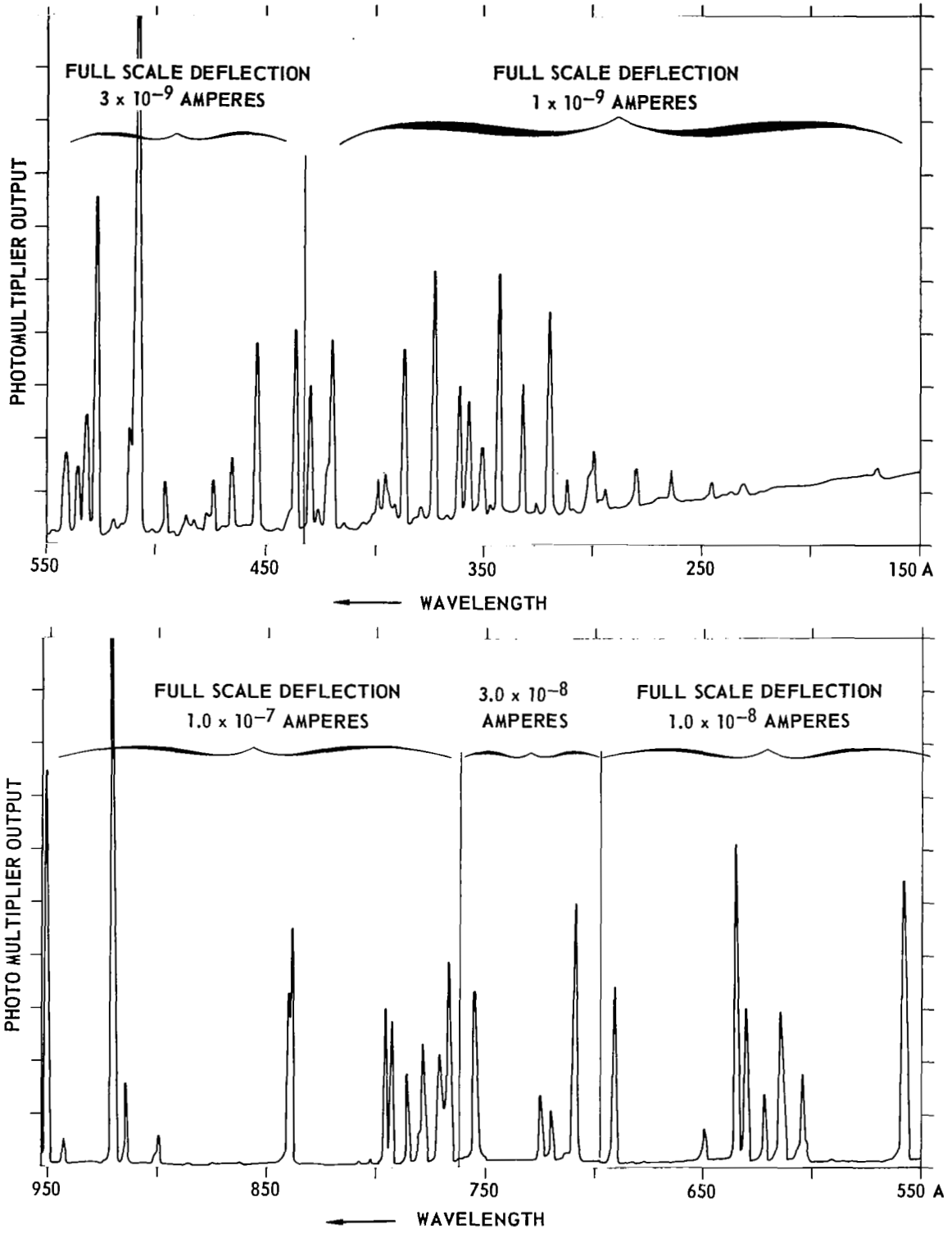

Figure 8. Line Spectrum From a Spark Discharge in Nitrogen.

source was positively registered into the firing position by a level mechanism and numbered lights indicated which source was in position. A vapor source shutter, operated externally, was provided to shield the aerosol coating from the heat of the evaporation filament during the initial melting period in order to prevent it from cracking and contamination. All evaporations were made at a pressure of approximately 5×10^{-6} mm Hg and completed within 10-15 seconds. The substrate was maintained at room temperature.

Other techniques of preparing thin unbacked films were tried which would have produced relatively less contaminated films. The glass slides were coated with a fresh film of Victa Wet-35B, obtained from Victor Chemical works, to provide a smoother surface for the metal film as compared to the surface provided by an aerosol solution. No appreciable success was achieved in floating the metal films from Victa Wet coated glass. Next pressed discs of ammonium chloride were used as a substrate for the metallic film. These discs were prepared by pressing the powdered ammonium chloride at about 80,000 pounds per square inch between die faces which were optically flat and mirror polished. It had been observed that ammonium chloride can be removed by sublimation in a vacuum when heated to $160^{\circ}C$ because of its high vapor pressure. In our experience, the ammonium chloride did not disappear completely and left a brownish color at the film surface. This technique was eventually abandoned. Attempts were made to use sodium chloride as a substrate. During floating-off of the film, only very small pieces were recovered which could not be used.

For transmittance measurements, the thin films were picked up on holders having a $\frac{5}{16}$" diameter hole. The same film holder was also used when the film acted as a filter for the preliminary selective detector using small glass capillary tubes. In order to use these thin films as filters as well as windows in the selective detector, thin mosaic borosilicate glasses, obtained from Mosaic Fabrication Inc., were used as supports for the films.

Thin aluminum films were prepared by evaporating Al of 99.999% purity from a three-strand tungsten helical coil. Small pieces of aluminum wire were hung from the W coil. Bismuth (obtained from J. T. Baker Chemical Company, and of 99.95% purity) was evaporated from a tungsten boat as well as a molybdenum boat while indium (obtained from Kern Chemical Company, and of 99.9999% purity) was evaporated successfully from a molybdenum boat. Films of antimony (obtained from A. D. Mackay Incorporated, and of 99.999% purity) could not be floated off successfully in one large piece, when evaporated from a molybdenum boat. It was observed that these films did not show electrical continuity when the film thickness was less than 500Å. The surface appearance of the film was also milky in nature compared to a silvery appearance obtained in other evaporation chambers. It was suspected that the solid base plate did not provide sufficient pumping speed during melting and evaporation. This deficiency in pumping speed was overcome by cutting two 3" diameter holes in the base plate beneath the evaporator coil. It was also felt that the antimony atoms had large mobility and a tendency to cluster around small regions.

Titanium and chromium both were successfully evaporated from a tungsten boat. Only titanium (obtained from A. D. Mackay Incorporated, and having 99.99% purity) films were successfully floated off in water and picked up on mosaic glass for use in selective detectors. On the other hand, chromium films could not be floated off in one large piece. Effort was then made to use aluminum and titanium films as a substrate for the chromium film. In each case either chromium acted as a reducing agent causing patchiness in the composite film or made the composite film curl up on itself. Using optically polished quartz as a substrate for titanium plus chromium film did not improve the film quality. The thickness of most of the films used was measured by means of a Tolansky interferometer.

Radiation Thermocouple Measurements

The Reeder (RUV-5VC) thermocouple consisted of two active junctions in series with opposing polarity. Each junction, when individually exposed to visible light, gave an electrical output signal which was of opposite sign. However, when both junctions were exposed to the same

light beam simultaneously, the output signal indicated the algebraic sum of the two. The resistances of the two junctions were measured to be 9 Ω and 20 Ω. By exposing the two junctions to a 5 microsecond white light pulse from a Strobotac type GR 1531-A light source, operating at 10 pulses per second, a peak output signal of 50 microvolts was observed on an oscilloscope. A rise time of 1 millisecond and a half voltage decay time of 5 milliseconds (in air) was also observed on the oscilloscope and is shown in Figure 9.

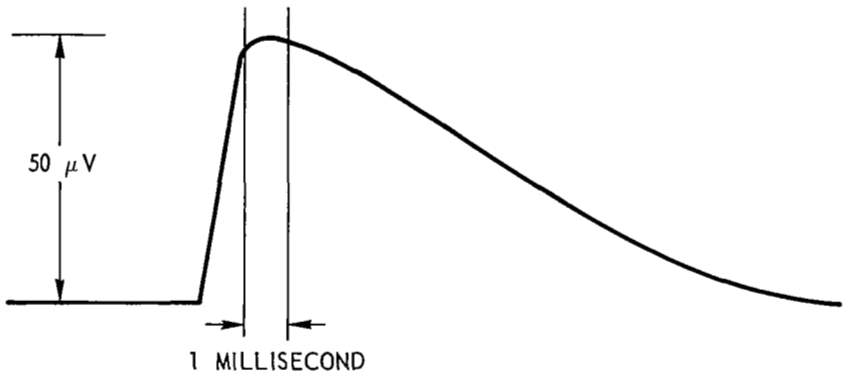

Figure 9. Thermocouple Output for a 5 Microsecond White Light Pulse.

In order to monitor the low level signal output of the thermocouple by means of the synchronous amplifier Model 103M built by Brower Laboratories which amplified signals only at 11 cps, some modifications were required in the operation of the light source. The pulse control unit was modified so that the light source could be operated at 11 cps and capable of being triggered from an external source. Operating the light source at this frequency resulted in an output signal of 0.6 microvolts from the thermocouple for the zero order spectrum at a S/N ratio of 3. Since the intensity in the first order spectrum is roughly 100 to 1000 times less than the intensity in the zero order, a major improvement was needed in signal to noise ratio. Using a break before the make-type electrical chopper to reverse the thermocouple output at 11 cps

while the light source was pulsed at 44 cps, we were able to increase the signal to noise ratio to 20, which was also not sufficient to register the first order spectrum.

Another approach to monitor the output of the thermocouple resulting from the scanned spectrum was made by operating the vacuum ultraviolet light source in the pulse burst mode at a 11 cps burst rate. The number of pulses per burst varied from 1 to 5. The objective was to successively add (integrate) a large amount of light radiation by the thermocouple in a rapid series of pulses and then let the source and the thermocouple cool down before starting another series of light pulses, as shown in Figure 10. This should result in a large 11 cps fundamental output from the thermocouple which could then be amplified.

To accomplish this mode of operation, the pulse generator in the light source system was modified to operate in two modes: (a) fixed rate 44 pps; (b) pulse burst with variable number of pulses per burst and burst rate synchronized with the synchronous amplifier. In the latter mode, the burst rate was controlled by a 0 - 20 volt negative waveform. This waveform was in turn synchronized with the synchronous amplifier reference signal. The number of pulses could be controlled from 1 to 5 per square wave input. The first pulse of the burst occurred at a higher voltage than subsequent pulses because of time constant limitations (Figure 10). Replacing Model 103M with an improved version of the synchronous amplifier Model 129 helped eliminate considerably the noise pick up. The pre-amplifier components were all RF shielded. All the inputs to the preamplifier and the outputs of the amplifier to the oscilloscope were provided with LC filters to keep the RF pick up from entering the preamplifier. Values of L and C used in the filter design are shown below.

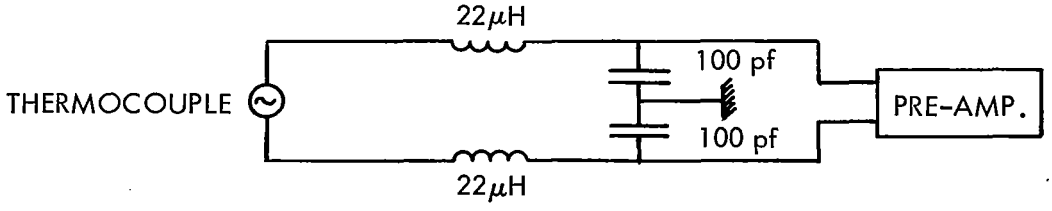

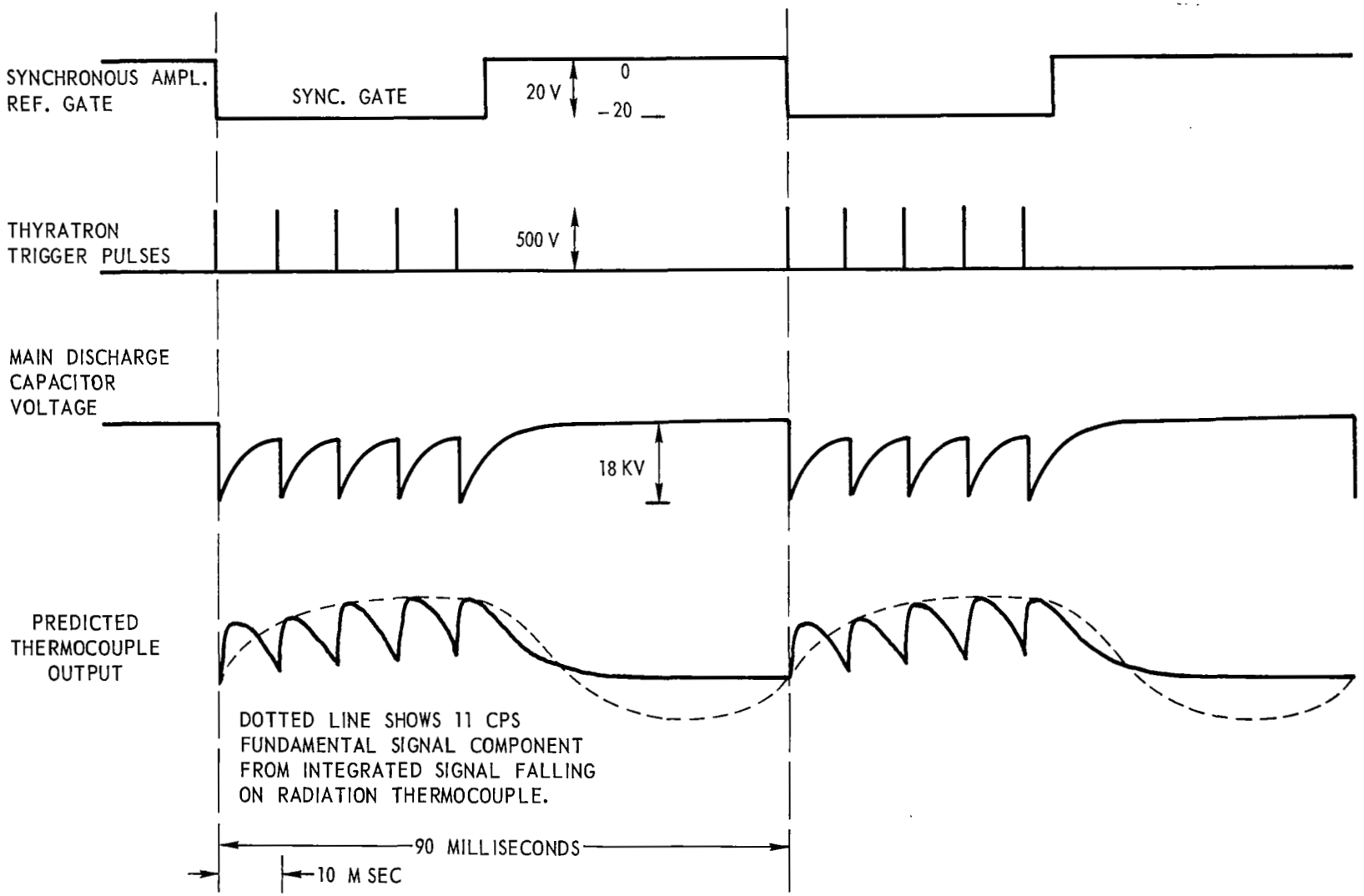

Figure 10. Light Source Input and Predicted Thermocouple Output.

Both the preamplifier and the amplifier were placed inside a doubly shielded cage and thus the noise level was reduced to 4 nv while the light source was operating and the shutter between the light source and the thermocouple was closed. The best integration time used in the measurements was 3 seconds. The response was noisy with 1 second integration time and too sluggish with 10 seconds. The synchronization did not change while the more sensitive scales were used for low light level signal measurements. By operating the source at an 11 cps burst rate with 4 pulses per burst, a trace of the spectrum was obtained which is reproduced in Figure 11. The lowest light level signal recorded by this system appears to be 10 nv and corresponds to radiation of 555 Å. Other more intense lines of higher wavelengths are recorded at less sensitive scales. At least it was shown that the electronic system of operating the light source in the pulse burst mode and the thermocouple amplifier system, when properly shielded, gave rise to signals which are readable.

After the radiation thermocouple output had been recorded, it was considered desirable to monitor the light intensity by the photomultiplier as well as the ion chamber. Figure 12 shows the photomultiplier output (in arbitrary units) as a function of pulses per burst. Also shown is the time averaged current at the power supply in milliamperes. Figure 13 shows an interesting property of the pulse burst mode of operation of the light source: the maximum output at a given number of pulses per burst is obtained at the minimum possible temporal spacing between pulses.

Construction of the Selective Detector

The design of the selective detector was conceived after preliminary results were obtained from the laboratory model, shown in Figure 14. Thin films mounted in the rod, T, which was attached to the exit-slit assembly of the monochromator, were brought into or out of the light beam. The ion chamber assembly was provided with a separate pumping system to evacuate it and a leak valve to control the flow of various gases. In order to limit the flow of gases from the ion chamber, a

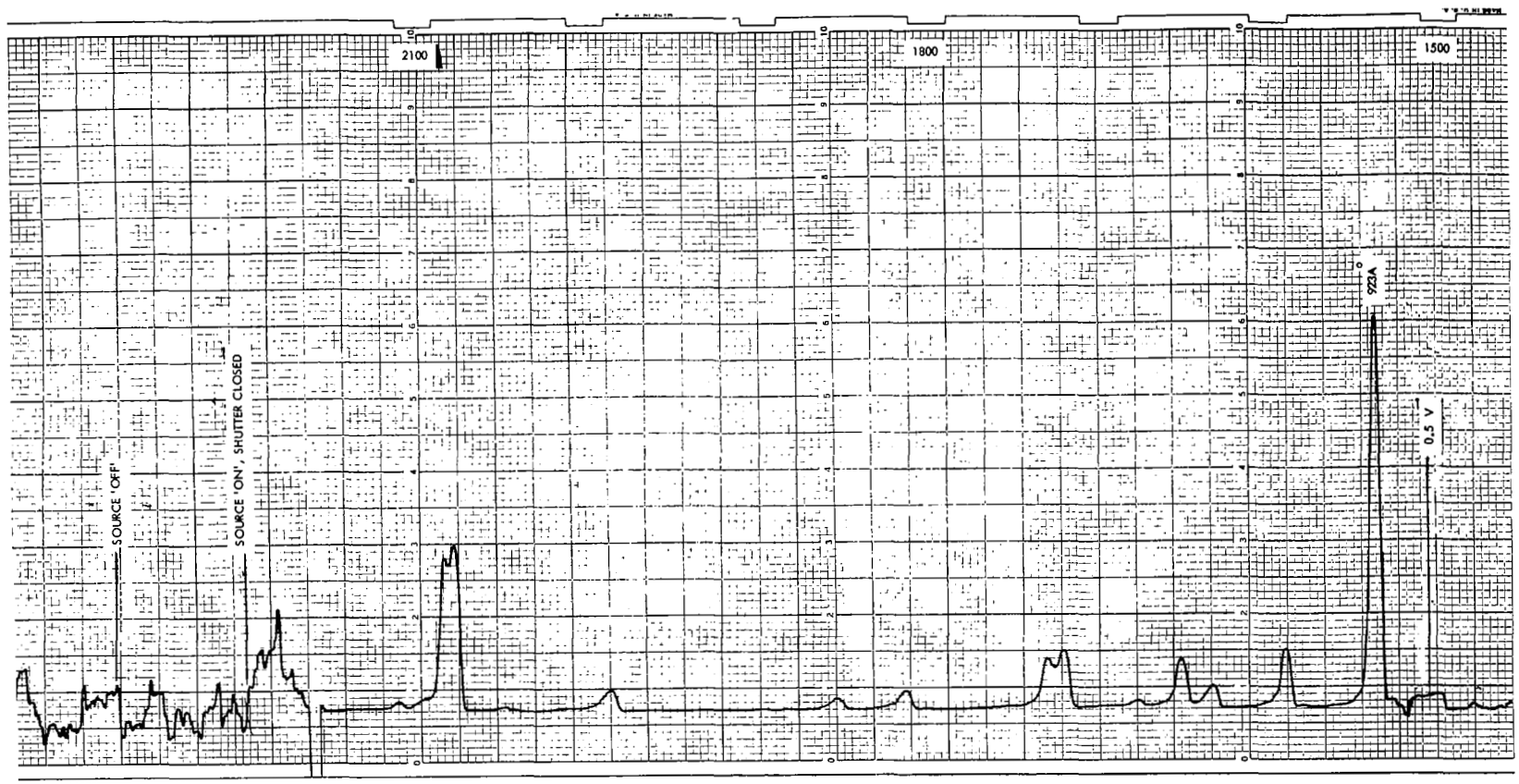

Figure 11 Trace Showing the Output of Reeder Thermocouple as a Function of Wavelength (Cont'd)

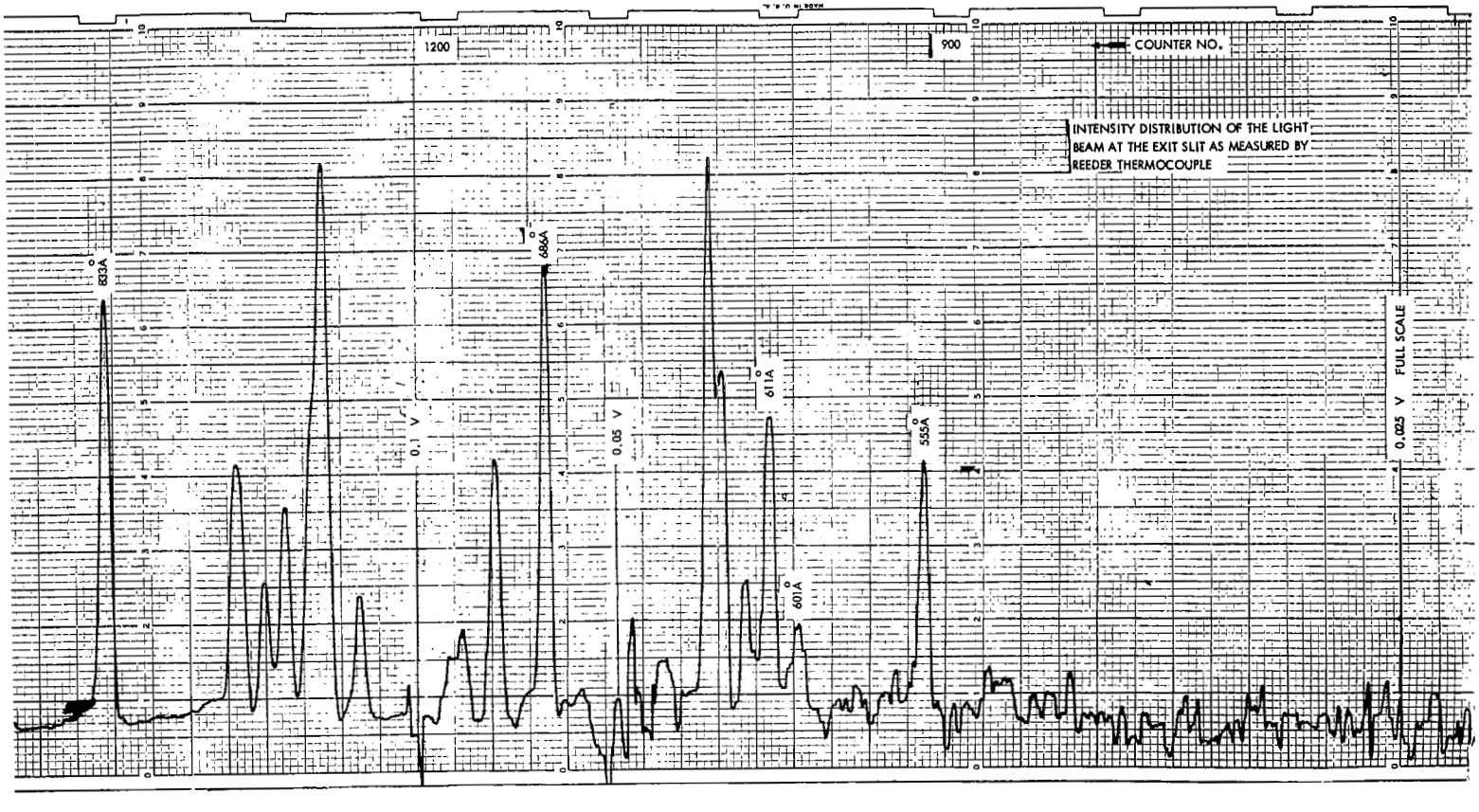

Figure 11 Trace Showing the Output of Reeder Thermocouple as a Function of Wavelength

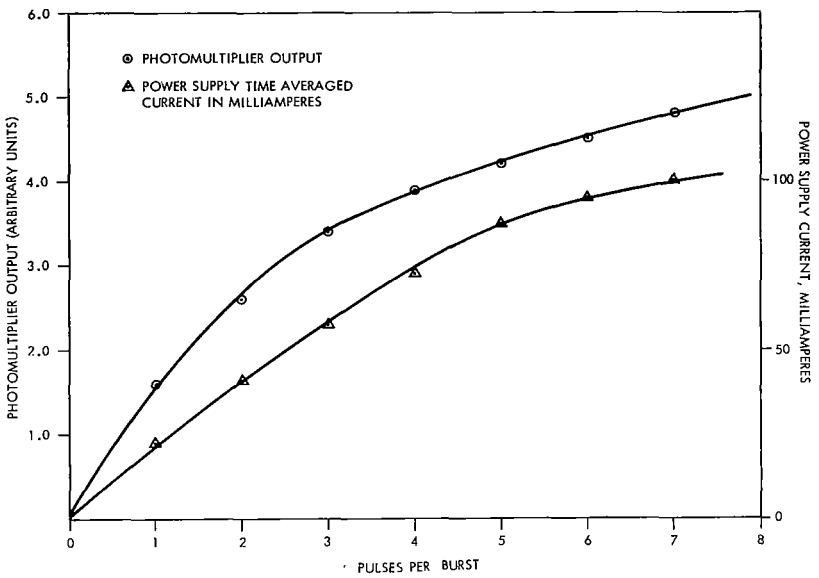

Figure 12. NSL R-1 Source Light Output as a Function of Pulses Per Burst.

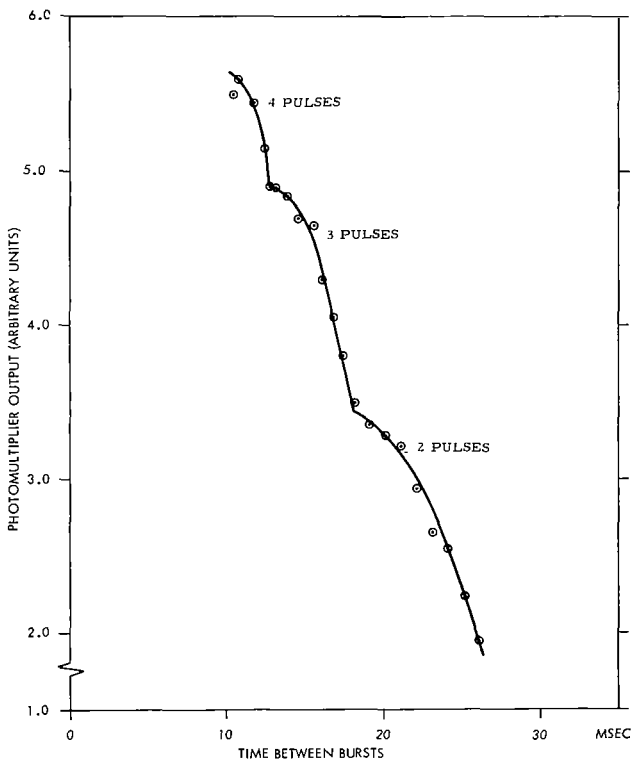

Figure 13. NSL R-1 Source Light Output as a Function of Temporal Spacing of Pulses.

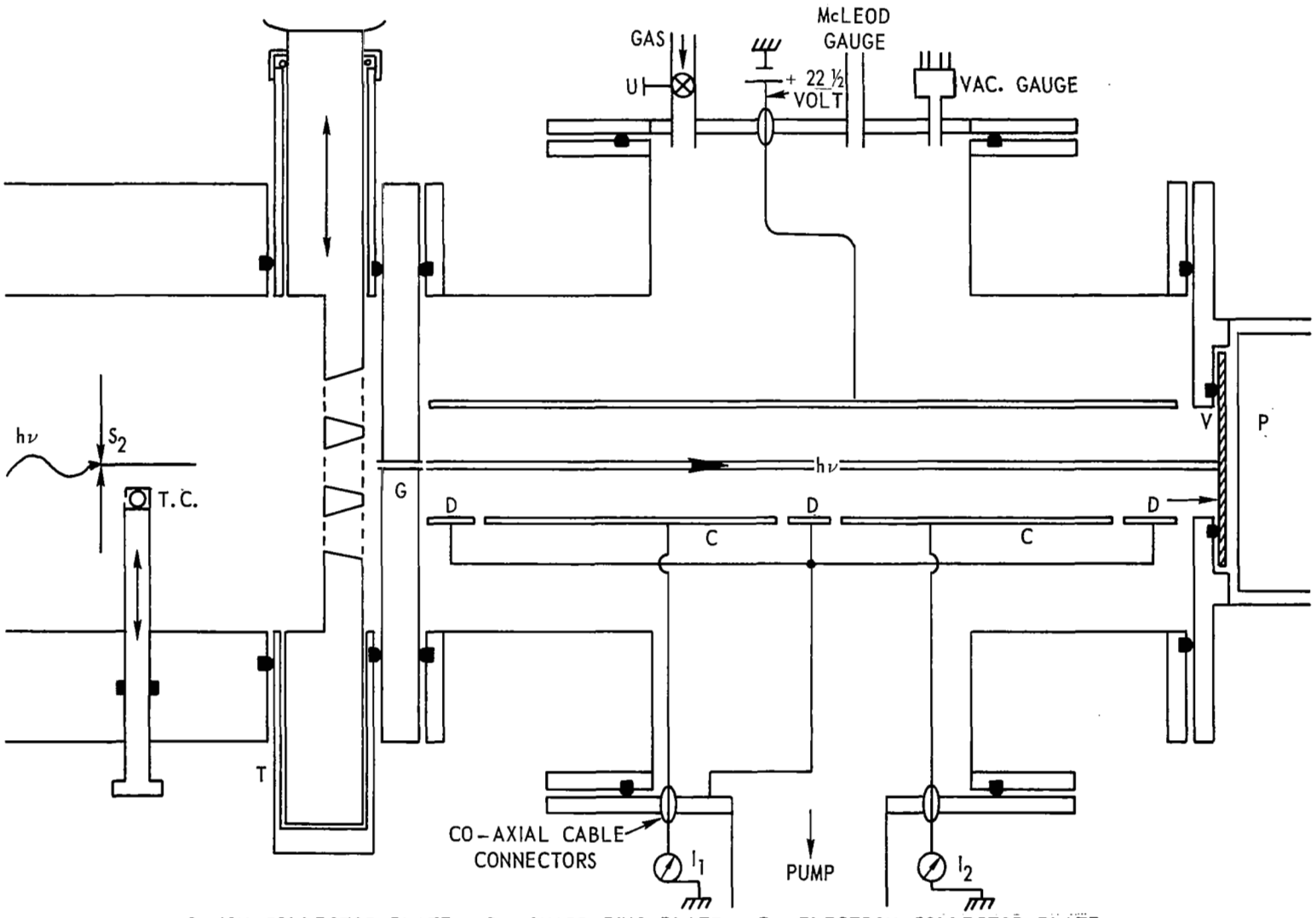

C: ION COLLECTOR PLATE; D: GUARD RING PLATE; E: ELECTRON COLLECTOR PLATE; P: PHOTOMULTIPLIER TUBE; S_2: EXIT SLIT; T: THIN FILM HOLDER; U: NEEDLE VALVE; V: SODIUM SALICYLATE COATED GLASS PLATE; G: GLASS CAPILLARY TUBES; T.C.: REEDER THERMOCOUPLE.

Figure 14. Laboratory Model of the Selective Detector.

brass plate fitted with fine glass capillary tubes, shown in Figure 15a, was intalled between the ion chamber and the thin film holder. The capillary tubes, 12.5 mm long and having an external square cross section, 400 microns on a side, were placed side by side in a rectangular slot 5 mm by 0.5 mm in dimension. The inside of these tubes presented a circular cross section with a diameter of 250 microns. The allignment of these tubes was accomplished by monitoring the vacuum ultraviolet radiation from the exit slit as it passed through them so that the signal was amaximum. Kasil (Potassium silicate base cement) was used in bonding these tubes which was later on heat treated to eliminate any residual moisture.

The ion chamber with a pressure of 2×10^{-6} mm Hg did not register any signal while the grating was set for the zero order spectrum. With the ion chamber cut-off from pumping and maintaining vacuum by pumping through the glass capillary tubes, it was possible to maintain air in the ion chamber at a pressure of 500 microns. This gave rise to a measurable signal even when the first order spectrum was scanned. The signal, due to 923 Å radiation, completely vanished when an aluminum film was inserted in the light beam, indicating strong rejection for long wavelength radiation.

Using an In film and krypton gas combination it was shown in quarterly report NSL 65-134-3 that the ion chamber signal was strongly dependent on the pressure of the gas. It was also encouraging to note that the combination of In film and krypton gas was responsive only to radiation between 887 Å (threshold of photoionization in krypton) and 740 Å, the absorption edge in indium. The photon flux entering the experimental chamber was increased by using a bundle of 25 capillary tubes each 8 mm long having 0.8 mm and 0.6 mm as its external and internal diameter respectively. Since the laboratory set up had two ion chambers each roughly two inches long, ion currents produced in each chamber were monitored simultaneously. It was found that most of the ionization took place in the first chamber indicating that the length of the selective detector need not be more than two inches.

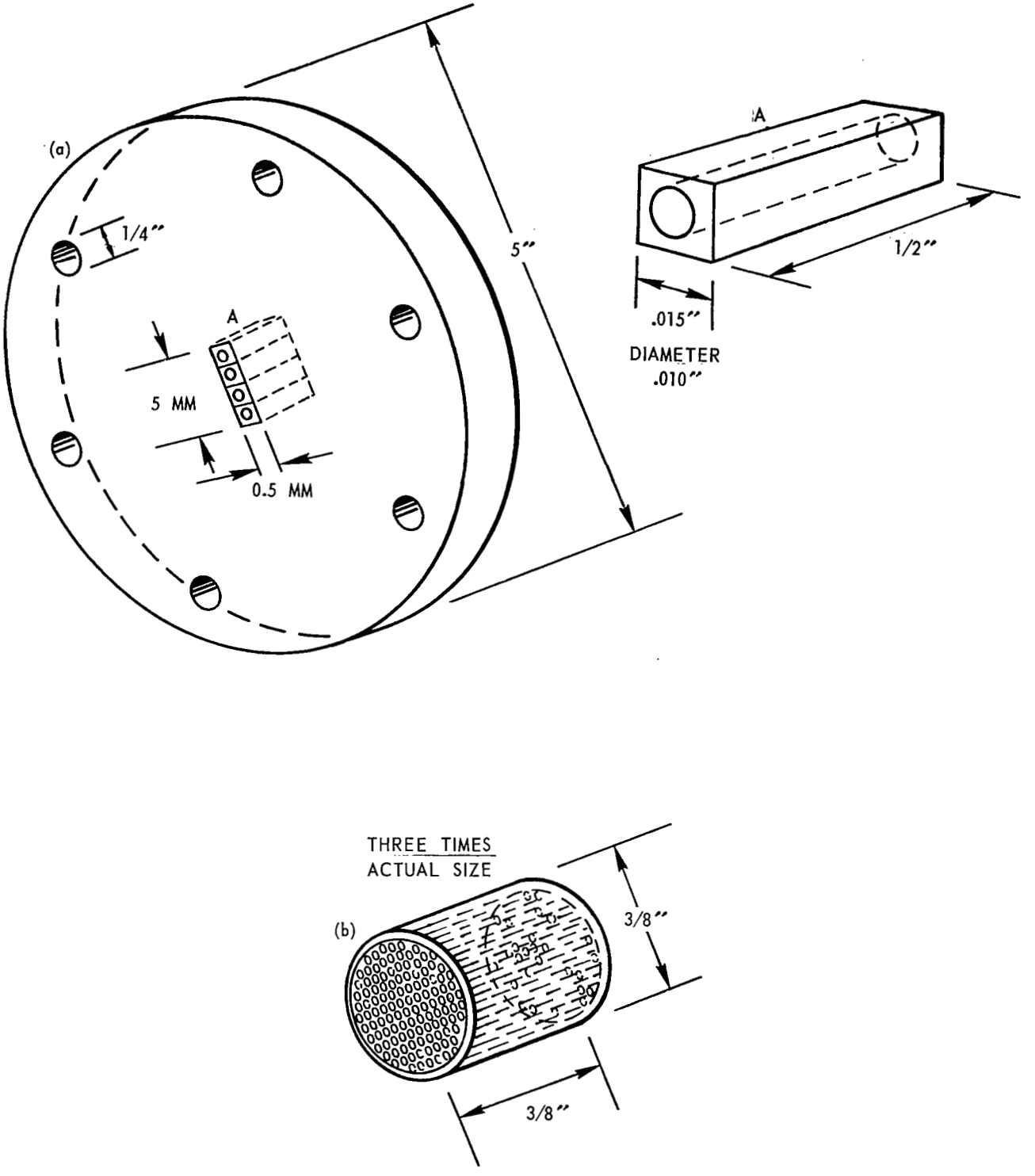

Figure 15. Bonded Glass Capillary Tubes.

Figure 16 shows the cut-away drawing of the first selective detector which was two inches long and 1.8 inches in diameter and made out of a copper tubing, the inside being coated with gold. The stainless steel collector wire, 1.1 mm in diameter, was not located in the path of the light beam and was kept at a positive potential with respect to the body. A $\frac{1}{4}$" opening provided an inlet for gases and evacuation of the detector. The $\frac{3}{8}$" opening in the face plate behind the film holder was filled with glass capillary tubes, 0.5 inches long and having a circular cross section with 0.015 inch and 0.010 inch OD and ID respectively, shown in Figure 15b.

Figures 17 to 20 show the various components of the portable selective detector as installed at the exit slit of the monochromator. The position of the capillary tubes behind the thin film is shown in Figure 17 with Figure 18 showing the thin film itself. The position of various pressure gauges and the leak valve is seen in Figure 19 along with the various isolating valves. Figure 20 shows the portable selective detector attached to the exit slit assembly but electrically insulated from the monochromator. The detector is kept at - 90 volts with respect to the monochromator so that the photoelectrons generated inside the detector are collected at the wire and recorded by the chart recorder with the help of a DC micro-microammeter

A response in the portable detector, when exposed to EUV radiation, without the filling gas, was observed. The current recorded was primarily due to photo-electrons released from the walls of the chamber when the filtered EUV radiation impinged on the wall opposite the capillary tube. The response due to photo-electrons from the ion chamber walls was not seen when the ion chamber was filled with gas having a lower ionization potential than the transmission cutoff limit of the film on the long wavelength side as is evident from Figure 21. Curves a and b are due to combinations of an Al film with Xe and Kr gas, respectively. Curve c of Figure 21 results from the combination of an Al film and Ne gas. The pressures of all gases were adjusted so as to get maximum response at one wavelength. Uncalibrated thermocouple gauges read

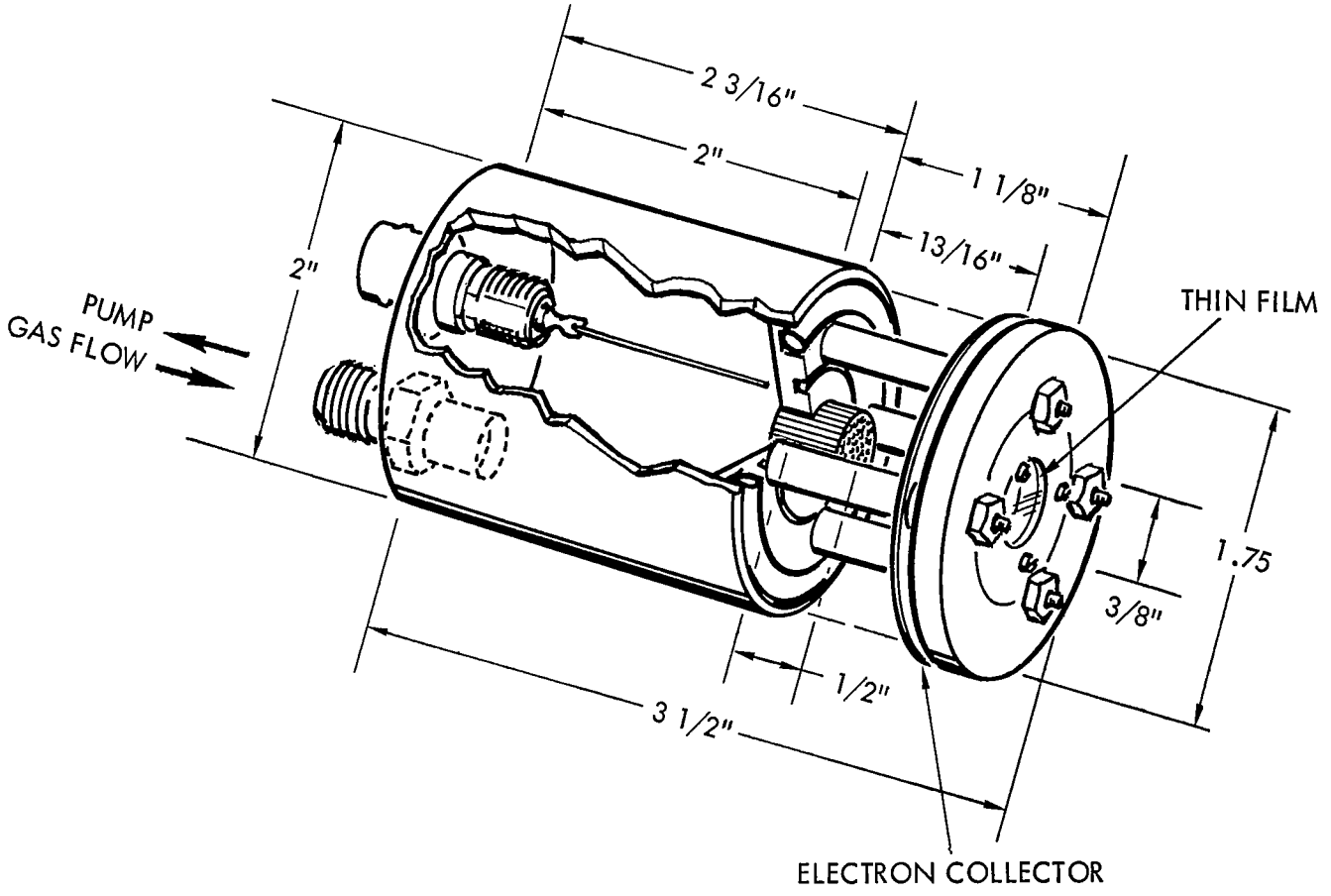

Figure 16. Cut-Away Drawing Showing the Various Components of the Portable Thin Ion Chamber Detector.

Figure 17. Photograph Showing the Capillary Tube of the Portable Selective Detector.

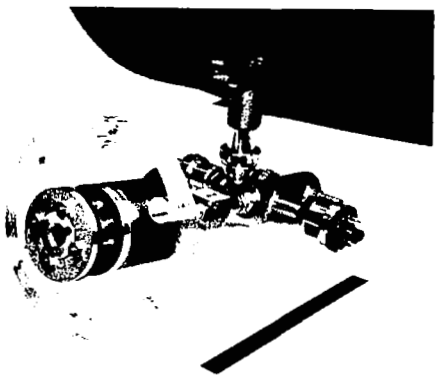

Figure 18. Thin Film Holder of the Portable Selective Detector.

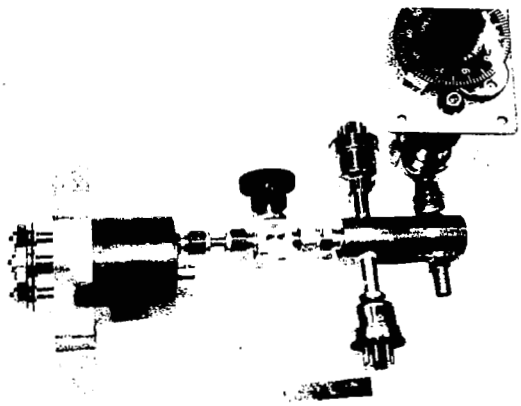

Figure 19. The Complete Portable Selective Detector with Pressure Gauges and Needle Valve.

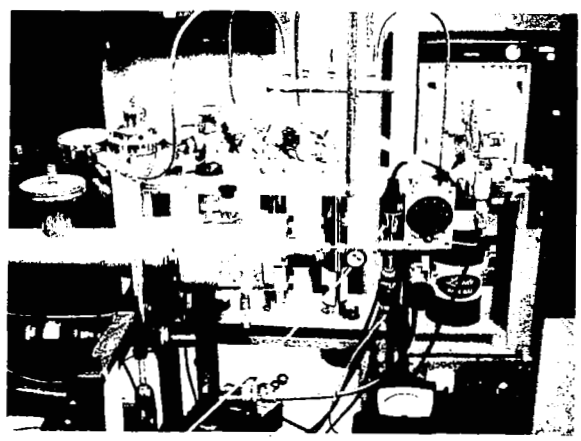

Figure 20. The Portable Selective Detector attached to the Exit Slit of the 1-M Seya Monochromator.

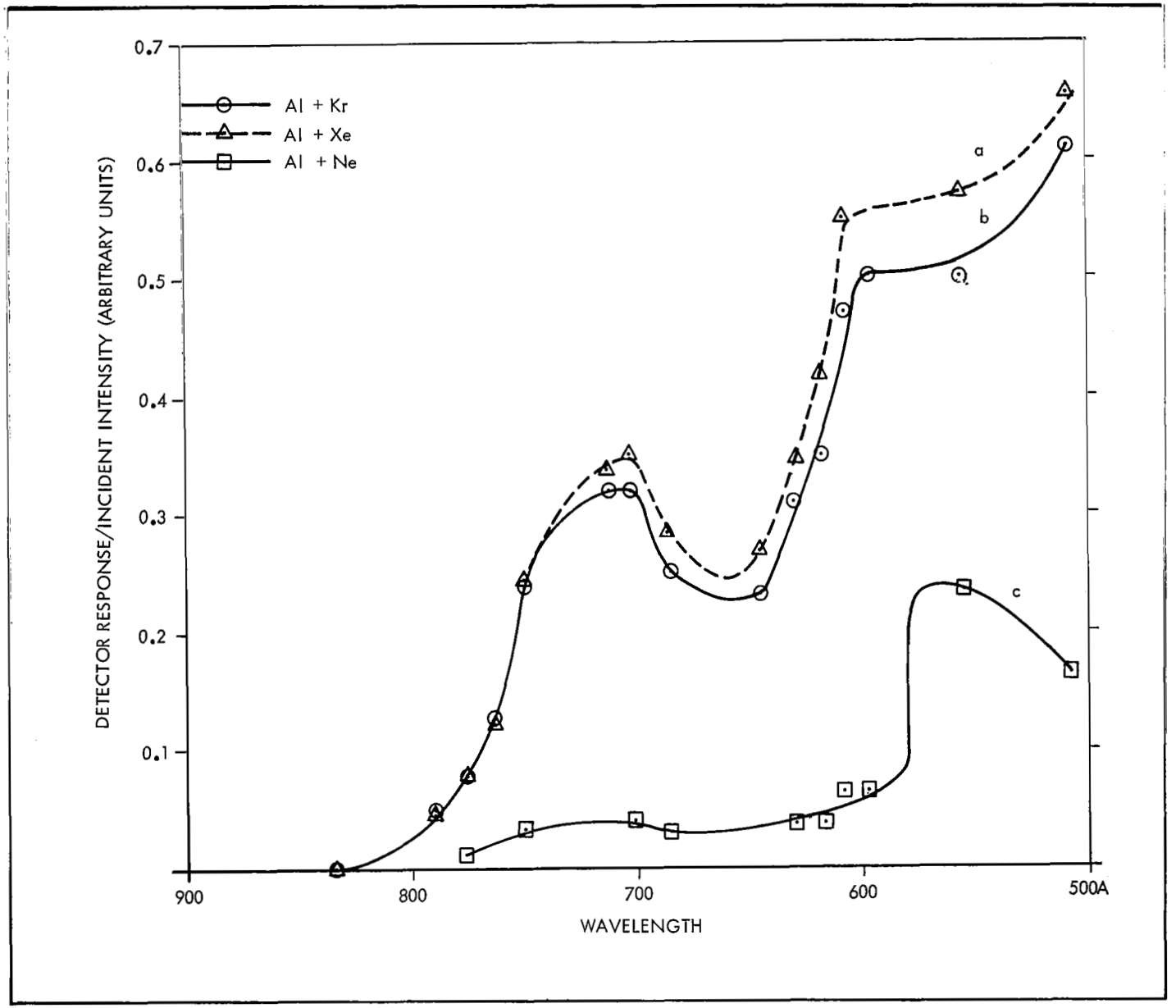

Figure 21. Response of the Selective Broad-Band Detector Using Al Film and Kr, Xe, and Ne Gas.

these pressures at 105 μ for krypton, 130 μ for xenon, and 300 μ for neon. Since the radiation between 580 Å and 840 Å was passed by the Al film and was not able to ionize Ne gas, it impinged on the ion chamber wall and produced photo-electrons giving rise to a response even for longer wavelengths than corresponding to the ionization potential for neon. Hence, the discrimination level for this detector had been reduced.

A different version of the portable selective detector was designed in the laboratory and fabricated by LND Incorporated, in which the rear wall of the chamber was made of alumina. The electrical connector for the collector current was mounted on a lexan plastic insulator which developed leaks around the joints. Before the capillary tube flange was installed, the alumina plate was checked for photoelectric emission current. It was noticed that an appreciable photoelectric signal was obtained without the film and capillary tubes in front of the chamber, and hence was not considered useful. Other ion chambers, not shown, having $\frac{1}{2}$ inch deep cavities at the rear wall covered with alumina were also found to be sensitive at those wavelengths which were able to pass through the thin film but could not ionize the gas.

At this stage, it was recognized that if the rear wall of the selective detector could be electrically isolated from the rest of the chamber, then the photoelectrons ejected from the rear wall could be suppressed by maintaining it at some high positive potential. This was accomplished in the new design of the portable selective detector, shown in Figure 22.

The ion chamber case was fabricated out of stainless steel tubing. A piece of Ni, $\frac{3''}{8}$ in diameter was used at the rear end to serve as a photocathode. A stainless steel mesh screen (100 mesh/inch) was used as a grid in front of the Ni photocathode to repel all the photoelectrons from the Ni photocathode while the cylindrical mesh screen was used in attracting the positive ions by maintaining it at some specified negative potential. This should result in an electron current at the

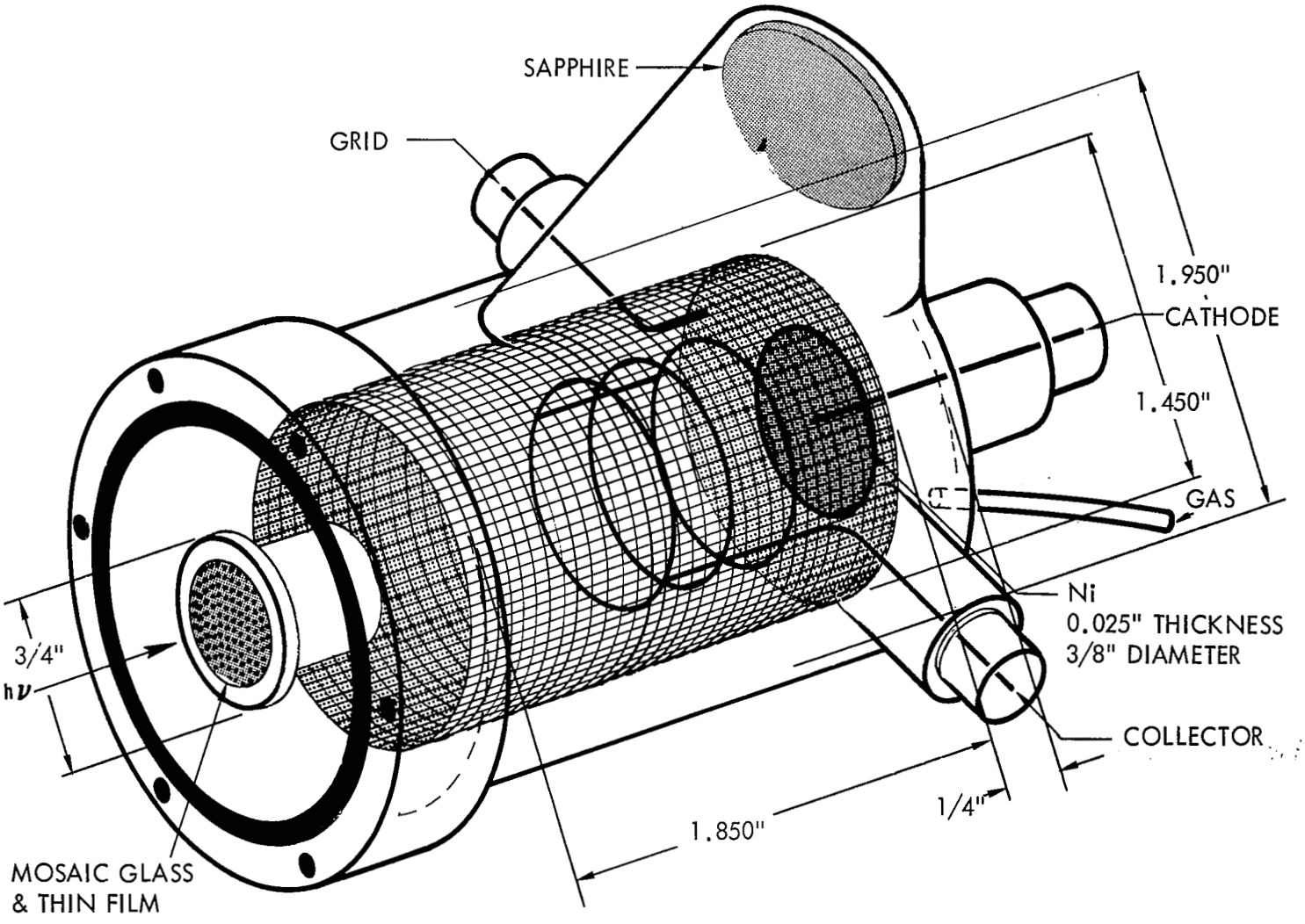

Figure 22. Three-Dimensional View of the Selective Detector.

circular ring electrode caused by electrons produced only by photoionization in the gas. In order to minimize the gas loss from the detector to the outside vacuum, long glass capillary tubes were replaced by mosaic glass obtained from Permeonics Corporation. This helped contain the gases for longer time periods. Each glass piece was $\frac{3}{4}$ inch in diameter and 0.015 inch thick, and carried 0.008" diameter holes over an area of $\frac{7}{16}$ " in diameter leaving an opaque boarder for making a vacuum seal to the front end of the detector. The optically flat face of the glass was used in supporting the thin films. Transmittance of mosaic glass was measured by pulling it into and out of the radiation in front of the exit slit. Using 923 Å radiation, it was found to be 28%. This transmittance would be close to 50%, when measured with a collimated beam.

In order to attach the mosaic glass to the front end of the selective detector, three different techniques were tried. Earlier results, reported in Quarterly Report 65-134-6, were obtained by using red sealing wax and keeping the thin film on the vacuum side. Some of the measurements possible with this new detector are summarized below.

1. Photoionization currents: the photocathode would be biased positive to eliminate photoelectrons produced at the photocathode of the detector, the grid would be biased negative, to collect ions and provide a collecting field, and the collector should be grounded through the electrometer to measure the photoionization currents.

2. The collector and photocathode could be biased positive, and the current could be monitored at the grid; this gives the current, if any, produced by the photoelectric effect at the grid. (The grid just in front of the photocathode is a mesh of 0.001" stainless steel that is 90% geometrically transparent.)

3. The grid could be biased positive and the collector negative, and the signal will be monitored at the photocathode; this would give the photoelectric current produced at the photocathode.

4. This design of the selective detector allows photoelectron retarding potential measurements, a technique which in itself is a form of selective detection. The voltage configuration would have the collector biased positive, monitoring of the signal at the photocathode, and a variable negative voltage on the grid to supply the retarding potential.

5. A sapphire window sealed to the ion chamber at 45^{o} to the light beam could be used to monitor the fluorescence radiation in the detector caused by vacuum UV radiation when it was filled with either air, oxygen or nitrogen.

The results obtained from the above mentioned detector pointed to some further improvement. Although we were successful in suppressing the photoelectrons from the photocathode, we did not observe sharp rejection of those radiation which could not ionize the filling gas. This can be seen from the spectral response characteristics of the detector using an Al film and neon gas (See Figure 39). Also a very peculiar pressure dependence of the selective detector response was observed at a fixed wavelength, (See Figure 37). The detector output increased as a function of gas pressure, and then decreased after attaining a peak over a very narrow pressure range. The peak response was attained at different pressures for each wavelength. Several arguments were given in support of these observations. For example, the long wavelength response was ascribed to impurity in gases, lack of circulation of gas in the detector, and photoelectrons ejected from the film. The strong dependence of the detector response on pressure at a fixed wavelength was ascribed to poor collection efficiency and leakage of gas either via the pumping line or around the film. These deficiencies were corrected in the final portable selective detector, shown schematically in Figure 23.

The gas inlet and outlet were separated so that gases can be introduced from the rear wall and pumped out from near the vicinity of the film, thereby allowing thorough evacuation of the detector. The cylindrical screen and circular collector electrode were replaced by

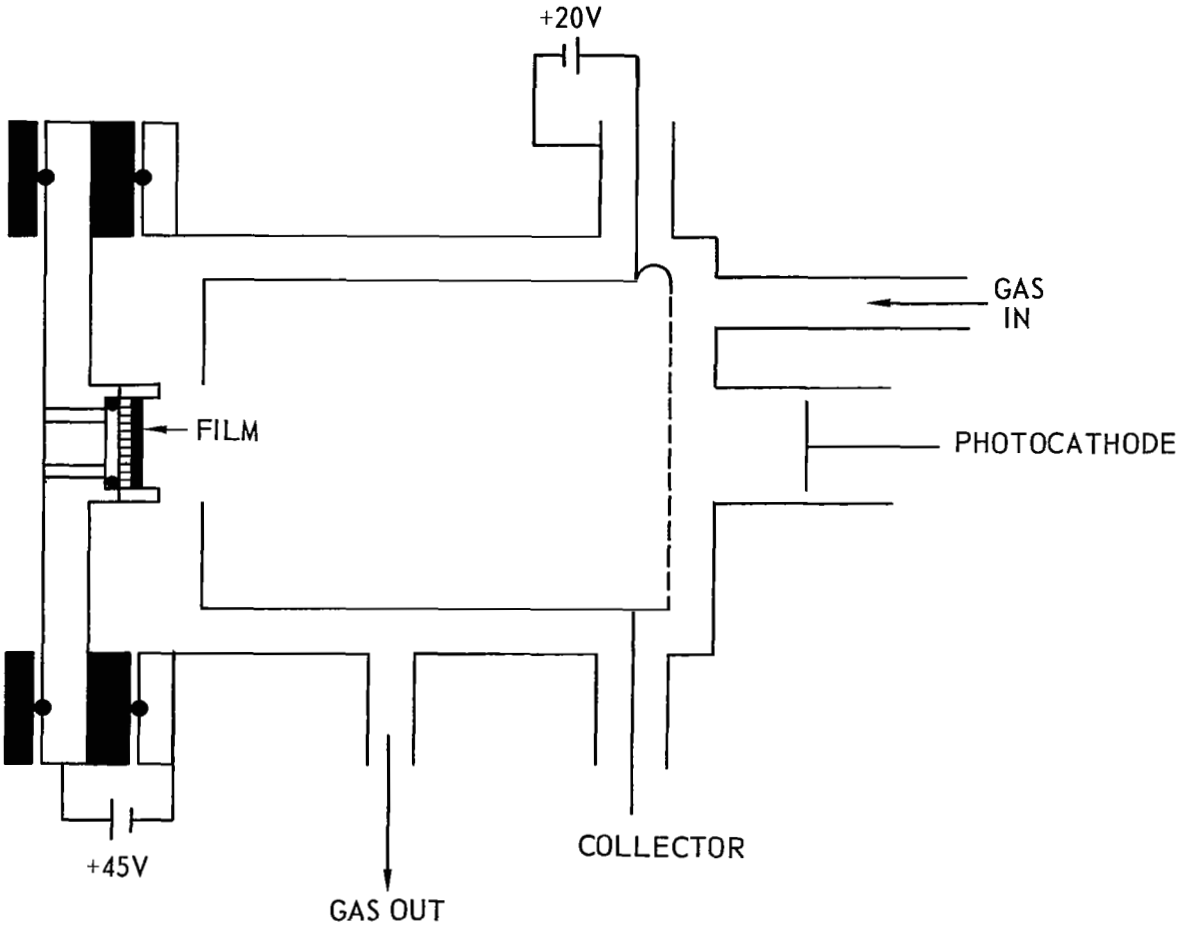

Figure 23. Schematic Diagram of the Selective Detector.

two semi-cylindrical electrodes. One of these electrodes was used to collect the positive ions produced in the selective detector giving the detector output while the other was kept at a low positive potential along with the grid in front of the photocathode to collect all the electrons. The thin film holder was also kept at a low positive potential to attract any photoelectrons released from the film now kept inside the chamber and repel the positive ions. The Ni photocathode material was replaced by a disc of tungsten. Conventional O-ring seals and quartz cement were used to stop leakage of gas around the film. A new pumping line was attached to the space immediately in front of the selective detector and the pressure there was monitored by a thermocouple gauge. Since these detectors are selective devices, a knowledge of their spectral response characteristics is absolutely essential in order to be able to interpret their current indications.

SECTION VI

RESULTS AND DISCUSSION

The results of the study conducted for the selective detection of vacuum ultraviolet radiation between 1000 - 100Å are presented here. First, the transmittance measurements of thin films are discussed. It is then followed by the results obtained from a limited study of the fluorescence in air. Then complete spectral response characteristics of the portable selective detectors are presented and followed by preliminary results on the photoelectric yield measurements and photodiode studies.

Transmittance of Thin Films

Figure 24 shows the transmittance measurements of an unbacked Bi film 1100 ± 100Å thick, and is characteristic of data obtained from other films of different thicknesses. Bismuth, obtained from J. T. Baker Chemical Company and of 99.95 percent purity, was successfully evaporated from a W boat at a pressure which varied from 7×10^{-7} mm Hg to 1×10^{-6} mm Hg, while the substrate was maintained at room temperature. The transmittance begins to rise from a value of 0.3% at 730Å to a maximum of approximately 10% at 530Å from where it drops abruptly to a value of 0.9% at 510Å indicating a sharp absorption edge at 520Å. The transmittance begins to increase again, approaching a second peak near 465Å from where it suddenly decreases to a value of 1.4% at 452Å indicating a second absorption edge near 460Å, both in good agreement with the results reported by Hunter et al. The third peak in transmittance occurs near 365Å where a third broad absorption edge sets in reducing the transmittance of Bi to less than 0.1% near 300Å.

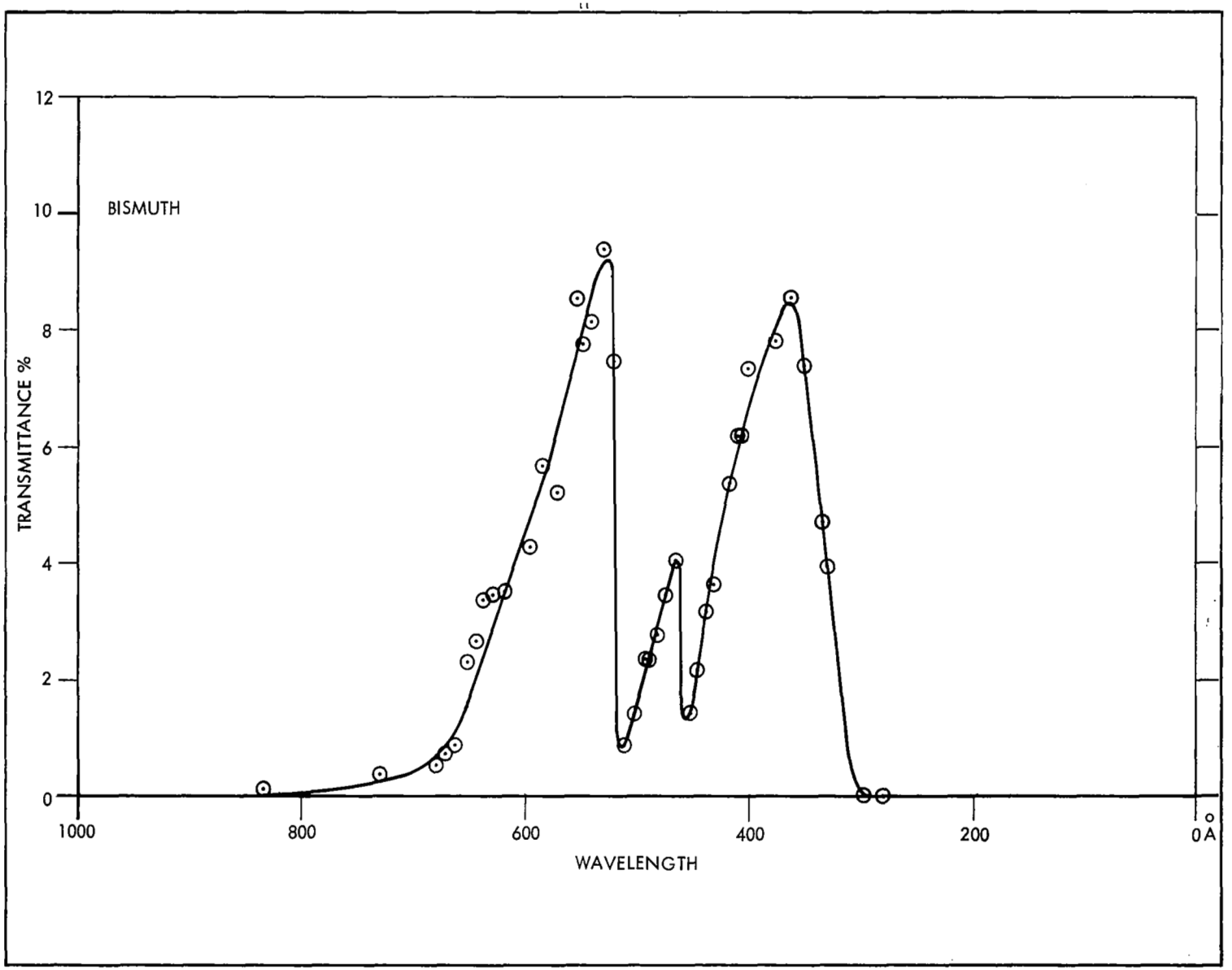

Figure 24. Transmittance of Bi Film as a Function of Wavelength with Least Exposure to Atmosphere.

Indium, obtained from Kern Chemical Company and of 99.9999% purity, was successfully evaporated from a molybdenum boat. The evaporation was achieved at a pressure of 5×10^{-6} mm Hg and lasted only 10 seconds. Figure 25 shows the transmittance measurements on an indium film, 1000 ± 100Å thick. The transmittance increases from a value of 0.4% at 1070Å to a maximum of 14% near 800Å then dropping to a value of 9.53% at 760Å. It is from this wavelength that transmittance decreases abruptly to a value of less than 0.1% near 730Å indicating a sharp absorption edge near 740Å. The film appeared silvery bright and wrinkle free. Figure 26 shows the transmittance of a tin film as a function of wavelength. Tin wire of 99.999% purity and obtained from A. D. Mackay Incorporated was successfully evaporated from a tungsten boat at a pressure of 2×10^{-6} mm Hg. The film thickness of approximately 800Å was measured using a Tolansky interferometer. Both tin films number 1 and 2 were placed inside the experimental chamber four days after their preparation. Transmittance increases from a value of 0.014% at 923Å to a maximum of 26% at 530Å and then suddenly decreases to a value of less than 1% at 510Å. The film again becomes transparent near 400Å and shows a continuous decrease in transmittance out to the limit of our measurements. This film was found to be completely free from pin holes and was, therefore, used in making fluorescence intensity measurements by exposing the air in the laboratory experimental chamber to zero order spectrum from the grating.

In order to explore the transmittance of tin in the short wavelength region, another tin film, approximately 600Å thick, was used. As shown in Figure 27, the transmittance increases from a value of 0.22% at 923Å to a value of 35% at 530Å and then drops sharply to 2% near 450Å attaining a minimum. It then rises to a peak of 8% at 400Å where it starts to decrease monotonically toward shorter wavelengths out to the limit of our measurements. The position of peaks and the valley in this curve agree well with those reported by Codling et al[90]. Their results report, in addition, another region of transparency below 150Å.

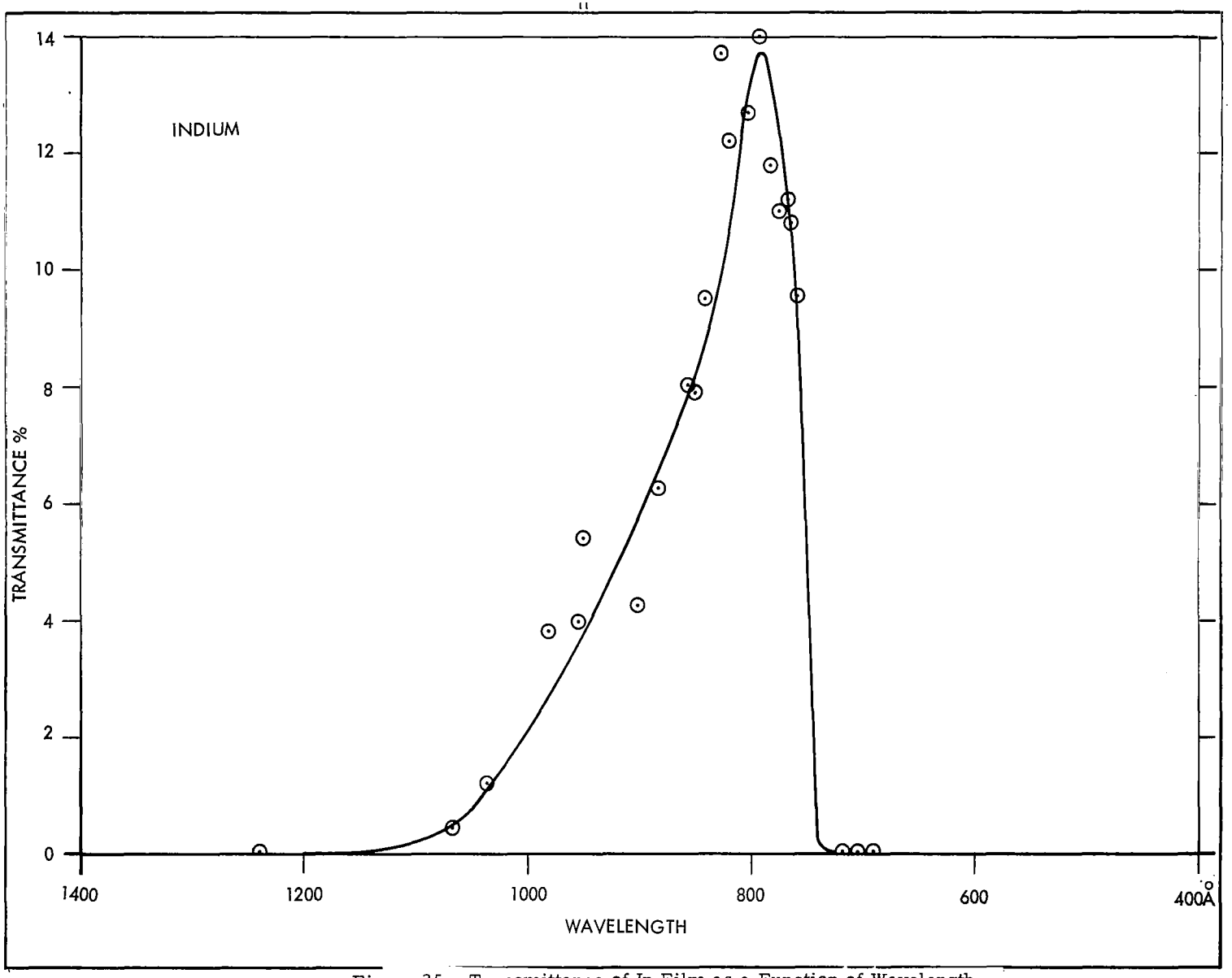

Figure 25. Transmittance of In Film as a Function of Wavelength.

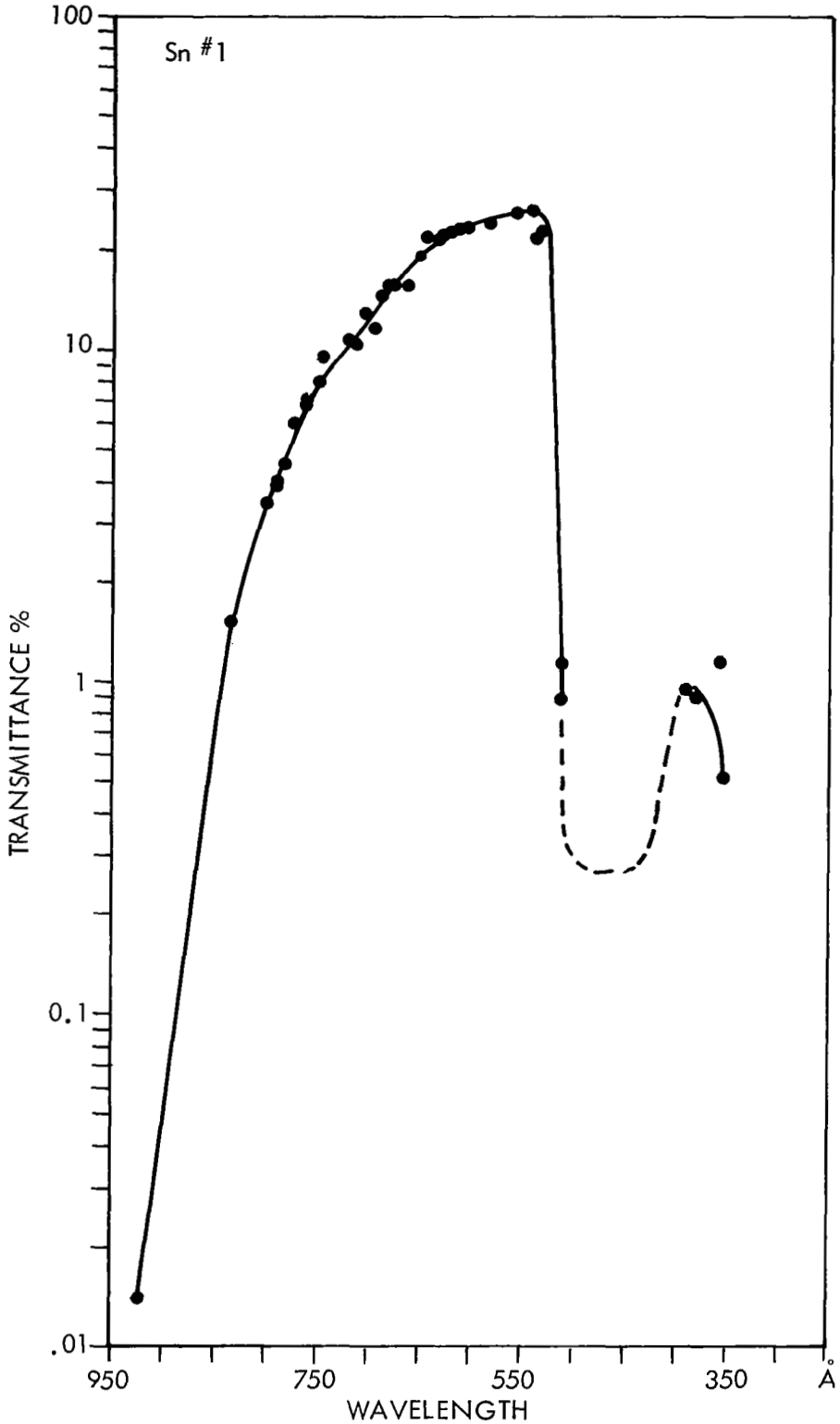

Figure 26. Transmittance of Tin Film No. 1.

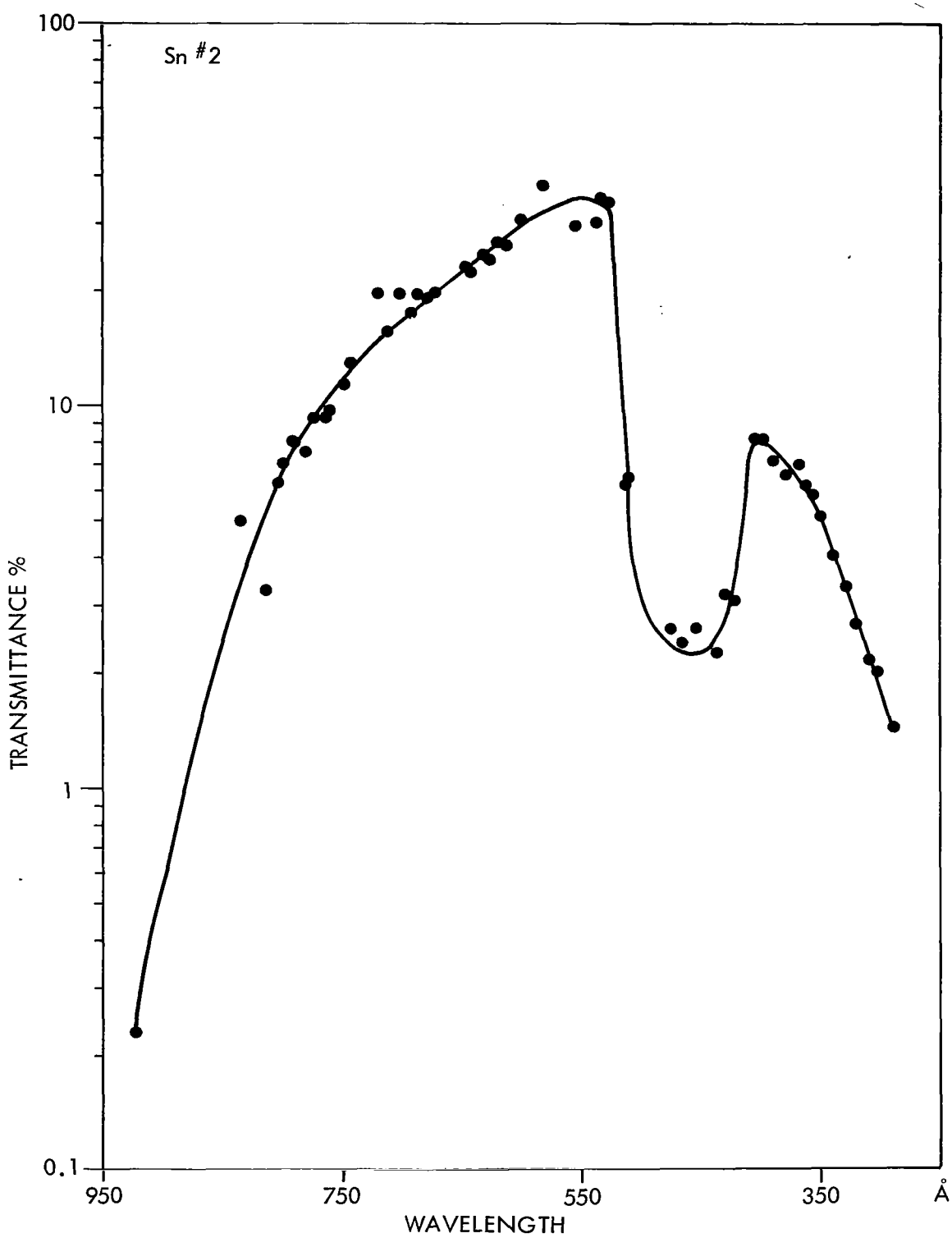

Figure 27. Transmittance of Tin Film No. 2.

Figure 28 shows the transmittance of an Al film 800Å thick. Aluminum of 99.999% purity obtained from A. D. Mackay Incorporated was successfully evaporated from a tungsten helical coil at a pressure of 2×10^{-6} mm Hg and picked up on brass holders. After keeping the film in the desiccator for 24 hours, it was transferred to the experimental chamber for measurement. The transmittance increases from a value of 0.25% at 833Å and continues to rise out to the limit of our measurements attaining a value of 60% at 250Å. Similar results were obtained from other Al films.

In order to prepare composite (Al + Sn) films, an aluminum film was evaporated first on a glass slide which had a water soluble coating. Without exposure to air and water, a thin coating of tin was evaporated on the aluminum film. The glass slide, when taken out of the vacuum system looked very shiny. During floating-off of the thin film, the film broke up into very small pieces indicating a loose structure and hence the film could not be picked up. Next the alternate procedure was tried. First, an aluminum film was floated-off and picked up on a brass holder. This film was then transferred to the evaporation chamber and was then coated with a thin film of tin. On opening the belljar, a strong film of Al + Sn was obtained and transmittance measurements made.

Figure 29 shows the transmittance characteristics of a film consisting of approximately 500Å thick film of aluminum and 200Å thick film of tin. The transmittance starting with a value of .004 at 833Å rises to a value of nearly .17 at 525Å and then suddenly drops to a value of .02 at 510Å. At still shorter wavelengths, the transmittance continues to decrease until 450Å where it attains a maximum of .04 and then decreases again.

In order to narrow the response of selective detectors to wavelength intervals of 50Å, attempts were made to prepare thin films consisting of chromium, having a transmission-onset near 500Å, and another metal having a transmission onset above 500Å like Al or Ti

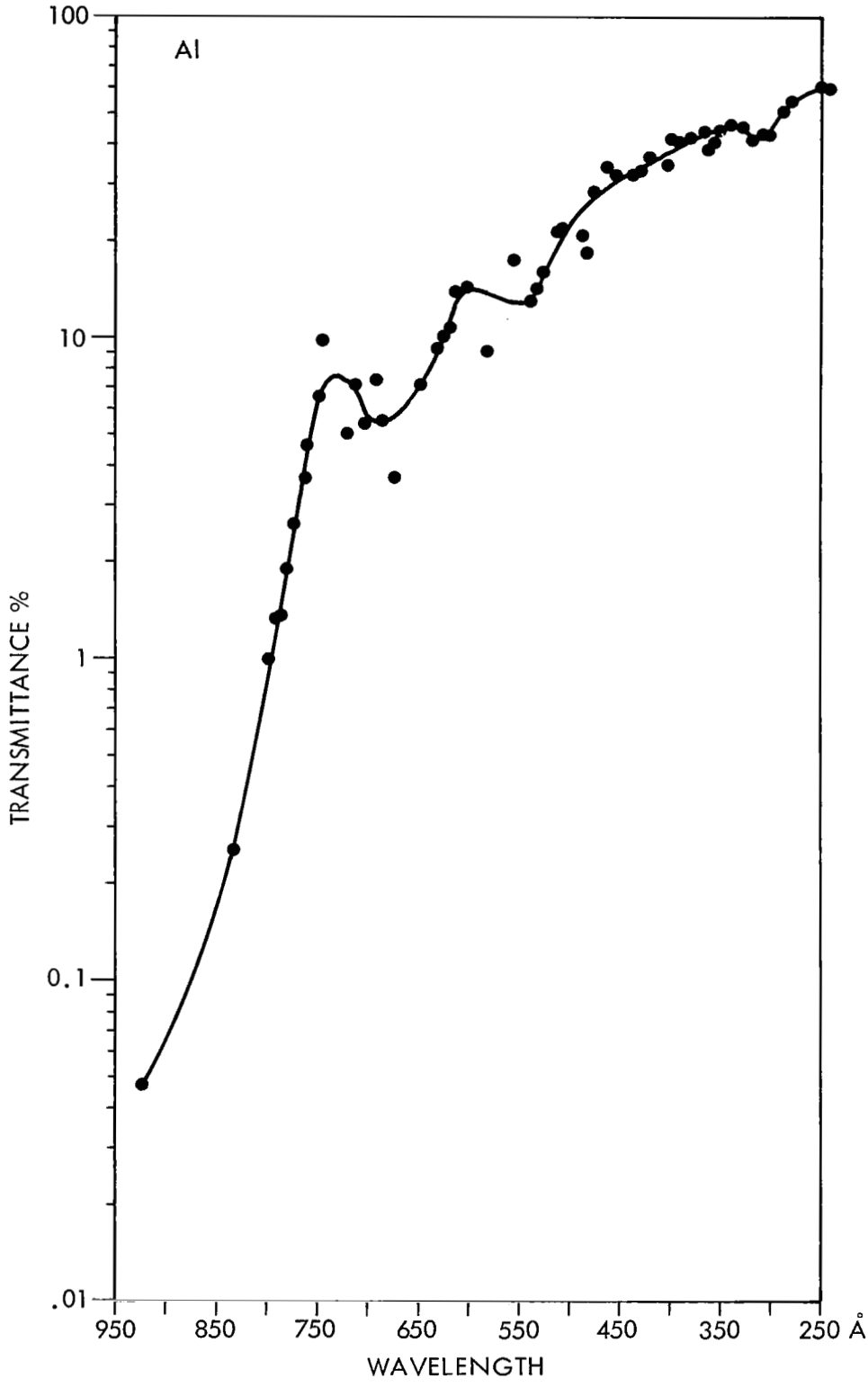

Figure 28. Transmittance of Aluminum Film.

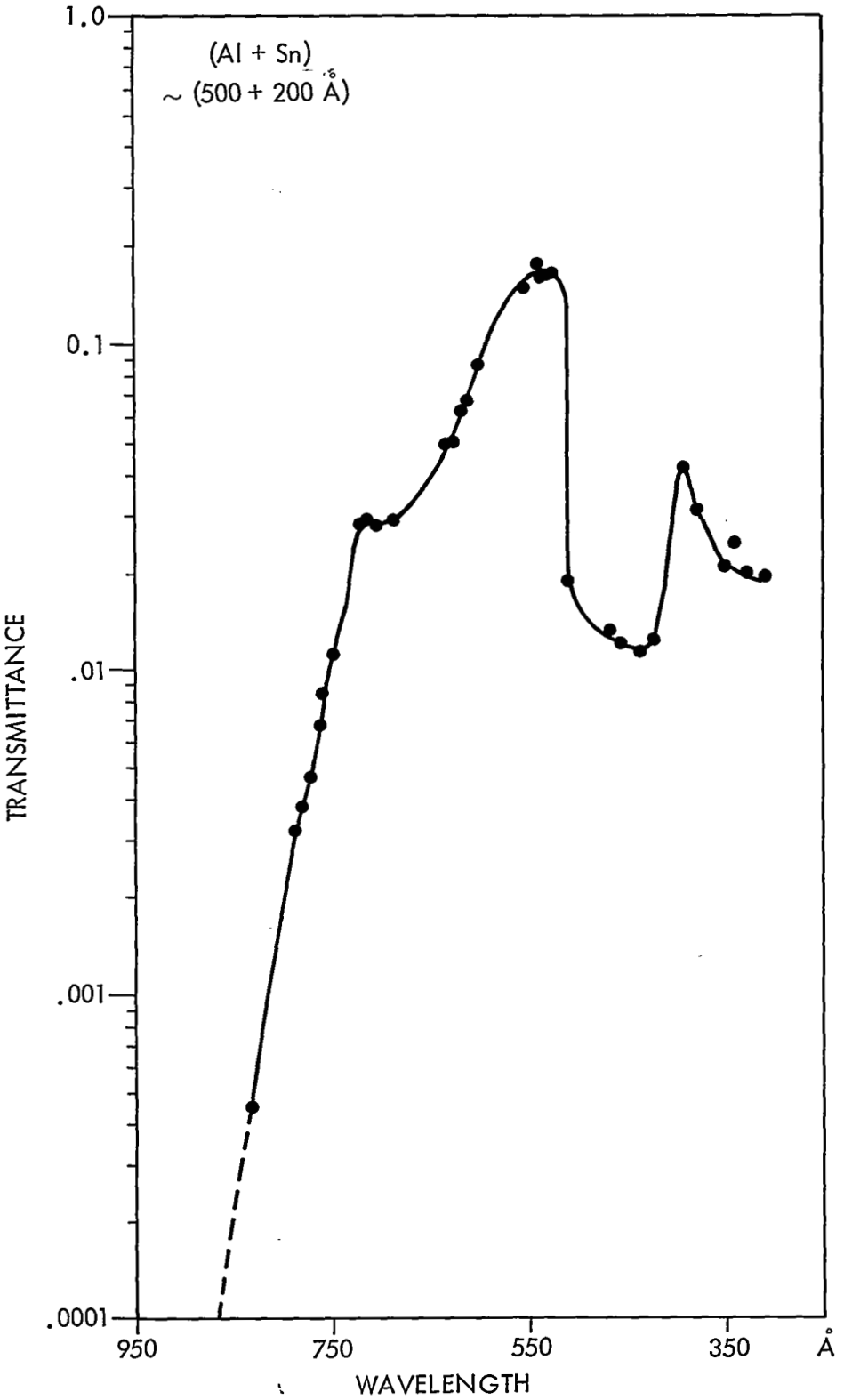

Figure 29. Transmittance of Aluminum Plus Tin Film.

with a transmission cut off below 500Å. The first attempt was made with aluminum and chromium.

Alumium films were prepared by evaporating Al from a tungsten filament on a glass slide which had been coated with a water soluble sugar-aerosol solution. The evaporation was carried out for five seconds during which time the pressure in the evaporation chamber rose from 6×10^{-7}mm Hg to 7×10^{-6}mm Hg. This film was floated-off in water after a week and picked up on mosaic glass and brass holders. The Al film on mosaic glass was transferred to the evaporation chamber for chromium evaporation. Evaporation of Cr was performed from a W boat. The pressure during evaporation, which lasted 10 seconds, rose from 5×10^{-7}mm Hg to 1×10^{-5}mm Hg. On opening the system, the mosaic glass, which looked opaque with Al film, looked transparent to visible light. On closer inspection, it appeared that Cr had reacted with Al. The same observation was made when Cr was evaporated on an Al film on a glass slide without exposing the Al film to atmosphere or water

For composite films of chromium and titanium, the following procedure was adopted. First titanium films were evaporated on glass substrates which had been coated with the water soluble sugar-aerosol solution. The Ti film was exposed to atmosphere so that it could attain an oxide layer and become stable. Then the Ti film on glass was kept in the evaporation chamber and chromium was deposited on it from a tungsten boat. On opening the bell jar, the glass slide was found to be coated only at a few places and the resultant coating appeared loosely bound to the glass surface. Attempts were then made to evaporate titanium and chromium both from the same tungsten boat. The resultant film had patchy appearance similar to the previously described film and could not be used. An optically flat quartz plate was used as substrate for further evaporations. Both titanium and chromium were successfully evaporated from the tungsten boat. The pressure in the evaporation chamber rose from low to high values in the 10^{-6}mm Hg range. Both films appeared silvery bright. The chromium film did not float off in water in one piece, but broke into a large number of smaller pieces. Evaporation of

Ti on Cr resulted in a composite film which had a patchy appearance. In some cases, the composite film of Cr on Ti curled up on itself as it floated off in water thus making it unusable.

Ti film, used in the portable selective detector, was prepared by evaporating it from a tungsten boat at 3 x 10^{-6} mm Hg pressure. The film was floated off in water and subsequently picked up on the mosaic glass. As the films used in the portable selective detectors covered the mosaic glass without leaving some portion which could be used for transmittance measurements, it was not possible to measure transmittance of these films.

In order to prepare thin films which are structurally strong, we obtained some Parylene pellicles type C. The basic member is a poly-para-xylylene, a completely linear, highly crystalline material, where one of the hydrogen atoms on the ring is substituted by a chlorine atom. It is a dimensionally stable thermoplastic which is synthesized by vapor phase polymerization. It exhibits excellent properties and is resistant to radiation. Its melting point is 750 deg. F making its practical upper use temperature 200 deg. F in air and 510 deg. F in an inert atmosphere.

Parylene C has better solvent resistance and barrier characteristics as compared to Parylene N, which has the better dielectric properties.

Some Parylene pellicles of type C, having a thickness of 230Å, as measured by capacitance measurement techniques, were obtained. The transmittance measurements on one such pellicle are shown in Figure 30. The transmittance starting with a value of 66% near 1800Å decreases continuously attaining a minimum of 5% near 800Å. It then increases at shorter wavelengths to a value of about 70% near 250Å. Since most of the other organic films also have the same transmittance characteristics, other samples will not be explored any further. However, it is pointed out that this pellicle may be a nice window material for the soft X-ray work.

Fluorescence Measurements

It was pointed out in Section IV of this report that fluorescence caused by the interaction of vacuum ultraviolet radiation with atmospheric

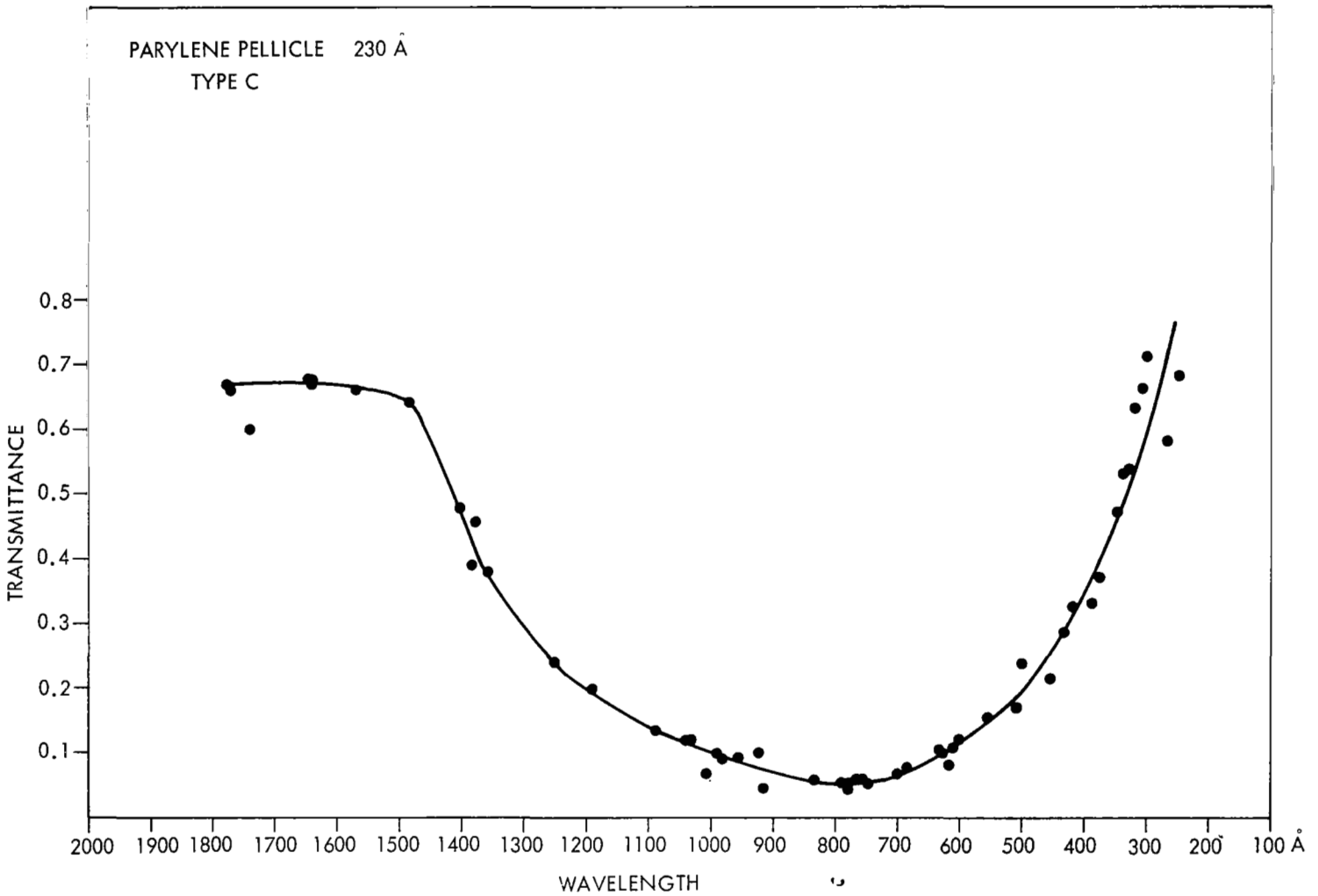

Figure 30. Transmittance of Parylene Pellicle Type C.

gases can be used to monitor the intensity of the exciting radiation. To observe the fluorescent radiation, the laboratory model of the selective detector, shown in Figure 14, was utilized. The glass window coated with sodium salicylate used as a radiation converter was replaced with a clean sapphire window. It was necessary to check that no visible light radiation caused either by fluorescence in the capillary tube or at the sapphire window be seen. Tin film No. 1 was placed in the zero order spectrum from the grating so that only radiation between 850Å and 510Å was allowed to enter the experimental chamber. Using an EMI 9526B photomultiplier tube at 800 volts, and no air in the chamber, an output signal was observed. This signal was eliminated when a lithium fluoride window was interposed in the incident beam indicating that fluorescence was either caused at the sapphire window or at the capillary tubes. The sapphire window was replaced with an ultraclean spectrasil window which resulted in a decreased output at the photomultiplier tube without any gas. When air was introduced at 50 μ pressure, the output signal increased by a factor of 15 above its background signal. This clearly demonstrated that in order to monitor the fluorescence radiation along the direction of the incident beam, the thin film, like Sn #1 film, should be completely pin-hole free and all windows of the chamber ultraclean.

The same chamber was then setup with Sn #1 film in the beam so that fluorescence radiation could be monitored at right angles to the exciting radiation six inches behind the capillary tubes. The output signal with air at 50 μ pressure was again observed but found to be decreased by a factor of 14 when compared to the signal obtained along the direction of the incident beam. This decrease in intensity is explained by the fact that in the direction of the incident beam, the photomultiplier tube is able to monitor the total fluorescent intensity whereas in the side-on position only a fraction of the total fluorescent region is viewed. The 50 μ air pressure was chosen so as to obtain a maximum signal in the side-on observation because at higher pressures, the attenuation of the incident beam increases exponentially at the point of observation.

The results of the typical side-on observation are shown in Figure 31. The units are arbitrary, but correspond roughly to fluorescent efficiency times the collection efficiency of the setup. Since the fluorescent intensity is rather small, no effort was made to analyse its spectral compositon. The curve in Figure 31 shows the general trend found by Judge et al.[91,92]

The knowledge and experience obtained from these experiments was then applied to the detection of fluorescent radiation in the portable selective detector, shown in Figure 22. The sapphire window was placed at such an angle so that the photomultiplier tube EMI 9526 B could view the region immediately behind the mosaic glass. This photomultiplier tube has a quartz window and was sensitive from 1650Å to about 7000Å. By observing the fluorescent region from an angle, any fluorescence at the sapphire window caused by the impinging incident beam was avoided. We were unable to read any signal over and above the dark current when the detector was slowly filled with air in the pressure range from 10^{-5} mm Hg to 1 mm Hg behind an aluminum film. Negative results were also obtained when the EMI 9526 B photomultiplier tube was replaced with solar blind EMR 541 F photomultiplier tube which was sensitive only over the wavelength region between 3000Å and 1500Å. The fluorescence measurements were not done while the selective detector was filled with rare gases as no flurescence is produced in these gases. It was, therefore, decided to study the spectral response characteristics of selective detectors by only measuring ion currents.

Spectral Response of Selective Detectors

Based on our earlier measurements on the portable selective detector using glass capillary tubes as reported in Figure 21, where no sharp cut-off in response at longer wavelengths was seen, a new selective detector was designed and fabricated. This detector, shown in Figure 22, used mosaic glass to support the fragile thin films and contained the gas with relatively little loss. The added feature of this detector was

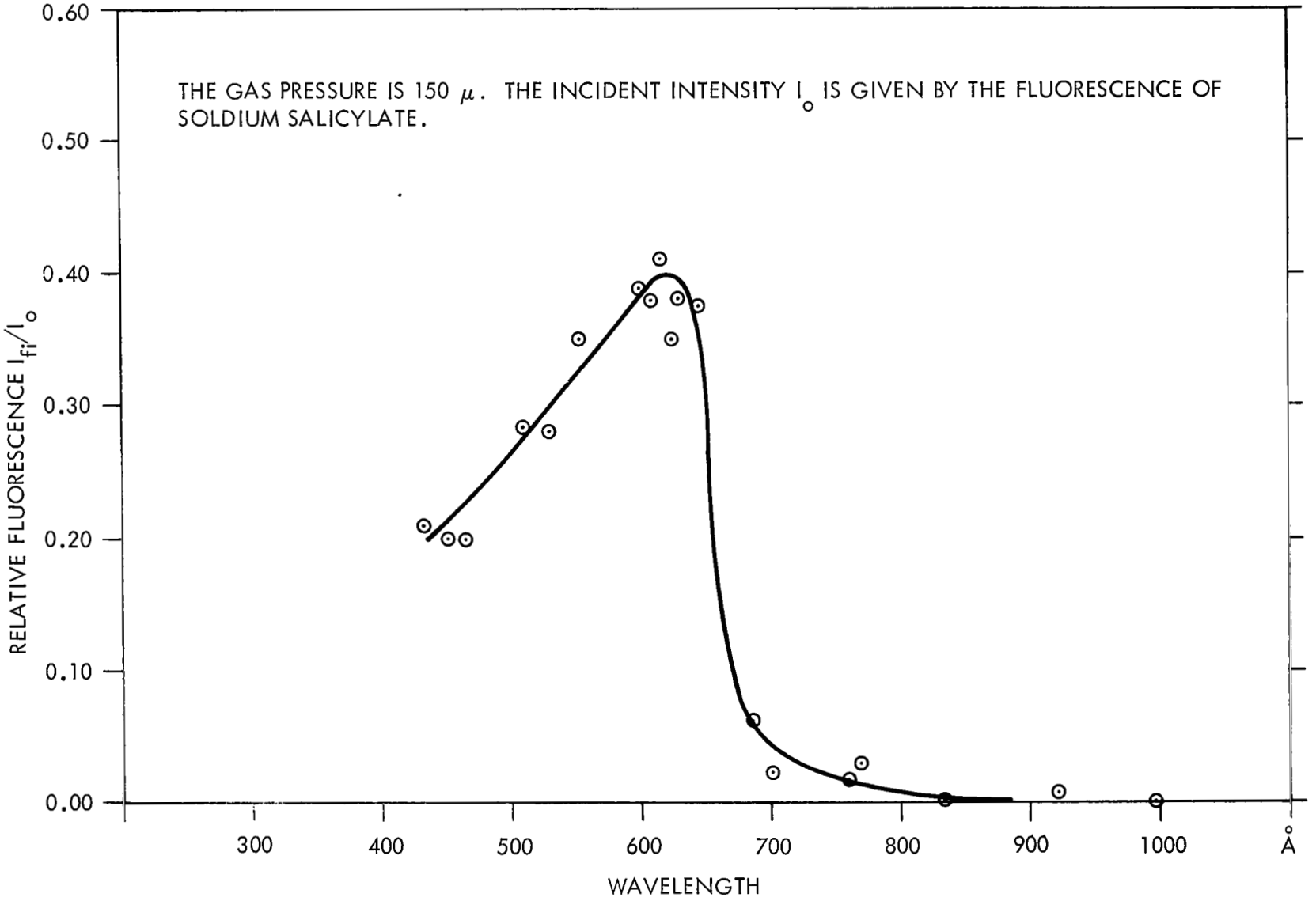

Figure 31. The Relative Fluorescence of Air as a Function of Wavelength.

manifested in its ability to monitor the vacuum ultratiolet radiation entering the ion chamber after it has passed through the thin film and mosaic glass. This was achieved by monitoring the current at the Ni photocathode due to emission of photoelectrons while the other electrodes were kept at some positive potential and the detector was completely evacuated. This eliminated the need of monitoring the vacuum ultraviolet radiation separately by means of a sodium salicylate coated photomultiplier. Using an aluminum film, approximately 600Å thick, and sealing the mosaic glass to the flange by means of red wax so that the thin film was outside the chamber, the following measurements were carried out.

Figure 32 shows the variation of photoelectric current as measured at the Ni photocathode when the potential at the grid and collector was varied from high negative values to high positive values. At positive voltages larger than 10 V, all the photoelectrons released from the Ni photocathode, when exposed to the zero order of the grating spectrum, were collected. The current reversed its sign when negative potentials were applied to the collector and the grid indicating that some electrons were released from the grid and were collected by the Ni photocathode.

When individual currents were measured at the grid and collector while the Ni photocathode, kept at -8.6 volts, was exposed to the zero order spectrum, it was observed that only 40% of the electrons were collected. The remaining being lost to the walls of the detector. Of these 40% only one third reached the collector and two thirds reached the grid.

With an aluminum film the response of the selective detector without any gas was below the limit of our measurements for all radiations above 840Å. The detector was then purged with various rare gases. With each gas chosen, the response of the detector was measured as a function of gas pressure at specific wavelengths and then maintaining the pressure for a maximum signal, a spectral scan covering the range from the zero order spectrum out to 925Å in the first order was taken. A minimum of three scans were made for each gas and averaged to reduce error due to fluctuations in the

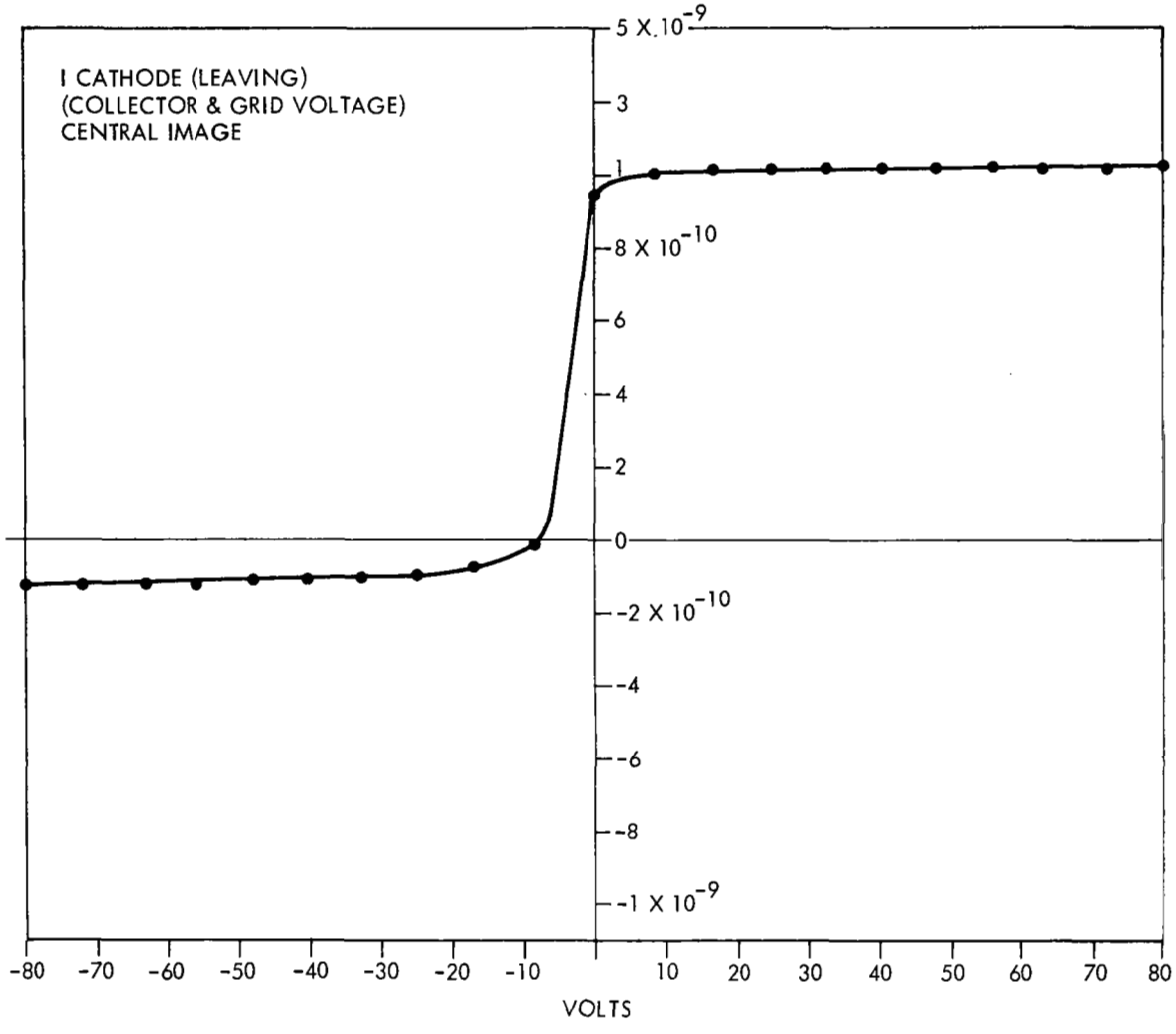

Figure 32. Photoelectric Current at the Cathode Versus Retarding Potential at the Grid and Collector.

light source. The constancy of the light source was checked by measuring the signal due to photoelectrons ejected from the Ni photocathode before the introduction of the gases and after the gases had been pumped out of the ion chamber detector.

Figure 33 shows the pressure dependence of the detector response at 686Å and 555Å. It is seen that the response of the detector increases as the gas pressure increases until the pressure reaches 120 μ, as measured on a CVC thermocouple, and then remained constant while the pressure increased to 200 μ. It then decreased with increase in pressure. This behavior was the same both at 555Å and 686Å.

Figure 34 shows the spectral response of the selective detector using an Al film and argon gas at 200 μ. The ordinate is the ratio of the electron current as registered at the collector to the output of the sodium salicylate coated photomultiplier tube. In arbitrary units, the response of the detector starts from a value of .003 at 923Å and increases to .03 at 787Å where the argon gas ionizes. The few pin holes in the Al film allow the longer wavelength radiation than 840Å to enter the ion chamber and ionize the contaminant gases present along with argon. The response of the detector continues to increase shortward of 787Å and has the characteristics of the transmittance curve of an Al film until it reaches a value of 0.65 at 650Å which it maintains down to 400Å where the decrease in absorption cross section of argon causes the total response to decrease. At 288Å, the response of the detector has a value of 0.09.

This decrease in response at wavelengths shorter than 400Å may also be due to increase in loss of more energetic electrons to the walls of the chamber, especially to the thin film flange, being accelerated by the negative potential at the grid. No measurable signal was registered at the Ni photocathode while the grid was kept at a high negative potential of -63 V and collector grounded. Also during these measurements, the pressure between the exit-slit and the selective detector increased from its value with no gas in the detector as registered by the ion gauge. The rise in pressure in the ion gauge became much more significant

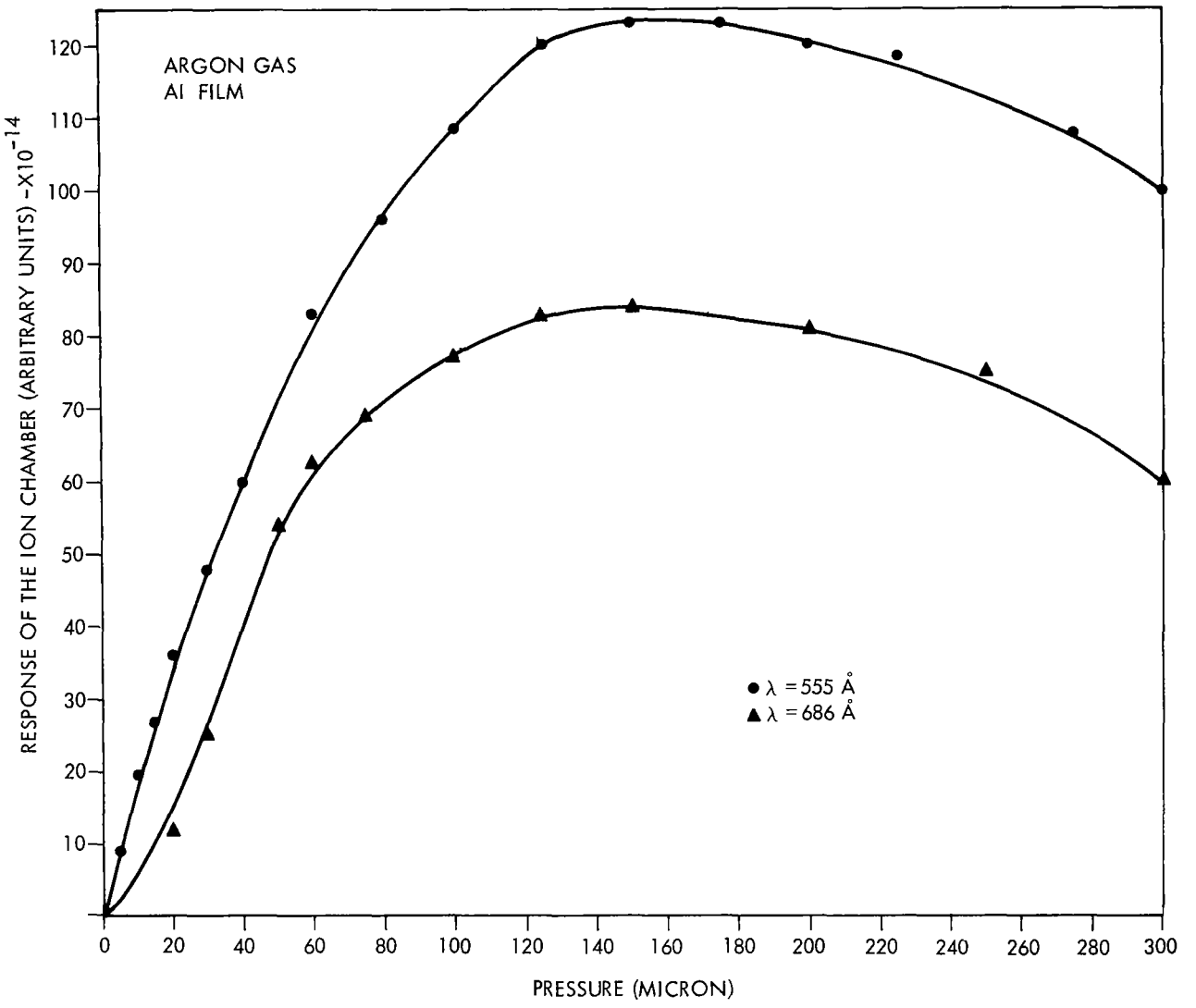

Figure 33. Detector Response as a Function of Argon Pressure at 686Å and 555Å.

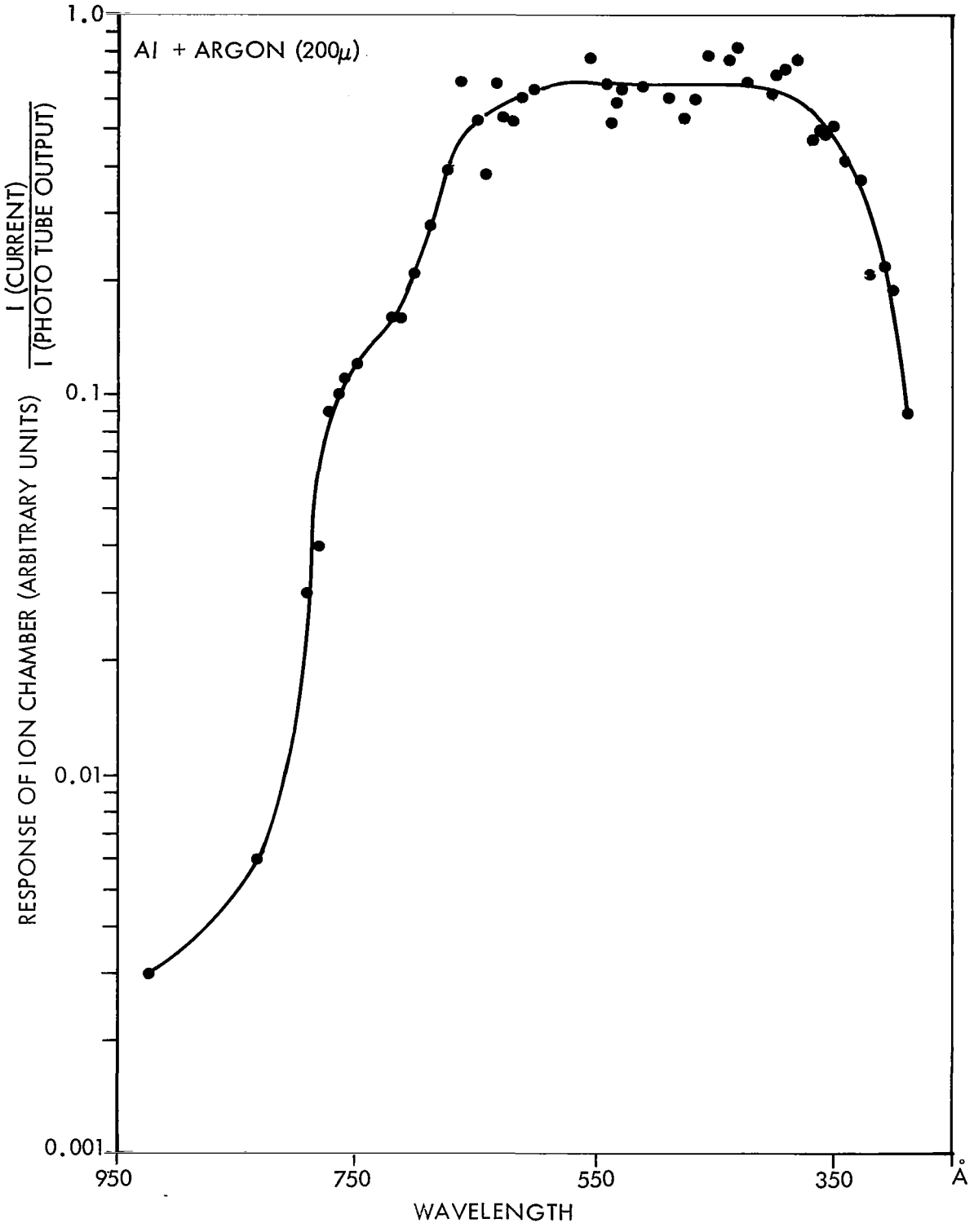

Figure 34. Spectral Response of the Selective Detector Using Aluminum Film and Argon Gas.

when the pressure in the detector increased above 200μ. This is reflected in the curve of Figure 33 where the response of the detector decreased for pressures over 200μ because more photons were absorbed before they entered the detector.

Figure 35 shows the collector current as a function of pressure of xenon gas at 686Å and 508Å. The response is markedly peaked for 686Å and is less pressure dependent for 508Å. The shape of the curve only confirms our earlier belief that more long wavelength photons are absorbed in the gas between the slit and the detector and, therefore, requires modification of our pumping system.

Figure 36 shows the response of the detector, using an aluminum film and xenon gas at a pressure of 200μ as a function of wavelength. Since the ionization potential of xenon gas lies at 1022Å, the response curve follows the shape of the transmittance curve of Al at longer wavelengths starting with a value of 0.01 at 833Å and rising to a peak of 0.8 at 430Å with a dip near 550Å (possibly caused by Al film). It then decreases down to 0.4 at 270Å because of a decrease in the absorption coefficient for xenon.

Figure 37 shows the pressure dependence of the selective detector consisting of krypton gas and an aluminum film at 686Å and 508Å. Again, we observe a marked dependence of the response of the detector for 686Å radiation and a uniform flat response for 508Å over wider pressure ranges.

Figure 38 shows the response of the selective detector as a function of wavelength using krypton gas at 220μ and an aluminum film. In this case, the response starts with a value of .003 at 923Å and rises smoothly to a value of 0.5 at 600Å. Then it shows a slight dip near 550Å and continues to rise to a peak value of 0.9 at 400Å. From there it decreases smoothly to a value of .4 at 270Å.

The spectral response of the selective detector consisting of neon gas at 500μ and an aluminum film is shown in Figure 39. Here is a combination where the ionization onset of the filling gas is at a wavelength much shorter than the transmission onset of the film. We find that the

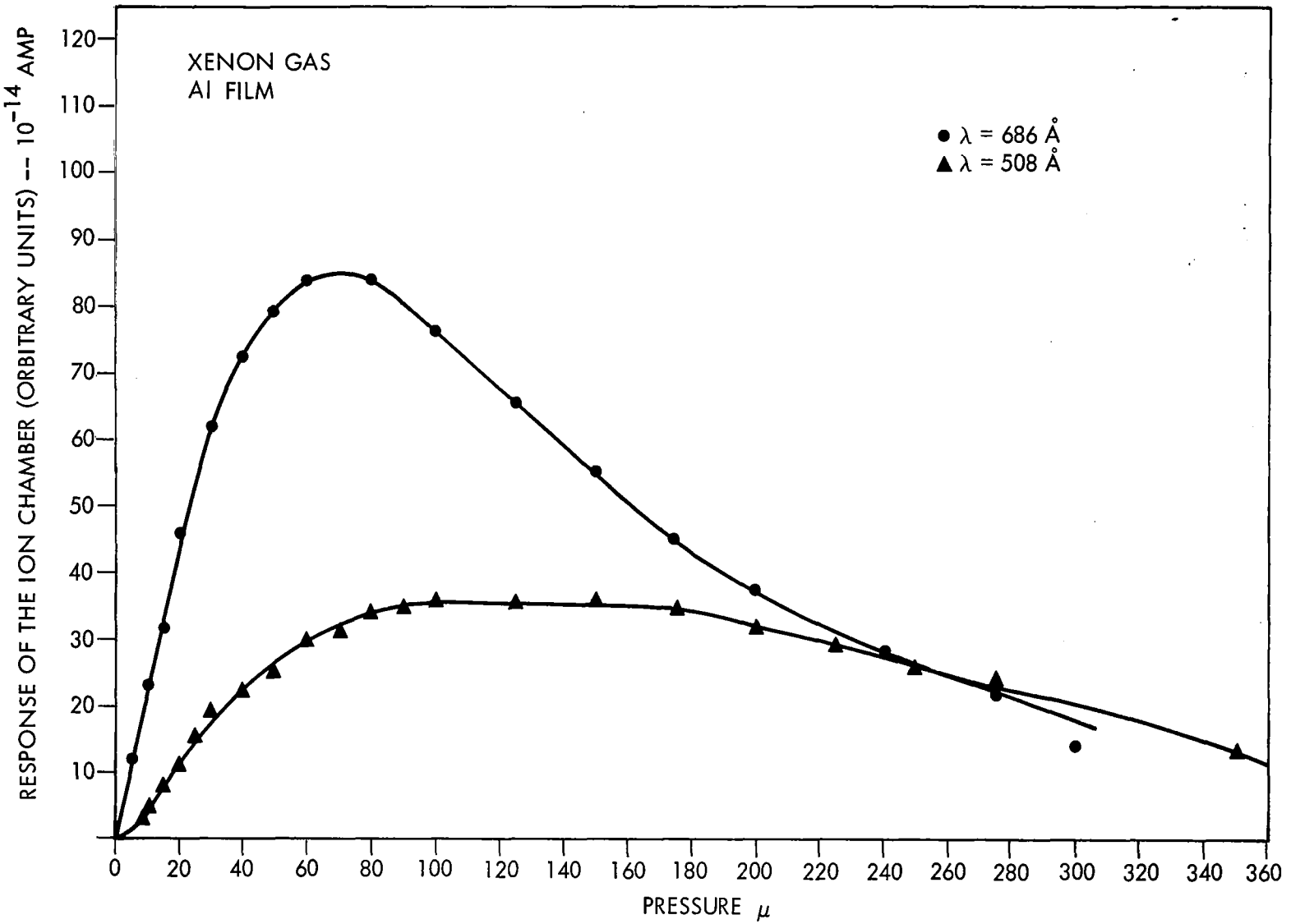

Figure 35. Detector Response as a Function of Xenon Gas Pressure at 686Å and 508Å.

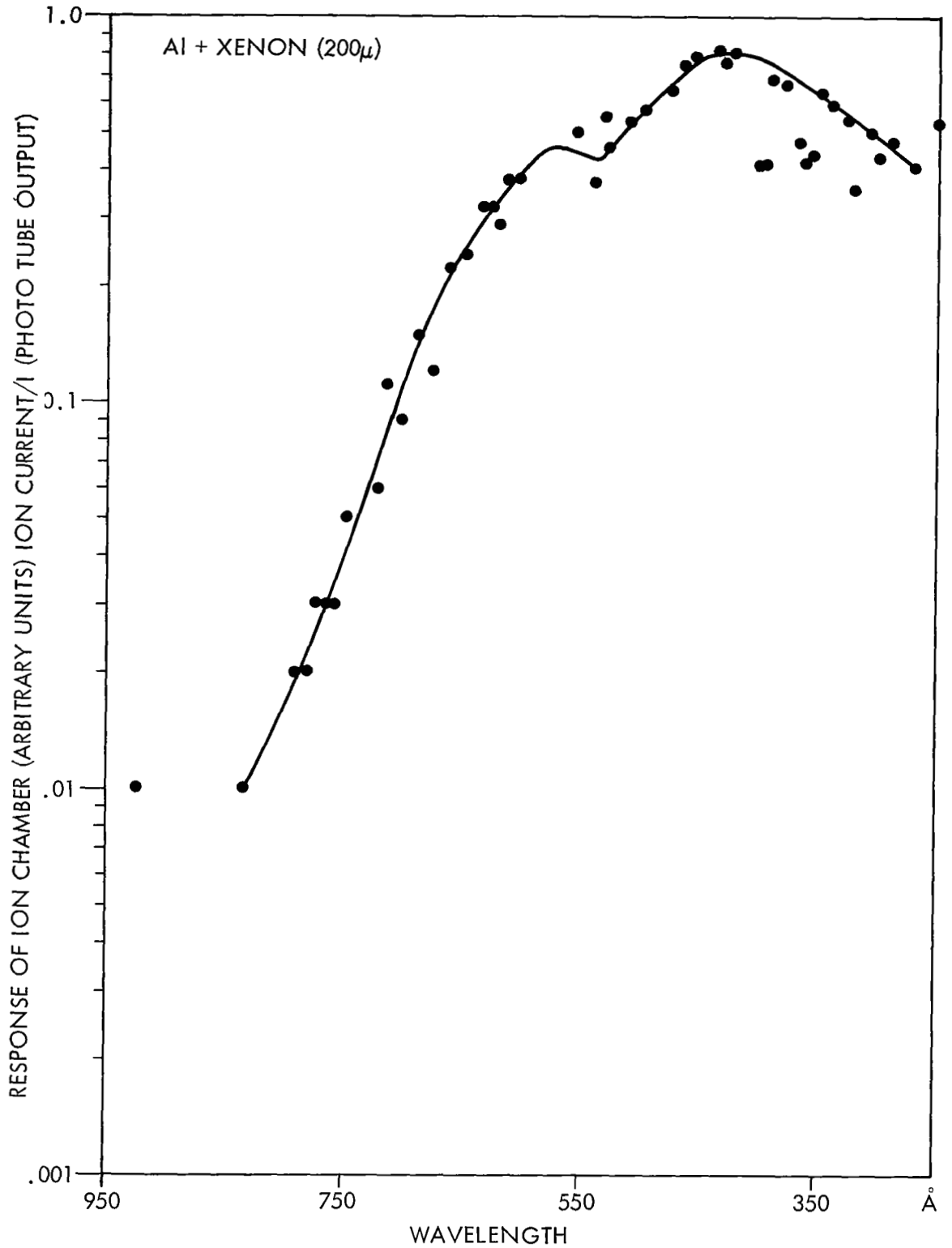

Figure 36. Spectral Response of the Selective Detector Using Aluminum Film and Xenon Gas.

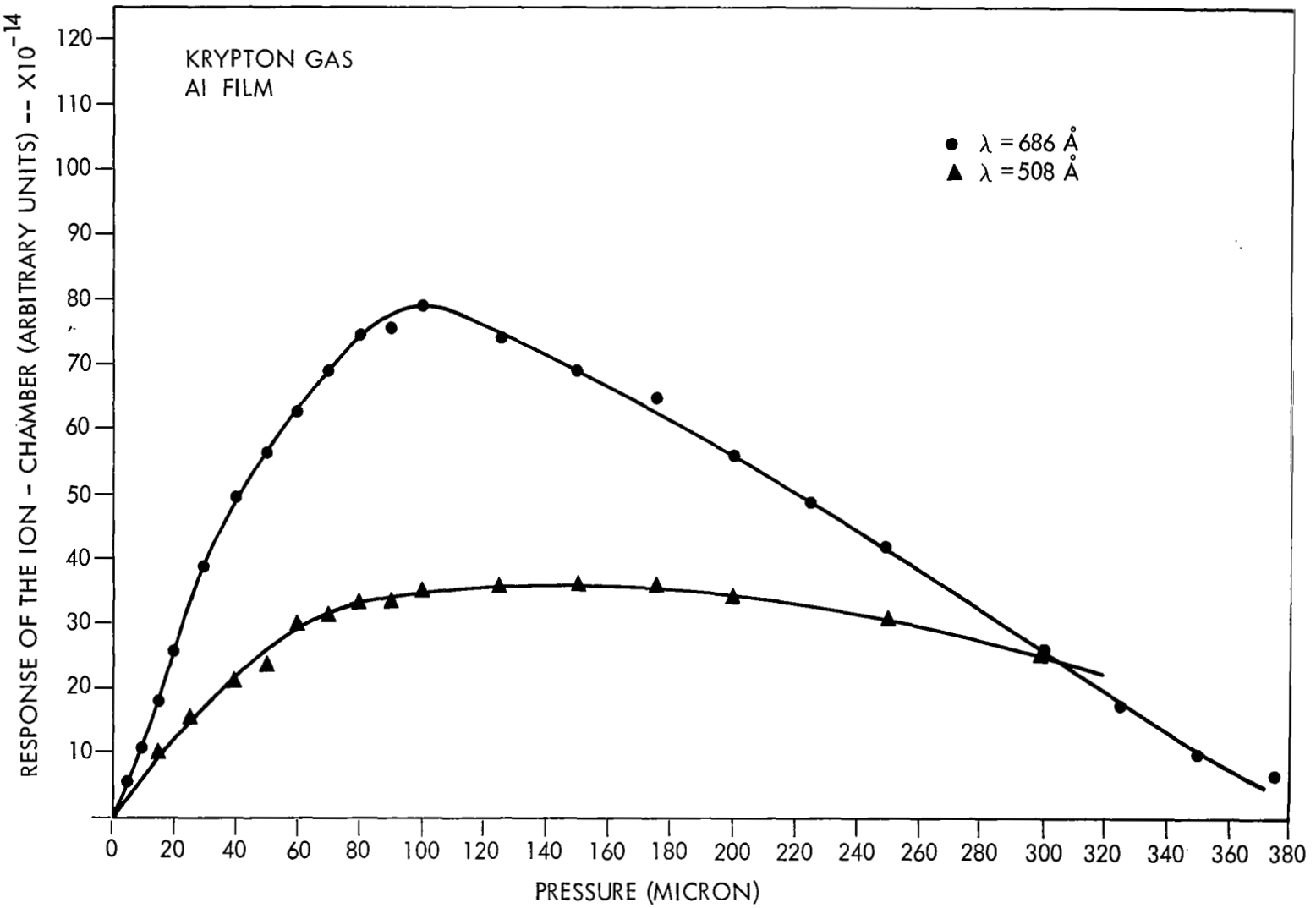

Figure 37. Detector Response as a Function of Krypton Gas Pressure at 686Å and 508Å.

detector response uniformly rises from a value of .001 at 923Å to a value of 0.1 at 600Å, from where it makes a big jump to 0.5 at 555Å and then rises to a value of 0.7 near 250Å.

If all of the gas in the detector were pure neon then the response at 600Å would have been below the limit of our measurements. This seems to indicate that we are never able to evacuate the detector chamber completely or our gases are not pure enough. We then made substantial modifications to our vacuum system so that no gas could find its way to the region between the exit slit of the monochromator and the selective detector. This was accomplished by providing a flap valve between the slit assembly and the diffusion pump and another pumping line immediately in front of the detector. Gas inlet and exhaust lines to the selective detector were separated. We also have modified the electrode system in the selective detector by replacing the mesh screen cylinder by two solid semi-circular cylinders. One of the cylindrical halves acts as a collector of positive ions and the other kept at a high (45 volts) positive potential and connected to the mesh screen in front of the W photocathode to collect all the electrons. The flange carrying the thin film and mosaic glass was electrically insulated from the grounded chamber and kept at a low positive potential to attract any photo-electrons released from the film.

Figure 40 shows the final laboratory set up of the selective detector shown schematically in Figure 23. Before making spectral sensitivity measurements, it was decided to make leak tests around the mosaic glass and thin film. This was achieved by monitoring the pressure in front of the detector by means of an ion gauge. In all the cases studied, the ion gauge reading showed a change from 1.5×10^{-5} mm Hg, when completely evacuated, to 3×10^{-5} mm Hg, when the detector was filled to 1 mm Hg pressure.

The bismuth film prepared for use in the selective detector was evaporated at a pressure of 5×10^{-6} mm Hg from a Mo boat. On floating, it was picked up on mosaic glass with 200μ hole sizes and kept in the

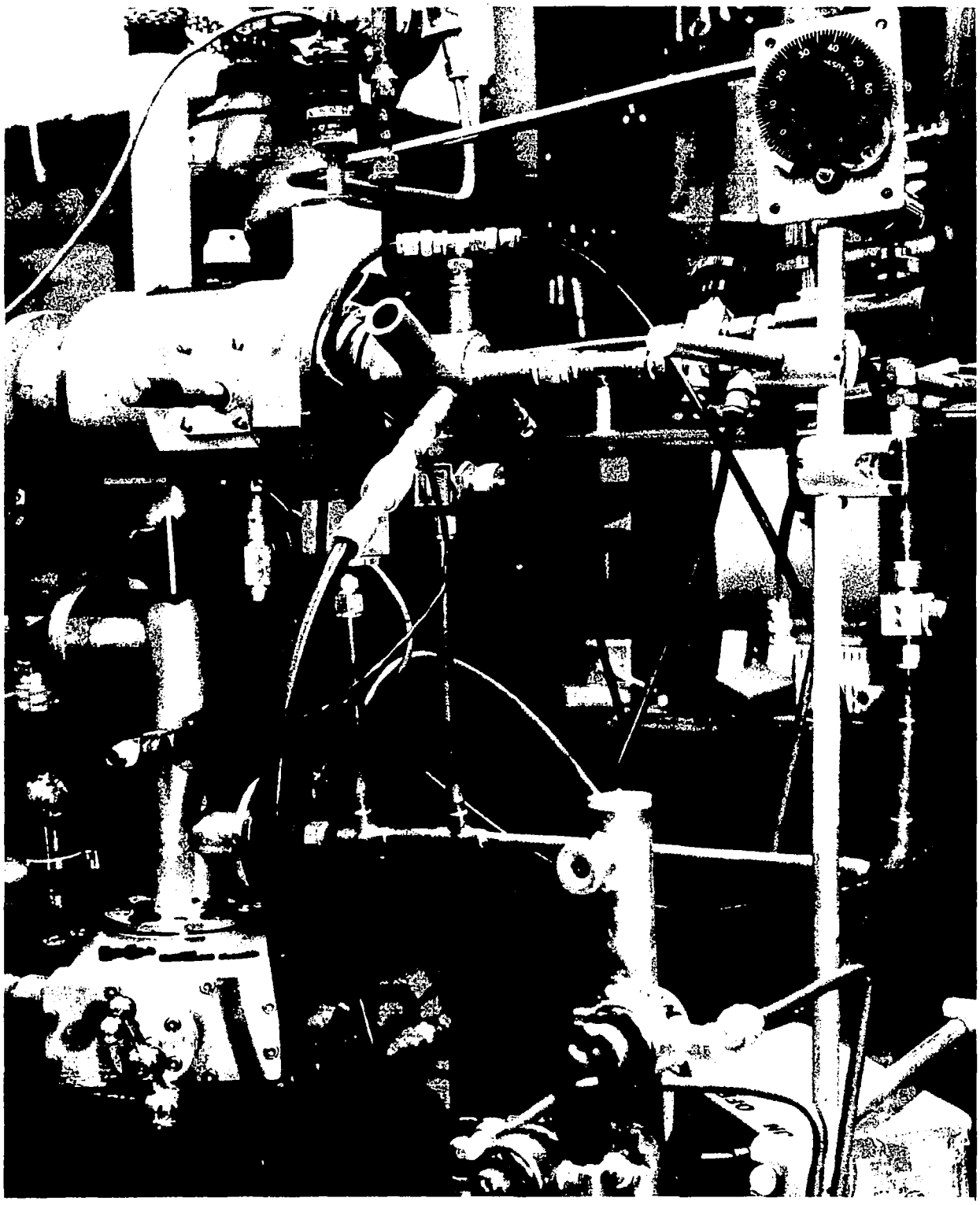

Figure 40 Laboratory Setup of the Selective Detector

desiccator for 24 hours before installation in the system. When the detector was maintained at a pressure of 1.33 mm Hg by introducing argon, the ion gauge reading increased from 1.8×10^{-5} to 3×10^{-5} mm Hg. This guarantees that there is relatively no loss of gas either through or around the thin film.

With complete evacuation of the detector, one should observe signals only at the photocathode and relatively none at the collector. However, a large signal should result at the collector, when the detector is filled with gases and a small signal at the photocathode. The following measurements were carried out with the bismuth film and neon, argon, and krypton gases.

(a) For zero order spectrum

	$I_{Collector}$	$I_{Photocathode}$
No gas	9.0×10^{-14} amp	114×10^{-14} amp
Argon at 950μ	900×10^{-14} amp	$< 1 \times 10^{-14}$ amp

(b) Figure 41 shows the current measured at the W photocathode with no gas in the detector. Only the 555Å radiation was strong enough to be registered. No observable signal was monitored at the collector in the 500 to 800Å region.

Figure 42 shows the pressure dependence of the detector output ($I_{Collector}$) at the zero order spectrum using argon gas. It is clear that the signal saturates around 475 microns of pressure and then remains constant out to 950 microns. A similar measurement at the photocathode resulted in no signal above 570 microns of pressure indicating that all the radiation reaching the photocathode had been absorbed.

Figure 43 shows the detector output ($I_{Collector}$) both at the zero order and first order when the ion chamber is filled with neon gas. The pressure of neon gas was well above 1mm Hg and could not be measured by the attached thermocouple. However, the ion gauge pressure increased to 2.7×10^{-5} mm Hg only. The spectral response is limited only between 525Å and the

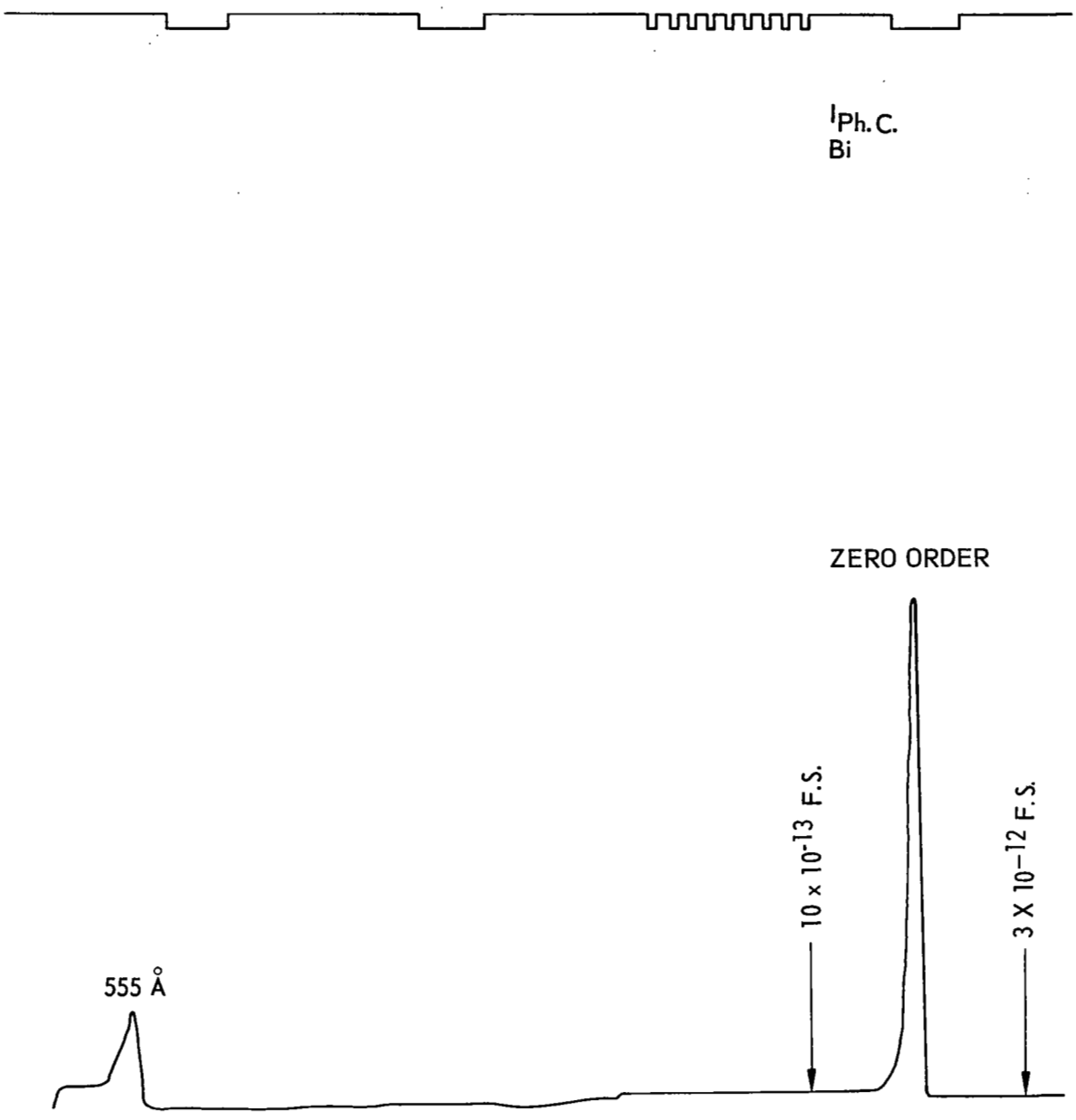

Figure 41. Photocathode Signal Using Bi Film Without Gas.

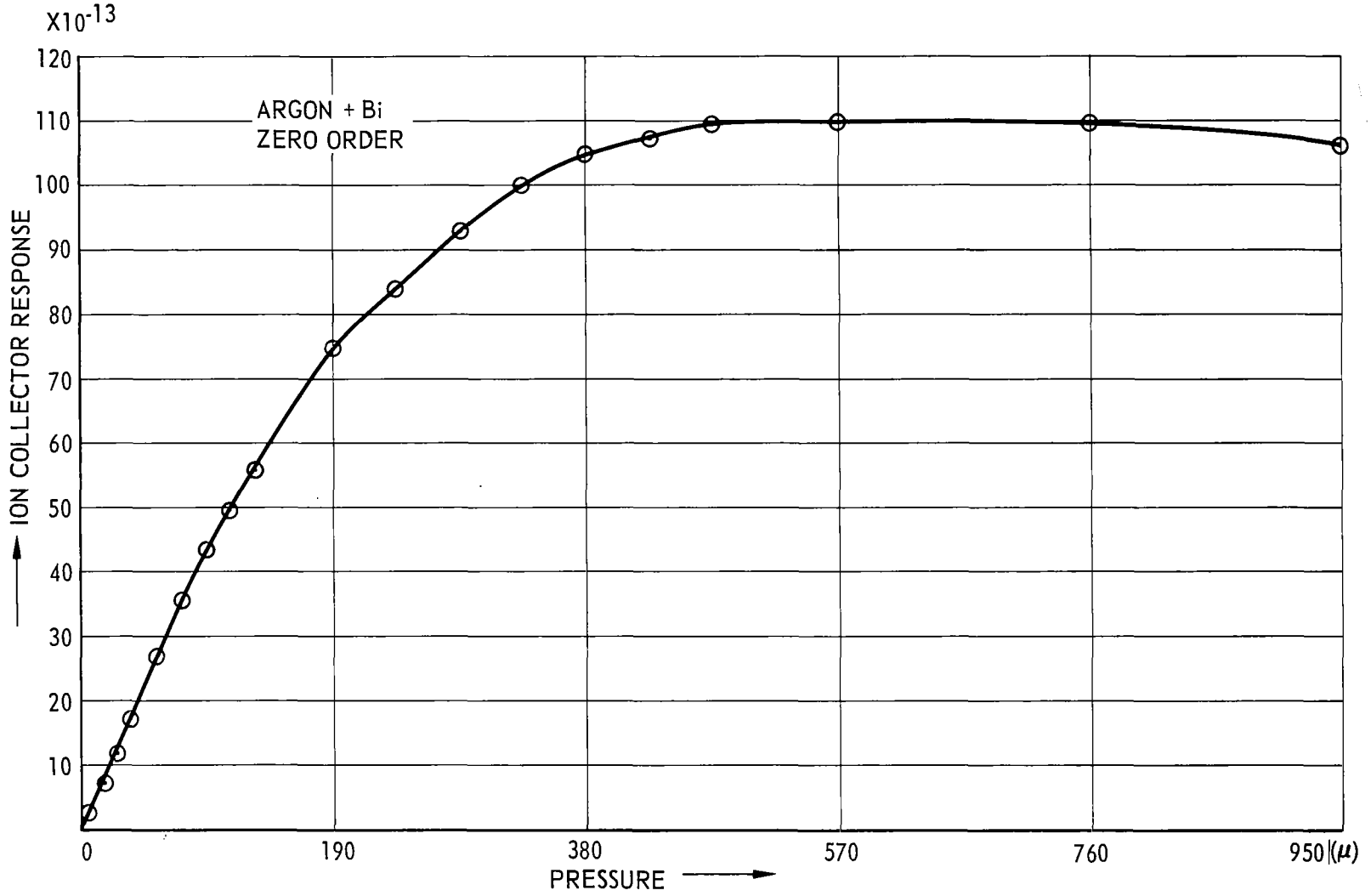

Figure 42. Pressure Dependence of the Detector Output Using Bi Film and Argon Gas at Zero Order Spectrum.

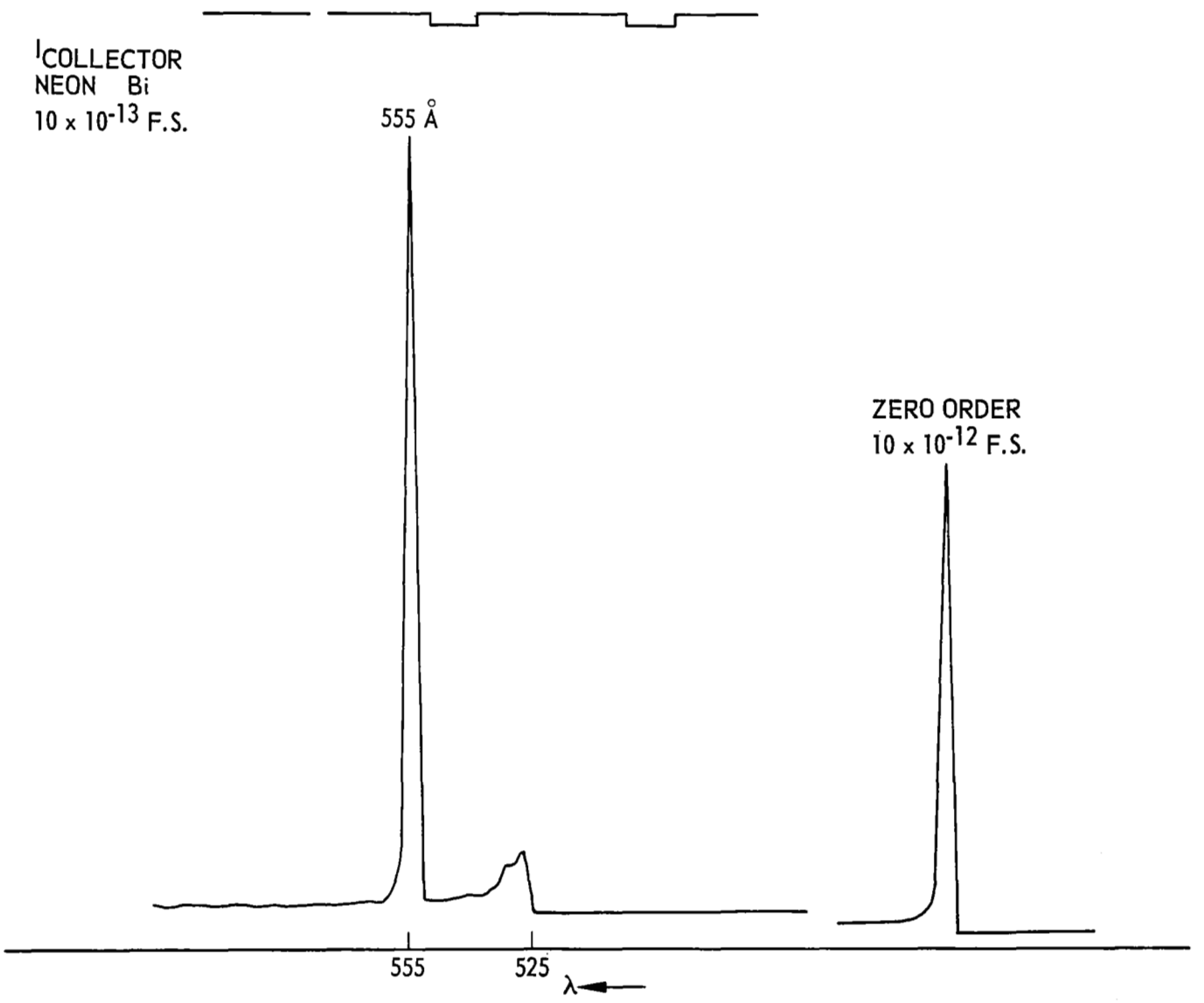

Figure 43. Spectral Trace of the Detector Output Using Bi Film and Neon Gas.

ionization limit of neon, namely 580Å. Since there were no strong lines between 555Å and 601Å, we were not able to see the sharp cut-off in response at 580Å. However, radiation above 580Å which is registered with argon and krypton filled ion chambers is not seen with neon.

Figure 44 shows the spectral trace of the detector output ($I_{Collector}$) using argon gas at 665 microns of pressure. It is shown that this detector is sensitive over the wavelength region between 520Å and 787Å, these being the cut-off in transmission of the film and the ionization onset limits of the gas respectively. Because of the large thickness of the film used, the response of the detector is negligible for wavelengths above 700Å. It should, however, be noted that the response of the detector having a Bi film and two different gases is identical over the overlapping region. This is also true when the gas chosen is krypton. Figure 45 shows the spectral trace of the detector using a bismuth film and krypton gas at 700 microns. The detector output showed no pressure dependence with krypton between 450 - 1000 microns of pressure and decreased slightly beyond 1 mm of pressure.

After the measurements on the detectors consisting of the Bi film and various rare gases were completed, attempts to prepare indium films were made. The indium film, evaporated from a Mo boat in only 5 seconds at a pressure of 1×10^{-6} mm Hg was successfully floated off in water and picked up on a mosaic glass. After drying it for 24 hours in the desiccator, it was mounted on the flange of the selective detector using a conventional O-ring seal. The following measurements were carried out one week later because of malfunction in the light source switching circuit.

First, a spectral run was made with the detector completely evacuated. The output measured at the cathode gave the amount of radiation entering the ion chamber after it had passed through the indium film and the mosaic glass. Figure 46 shows the spectral trace representing the intensity of the radiation entering the ion chamber as measured at the tungsten photocathode by the photo-emission current. The collector is kept at 45 volts negative while the other cylindrical electrode

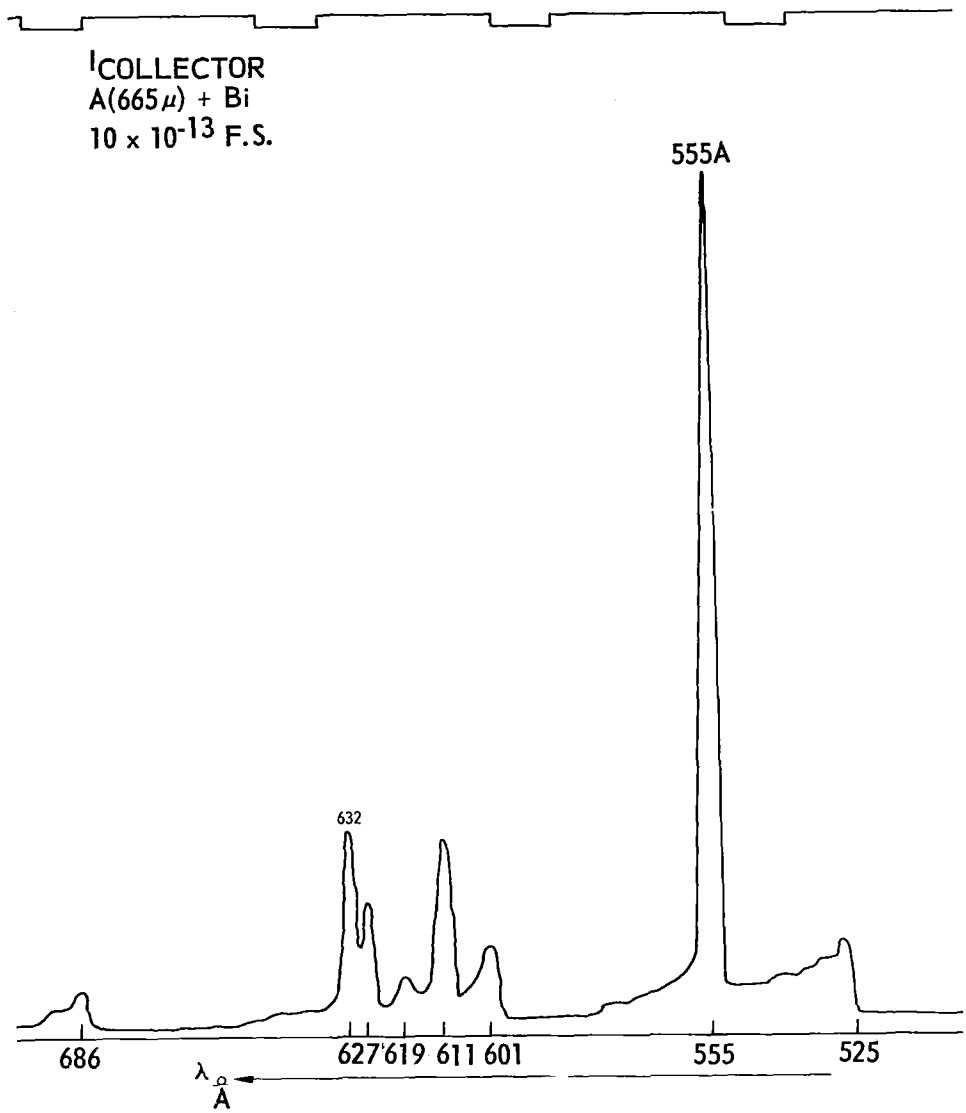

Figure 44. Spectral Trace of the Detector Output Using Bi Film and Argon Gas.

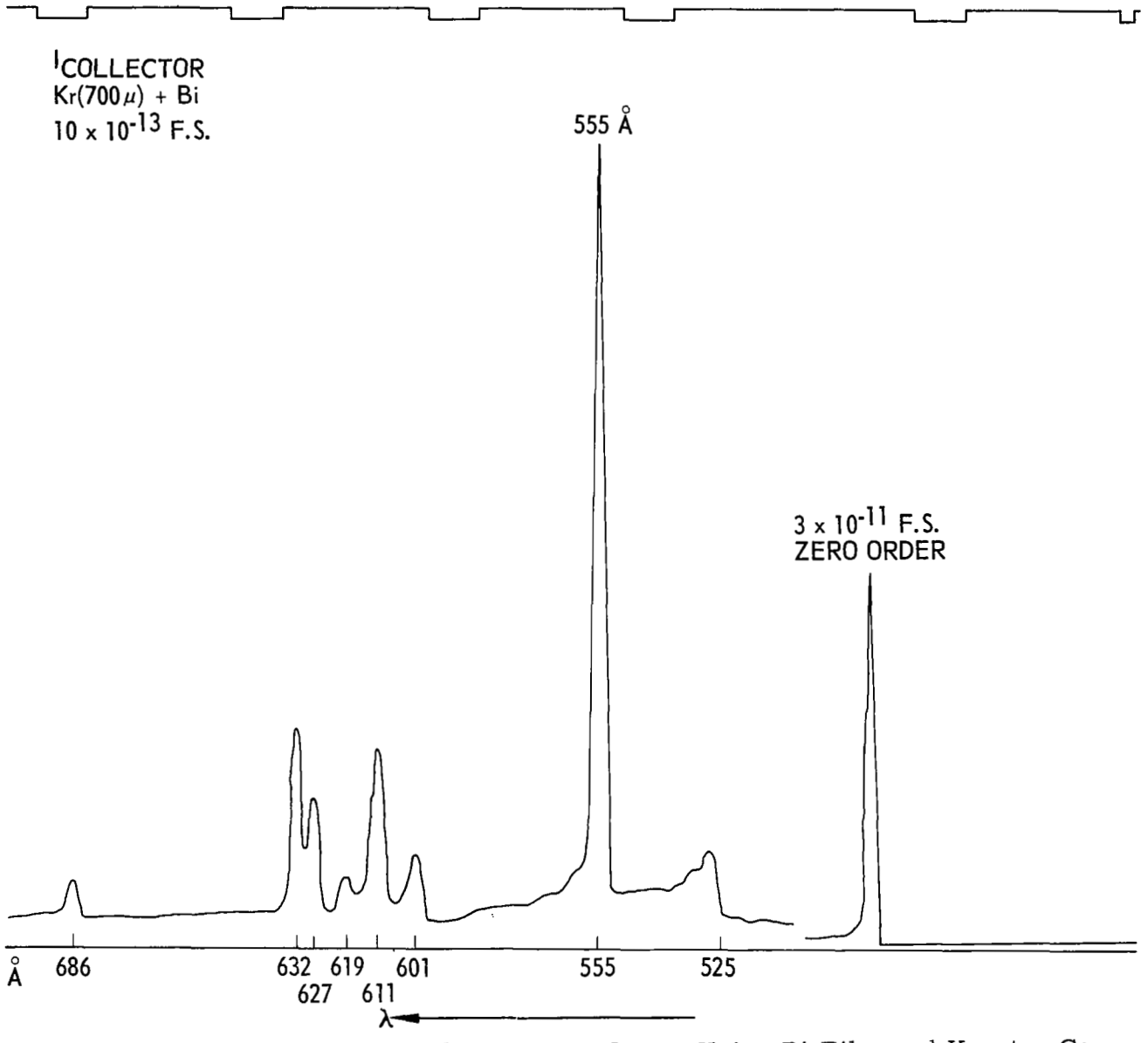

Figure 45. Spectral Trace of the Detector Output Using Bi Film and Krypton Gas.

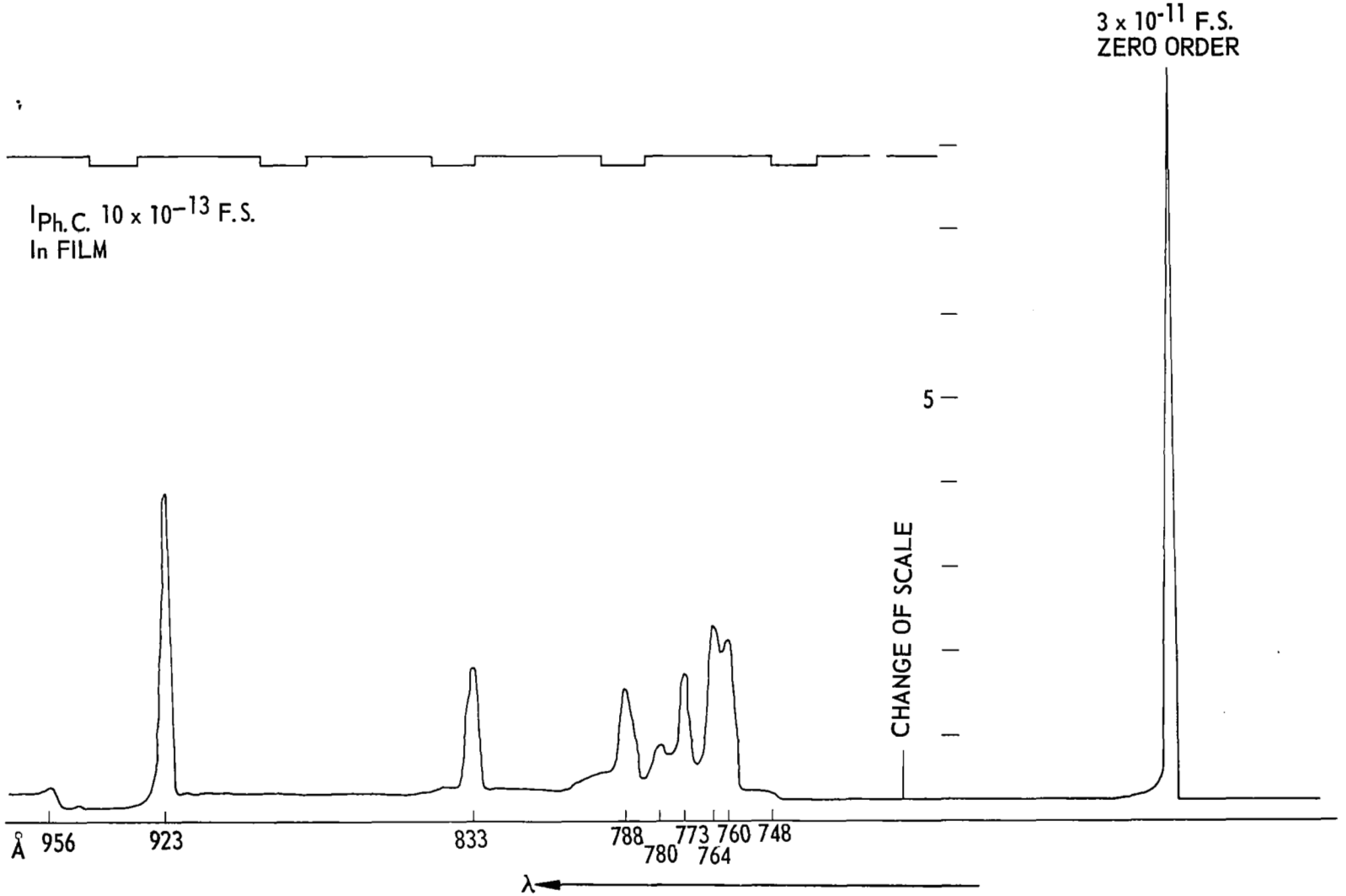

Figure 46. Photocathode Signal Using Indium Film Without Gas.

and the grid are kept at 20 volts positive. In all the measurements, the film flange is kept at 45 volts positive. When the signal was measured at the collector, the cathode was kept at 45 volts positive. The collector signal at the zero order was measured at 1.5×10^{-12} amp. while the response in the first order spectrum over the wavelength range between 740 - 1100Å was less than 1×10^{-14} amp.

Argon was then introduced in the ion chamber and maintained at 760 microns. Figure 47 shows the ion current collected at the collector both for the zero order spectrum and the first order spectrum. It is evident that the response is limited to a very narrow wavelength interval of 47Å between 787Å and 740Å. Even though radiation of higher intensity enters the ion chamber, it is not producing any signal at the collector. By fixing the grating position at 773Å, the pressure dependence of the output current at the collector was measured. Figure 48 shows the ion current at the collector as a function of pressure and indicates the constancy of the response between 475 and 950 microns. Simultaneous measurement of the signal at the photocathode, shown in Figure 49, in an atmosphere of argon gives indications of radiation only between 787Å and the transmission onset of In at approximately 1100Å.

Measurements of the detector response using krypton gas are reported in Figure 50. It should be noted that the range of spectral sensitivity has been increased to 148Å between 740Å and 888Å. The response in the zero order has almost doubled from that in which argon was used. A small indication at 923Å is ascribed to an impurity content in krypton. The pressure dependence using the zero order spectrum is indicated in Figure 51. Simultaneous measurement of the photocathode output, as shown in Figure 52, results in a lower signal at the zero order and at 923Å radiation with reduced intensity (effect of krypton gas on W photocathode).

If the photoelectric yield of W is known under various gaseous environments, then two simultaneous measurements, one at the collector and the other at the photocathode will result in photon flux measurements in two different wavelength intervals with no overlap.

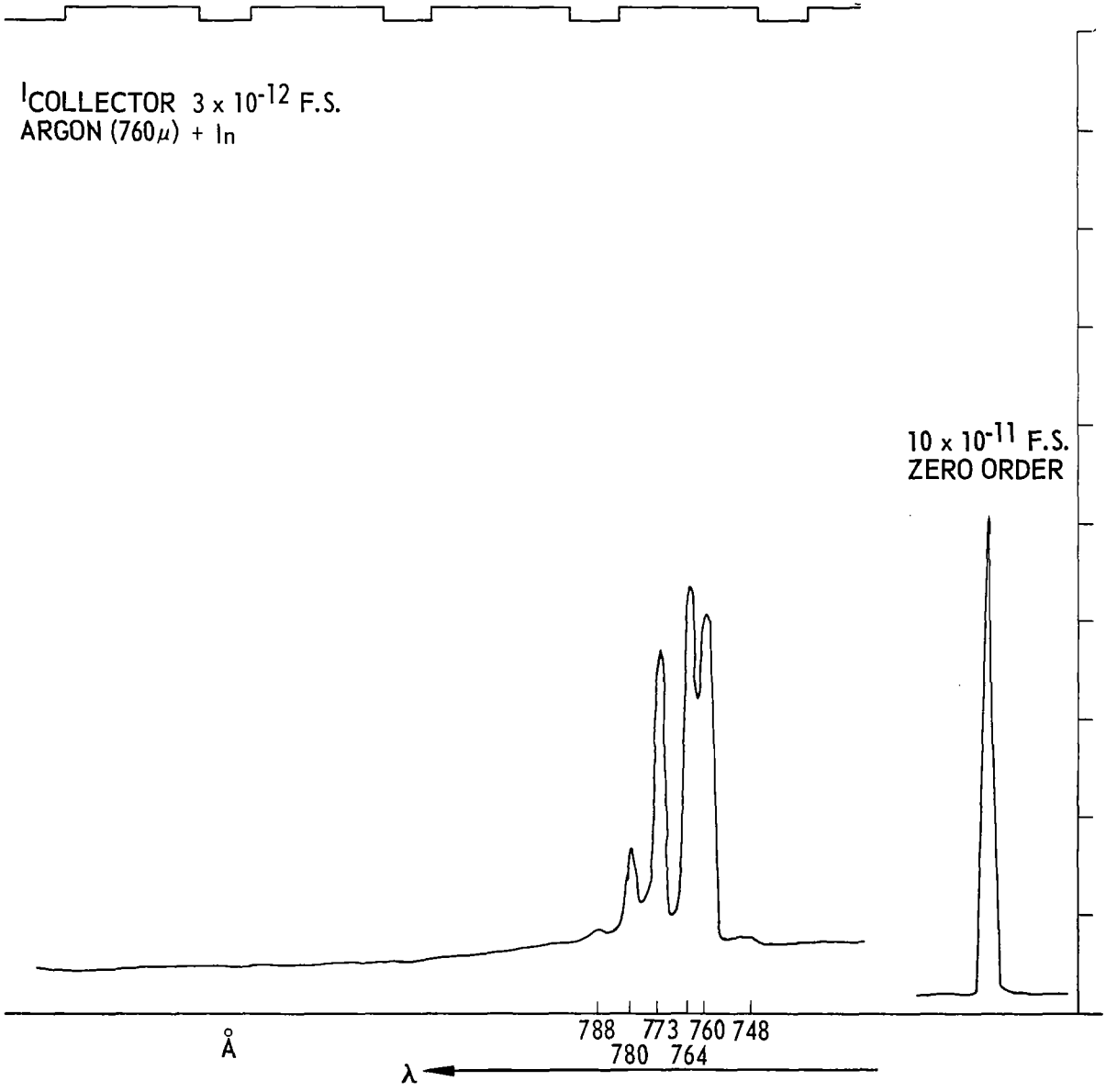

Figure 47. Spectral Trace of the Detector Output Using In Film and Argon Gas

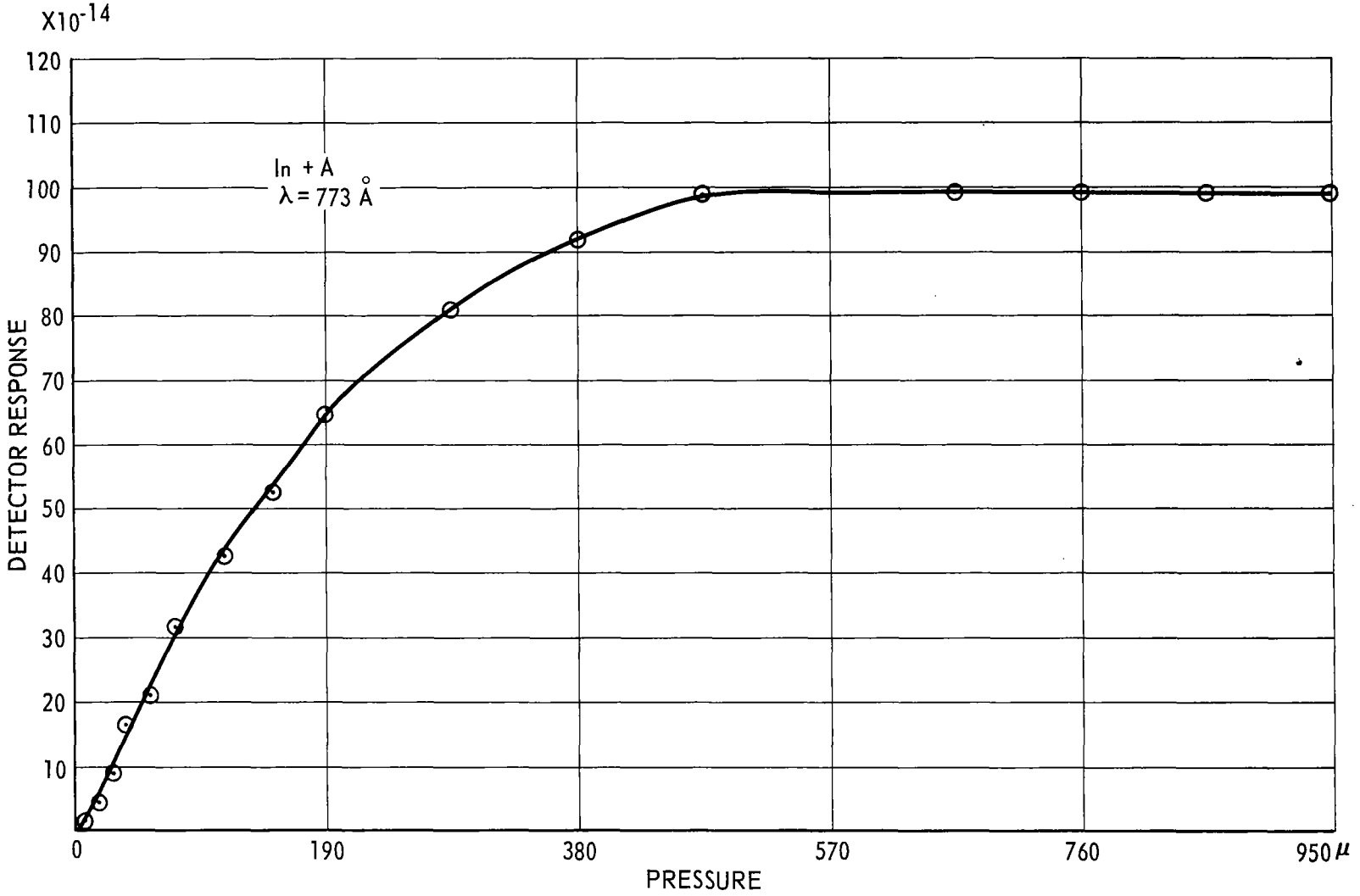

Figure 48 Pressure Dependence of the Detector Output Using in Film and Argon Gas at 773 Å

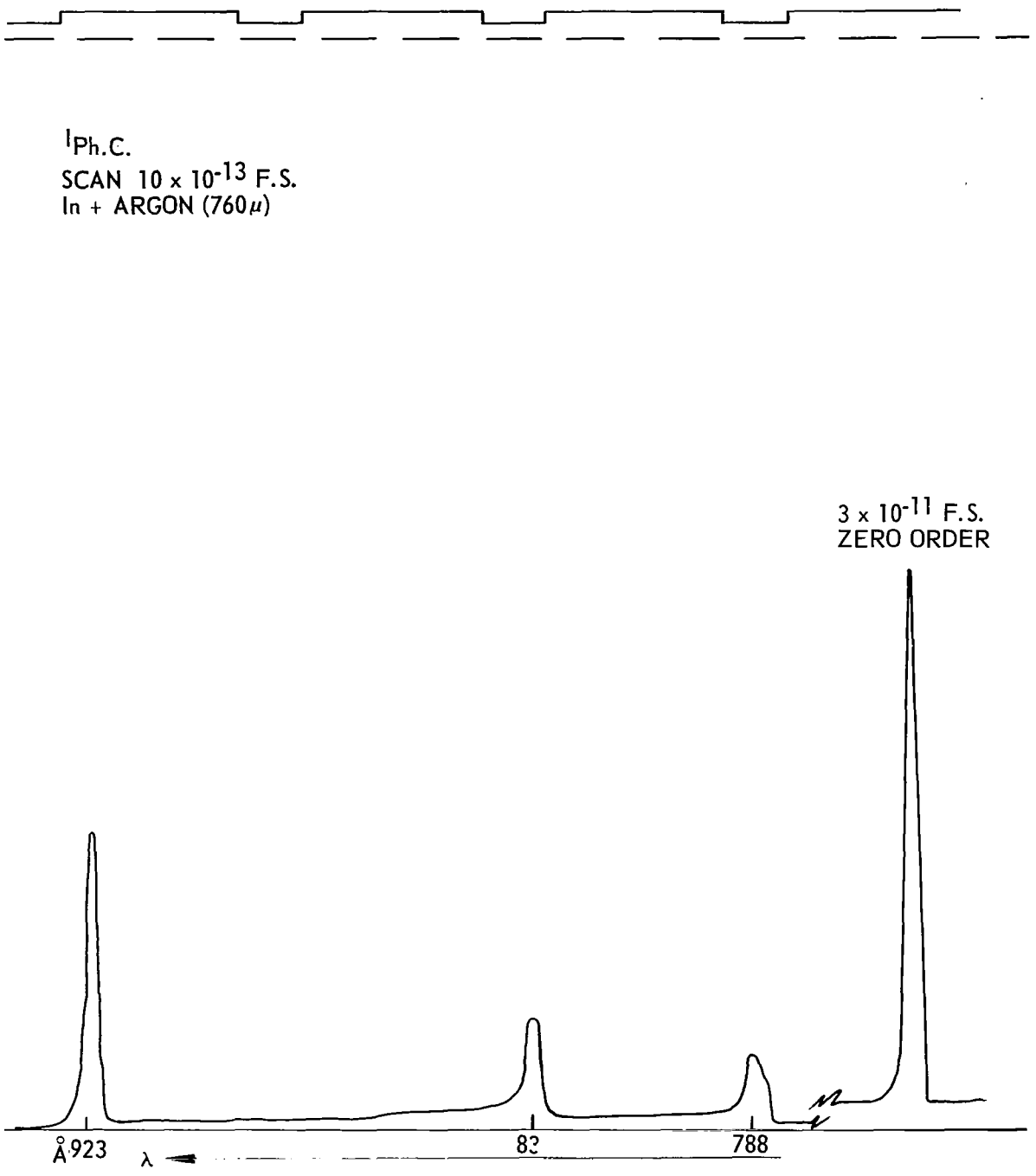

Figure 49 Spectral Trace of the Photocathode Output Using In Film and Argon Gas

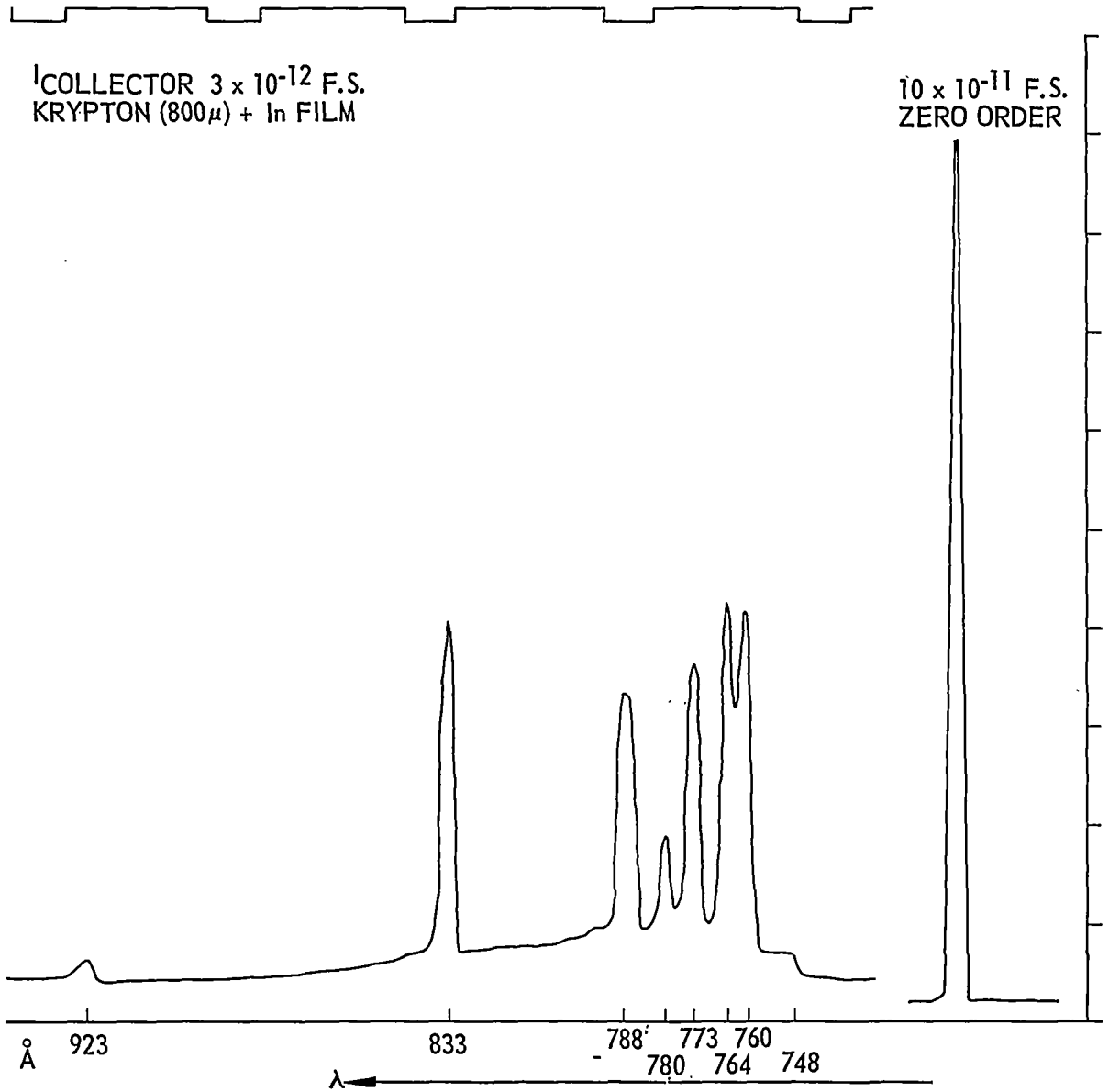

Figure 50 Spectral Trace of the Detector Output Using In Film and Krypton Gas

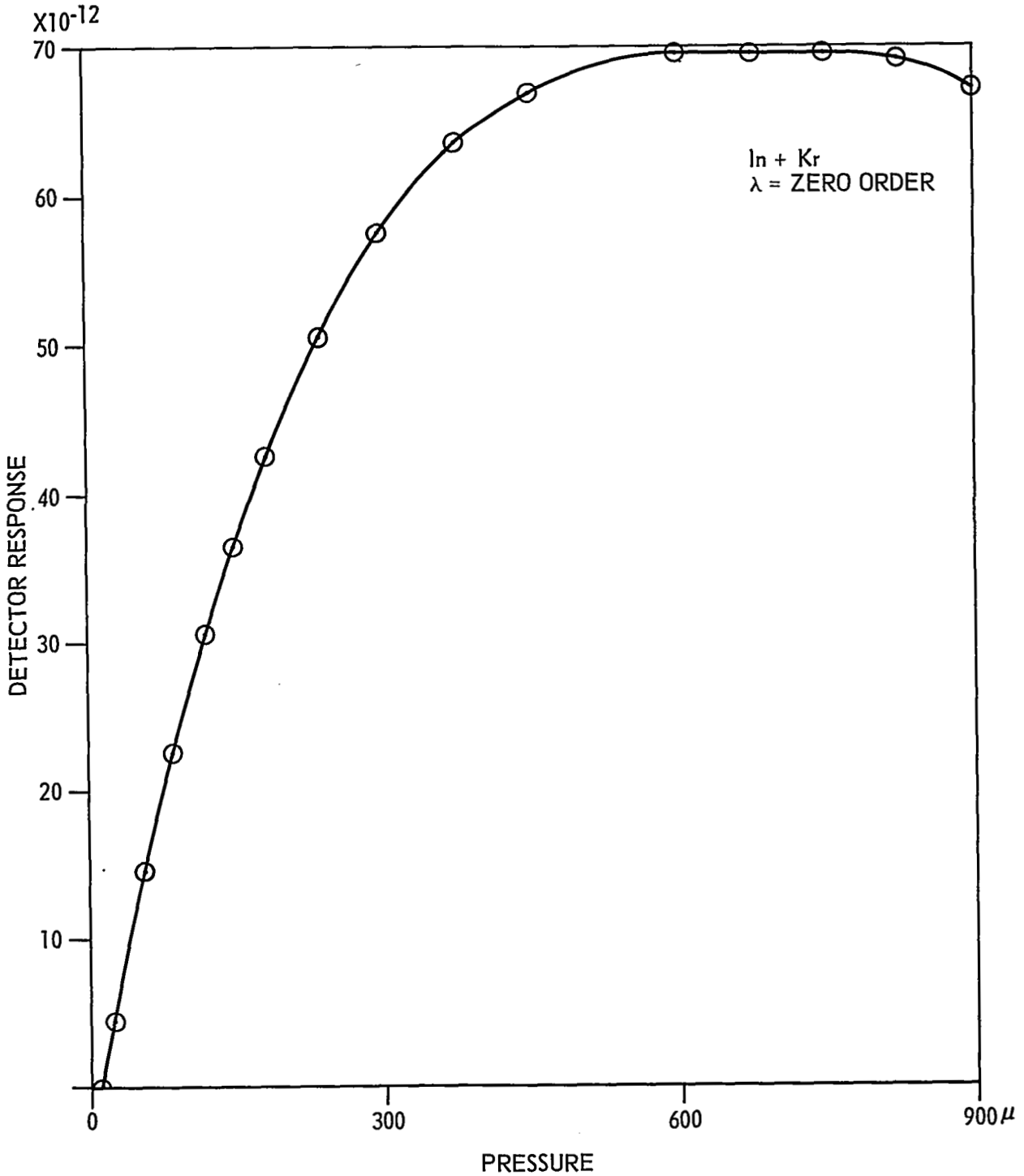

Figure 51 Pressure Dependence of the Detector Output Using In Film and Krypton Gas

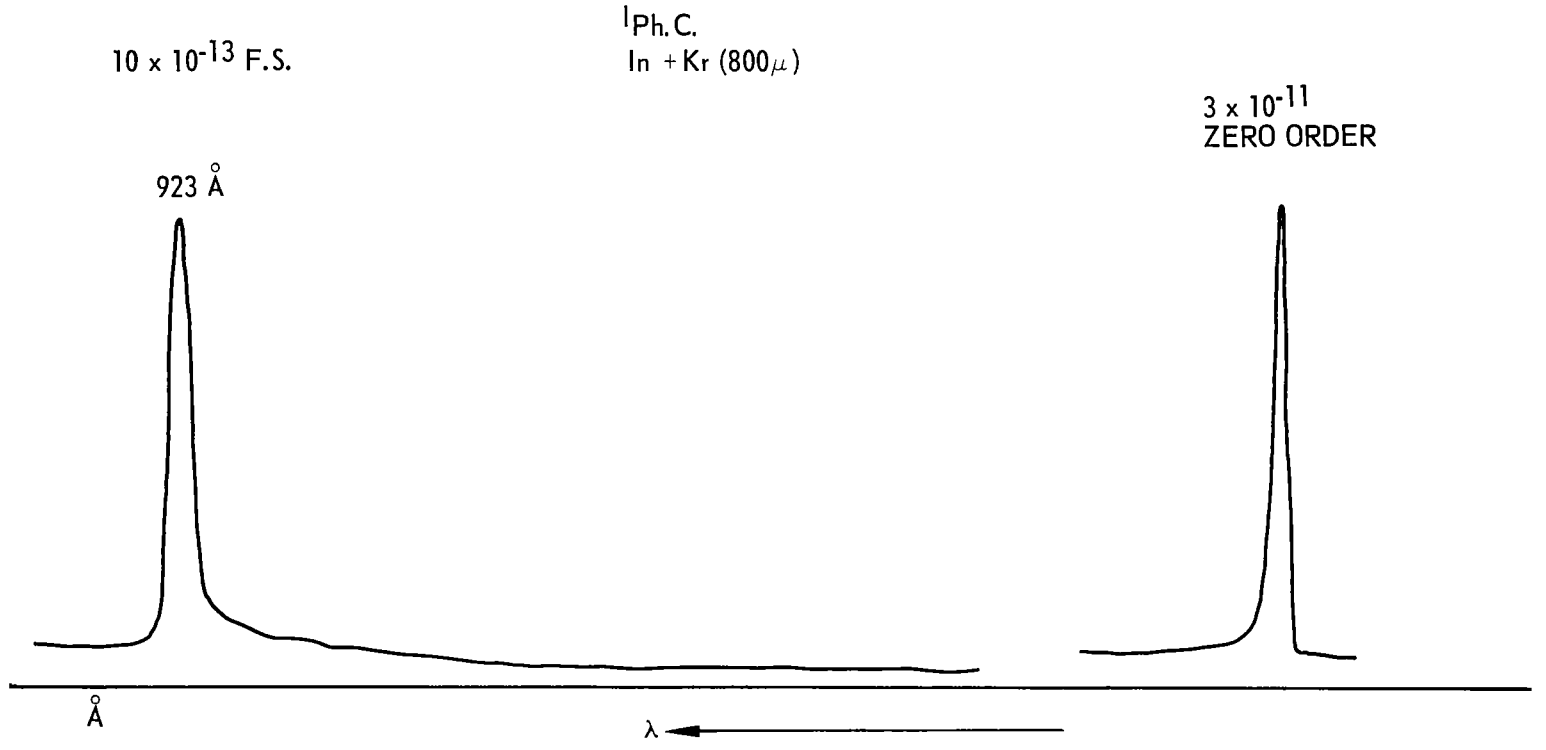

Figure 52 Spectral Trace of the Photocathode Output Using In Film and Krypton Gas

Using xenon gas at 520μ of pressure in the ion chamber increases the spectral sensitivity over the wavelength interval between 740 and 1022Å. Figure 53 shows the spectral trace of the detector output as measured at the collector of the selective detector both in the zero order and in the first order of the spectrum. The response at the zero order spectrum has increased from that when krypton was used. Simultaneous measurement at the photocathode resulted in a current of only 4×10^{-14} amp compared to a value of 2.7×10^{-11} amp when no gas was present. This small signal is representative of the radiation which is filtered both by the gas and the indium film and lies between 1022 and 1120Å. Figure 54 shows the pressure dependence of the detector output with xenon gas and an In film at 773Å radiation.

It should, however, be stated that all the measurements reported thus far were taken by using nitrogen in the light source and covered the wavelength region between 1000Å and 520Å.

In order to cover the wavelength region below 500Å, a fresh film of Ti was prepared by evaporating it from a tungsten boat at 3×10^{-6} mm Hg pressure. This film was floated off in water and subsequently picked up on a mosaic glass. After drying it in the desiccator over night, it was cemented to the flange by means of quartz cement. This cement, when heated to 300 degrees F, adheres to metallic surfaces very smoothly and has a very low vapor pressure at room temperature. Immediately upon application of this cement to the flange, the mosaic glass supporting the film is placed gently over it and pressed down uniformly. After checking the ion chamber for any leakage around the film, the following measurements were carried out.

As before, the selective detector was evacuated to a pressure of 2.2×10^{-5} mm Hg. The light source gas was changed from nitrogen to argon to obtain more incident radiation between 900Å and 300Å.

Figure 55 shows the spectral response of the selective detector using a titanium film and argon gas at 1.2mm Hg pressure and the intensity of radiation at the exit slit of the monochromator as measured by a 9514S EMI

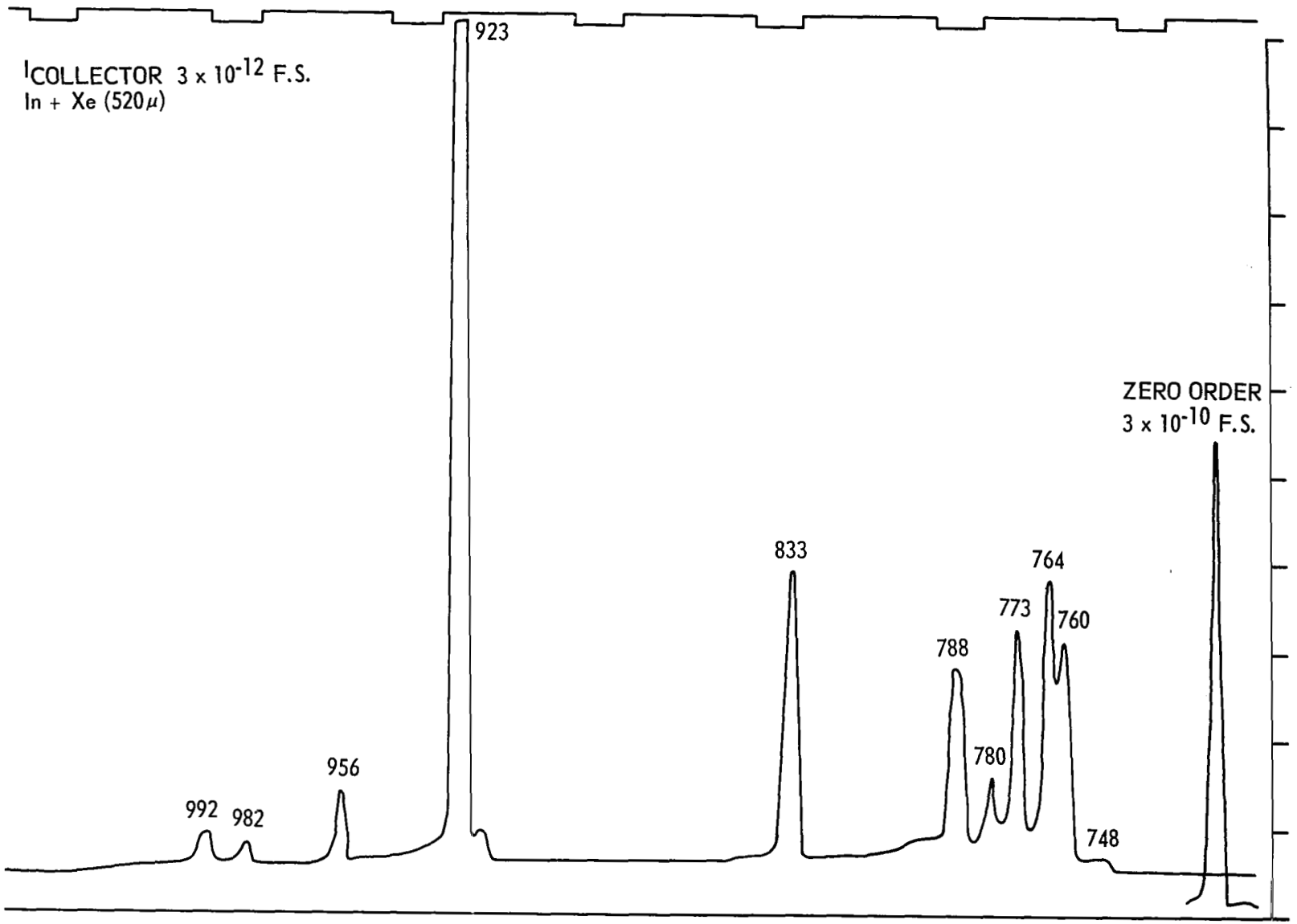

Figure 53 Spectral Trace of the Detector Output Using In Film and Xenon Gas

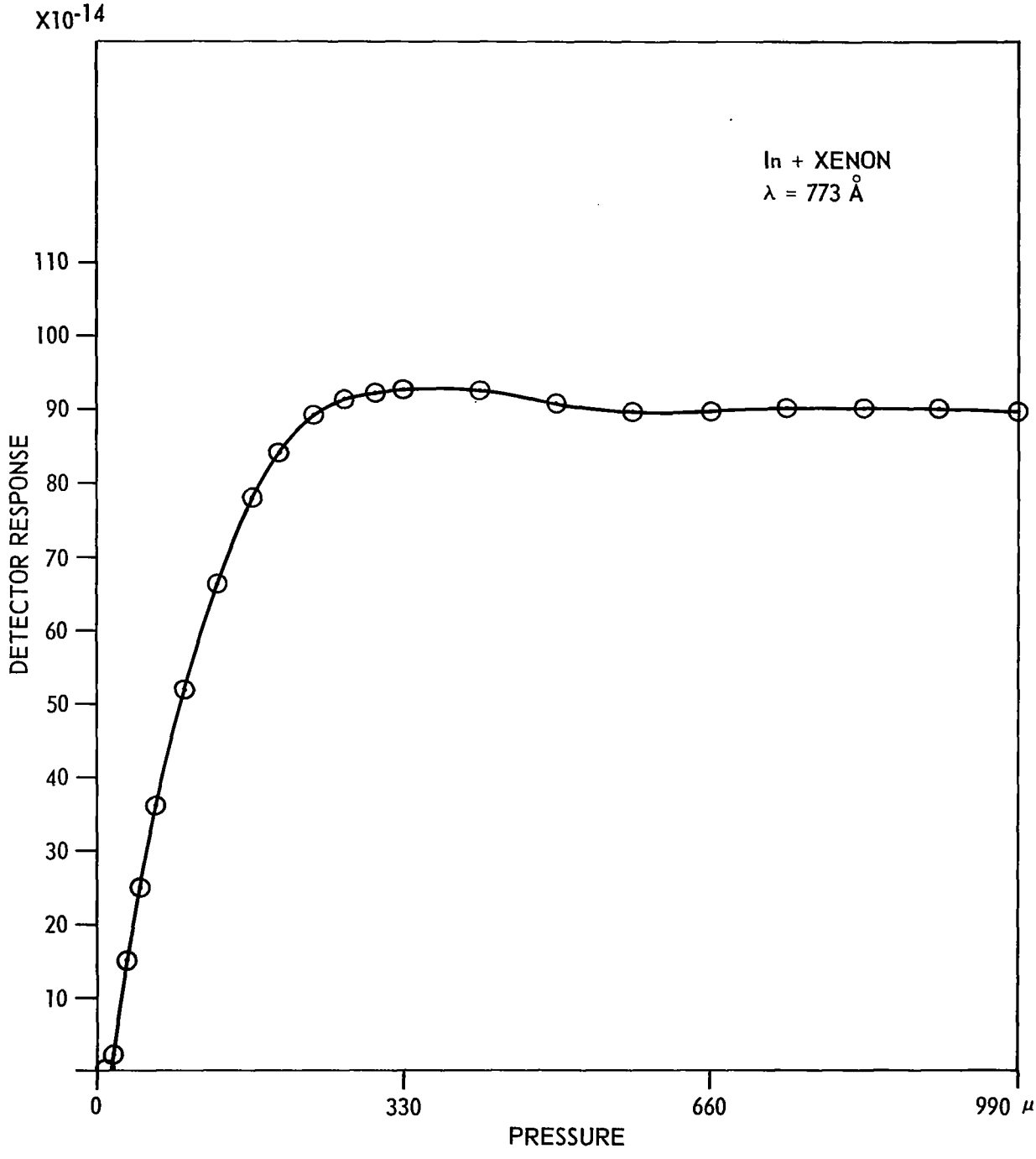

Figure 54 Pressure Dependence of the Detector Output Using In Film and Xenon Gas

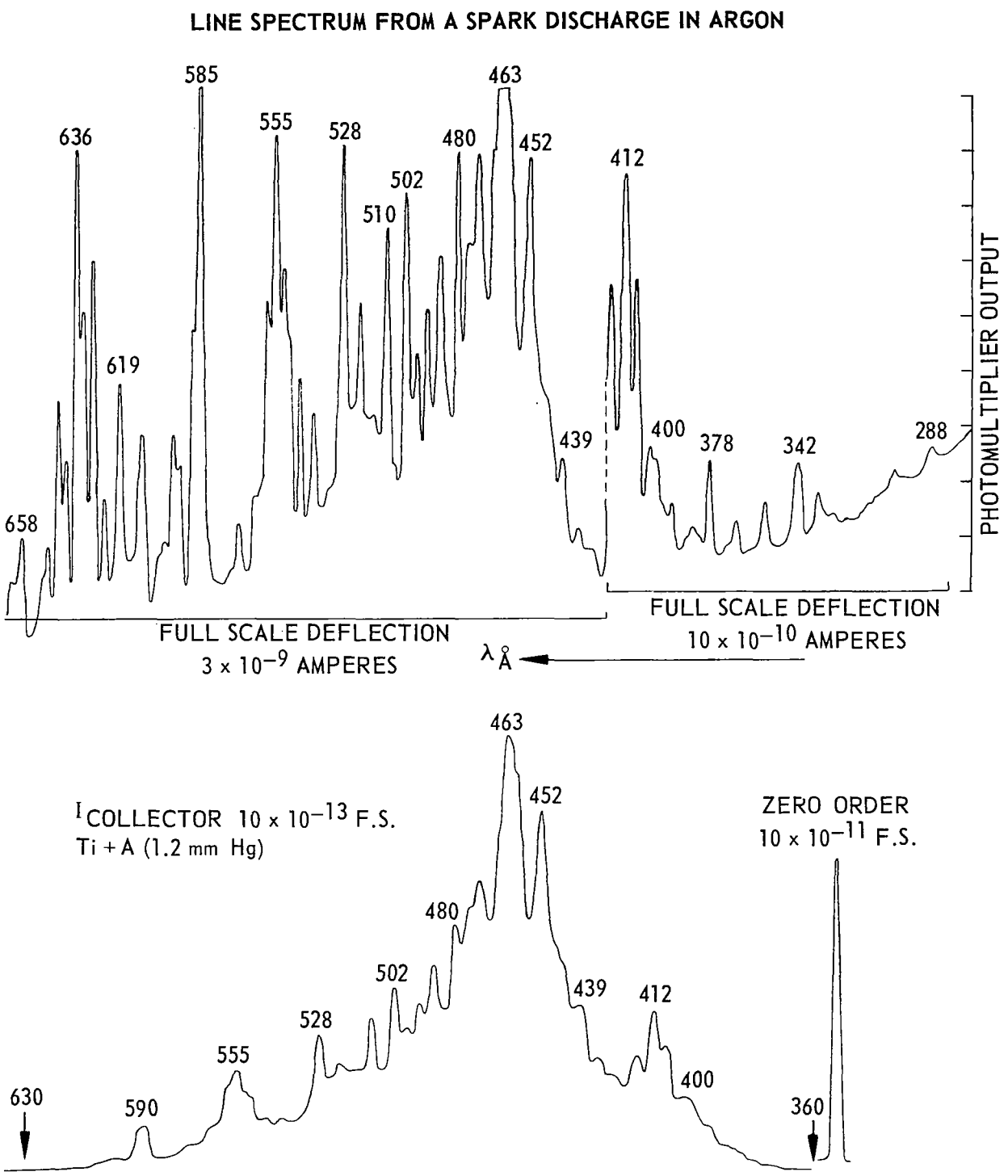

SPECTRAL RESPONSE OF THE SELECTIVE DETECTOR USING Ti FILM AND ARGON GAS

FIGURE 55

photomultiplier tube which had been sensitized by a uniform coating of sodium salicylate to respond to these radiations. The collector current, due to positive ions generated by the zero order spectrum in the chamber, is measured on the 10 x 10^{-11} amp scale (shown on the right of the lower trace) while the current due to positive ions generated by the radiation in the first order spectrum is measured on the 10 x 10^{-13} amp scale. Since argon is ionized at all photon energies larger than the photoionization threshold energy of approximately 15 ev and titanium transmits all radiation between 680Å and 325Å with maximum transmittance near 400Å,[52] we should observe the ion current at the collector between these ranges. The reason for no signal on the long wavelength side of 630Å or on the short wavelength side of 360Å is the low transmittance of the titanium film used here. This fact is supported by the traces, shown in Figure 56, where the upper trace shows the intensity of radiation at the exit slit of the monochromator as measured by the photomultiplier tube and the lower trace shows the photocurrent at the tungsten photocathode caused by the radiation which is filtered by the titanium film on the mosaic glass when no gases are present in the detector. The zero order response, shown on the right side of the lower trace, is measured on the 10 x 10^{-12} amp scale which is an order of magnitude less than the one obtained at the collector when complete absorption takes place in argon.

Fixing the grating for the zero order spectrum, we measure the ion current at the collector as a function of pressure of argon gas in the ion chamber. Figure 57 shows the results of these measurements. The current due to positive ions increases with pressure up to approximately 400 microns where it attains its maximum and remains constant until the pressure increases to 1 mm Hg. Measuring the current at the tungsten photocathode at this pressure resulted in a signal of less than 1 x 10^{-14} amp, indicating complete absorption.

After measurements with argon gas in the ion chamber were completed, the system was evacuated and subsequently neon gas was allowed to flow through the ion chamber until all traces of argon gas were eliminated. Figure 58 shows the spectral response of the detector using a titanium

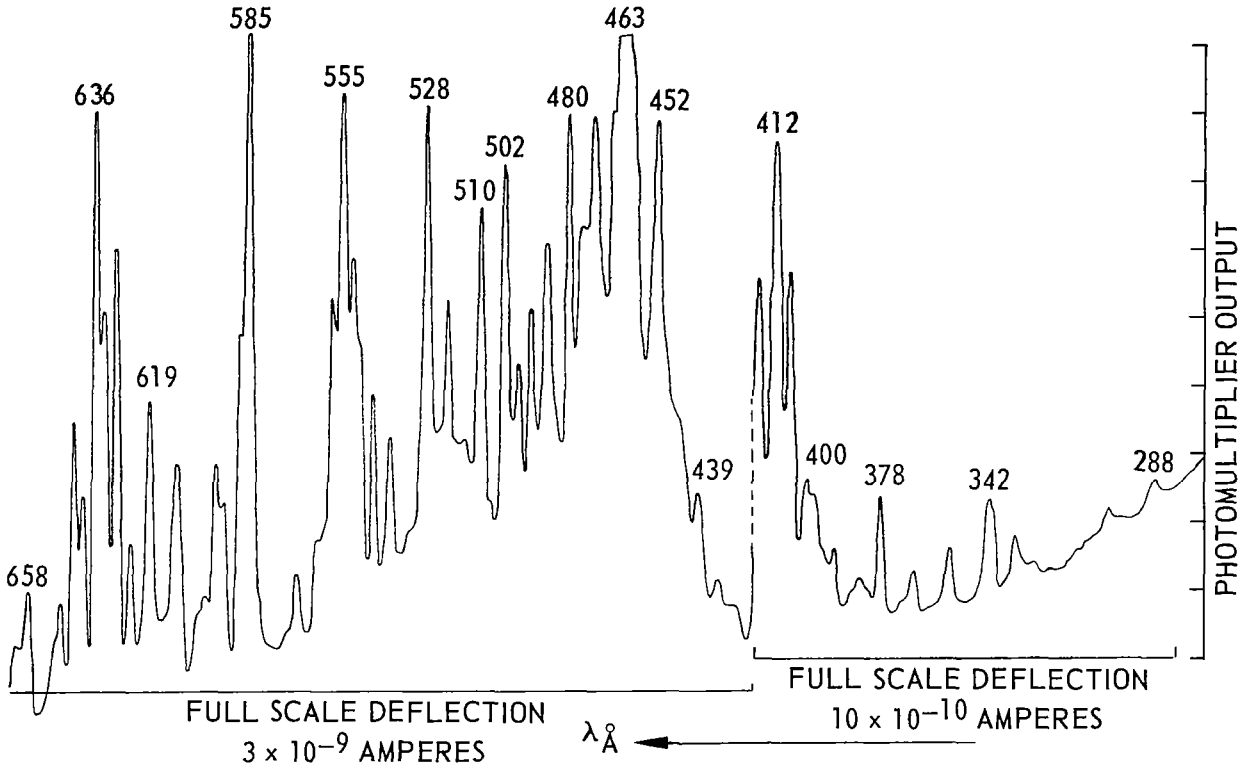

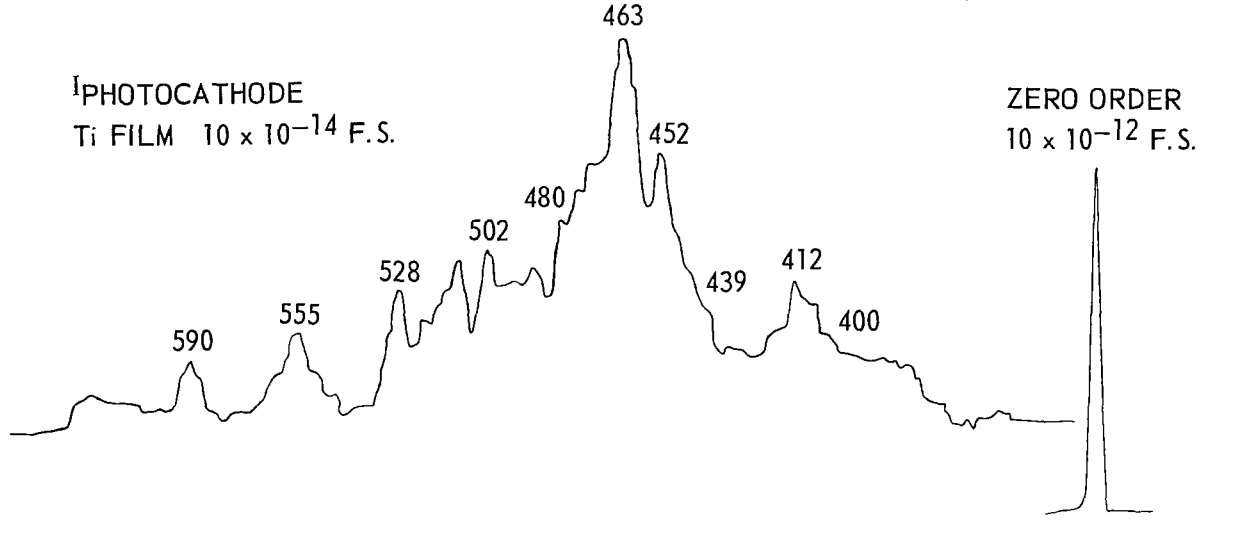

SPECTRAL RESPONSE MEASURED AT THE PHOTOCATHODE USING Ti FILM WITHOUT GAS

FIGURE 56

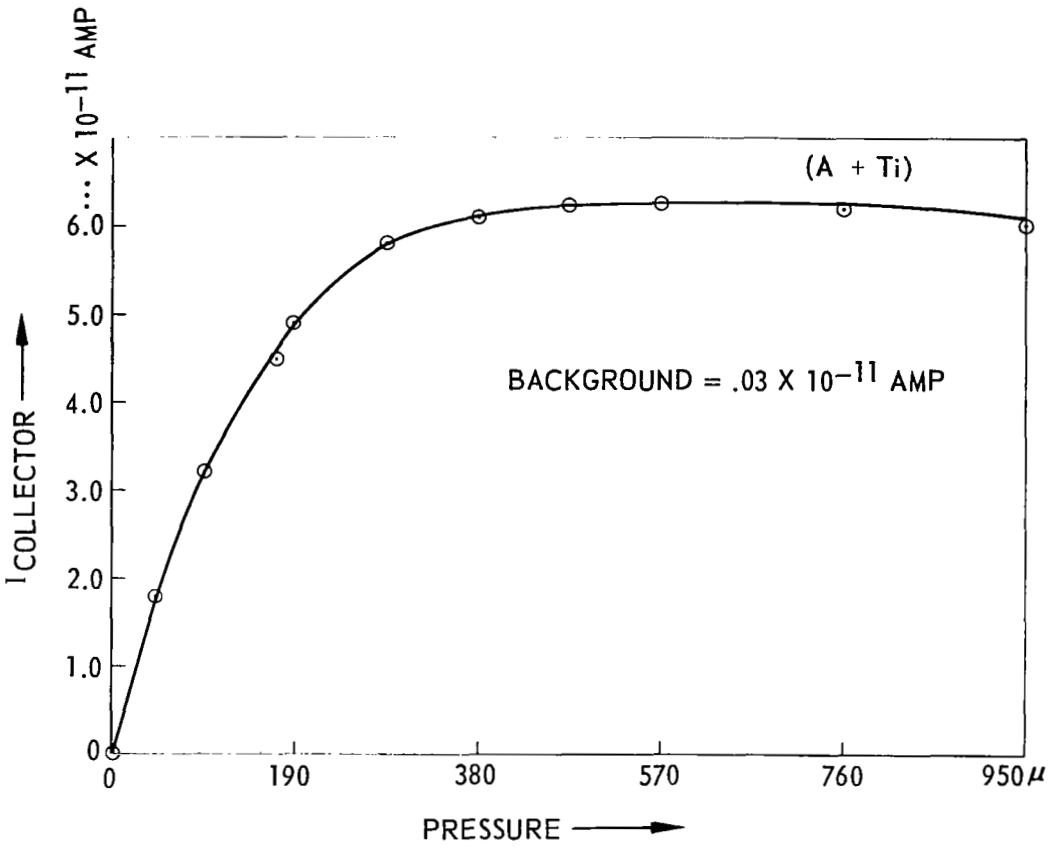

Figure 57 Pressure Dependence of the Collector Response Using Ti Film and Argon Gas

film and neon gas. The lower trace indicates the ion current at the collector for pressures of neon gas at which the signal for the zero order spectrum is a maximum and the ion gauge pressure is the same as that for argon. On comparing the collector current in the lower traces of Figure 55 and 58 in the overlapping region, it is found that the output signal is the same indicating that the photon flux at any wavelength, which is able to ionize both argon and neon, is independent of the gas chosen. It is important to note, however, that since the photoionization threshold for neon lies near 580Å, no collector current is measured at 590Å. Hence, the combination of the titanium film and neon gas has a limited spectral response between 580Å and 360Å. It should also be mentioned that we looked for collector currents at longer wavelengths than 600Å, but no measurable signal was observed even with stronger radiation.

Figure 59 shows a typical trace (lower) of the spectral response of the detector using a titanium film and helium gas together with the trace corresponding to the photon flux at the exit slit as measured by the photomultiplier tube (upper trace). Since the threshold for photoionization in helium lies at 504Å, no collector signal is seen at wavelengths longer than 504Å. Such a combination of a Ti film and helium gas is responsive to all radiations between 504Å and 360Å. Since the measurements with this combination were taken on a different day, it is not possible to compare the signals in the overlapping region with those of Figures 55 and 58. The light source is also not completely reproducible from day to day. The signal at the photocathode for the zero order without any gas in the ion chamber was also found to be lower than the one on the previous day.

The results reported so far, although somewhat limited, can be discussed in the following manner:

Our main object in the utilization of these detectors is to obtain photon fluxes in a specified wavelength interval. We measure the photoelectric current produced at the W photocathode by all the radiation entering the detector chamber. Since the photoelectric yield,

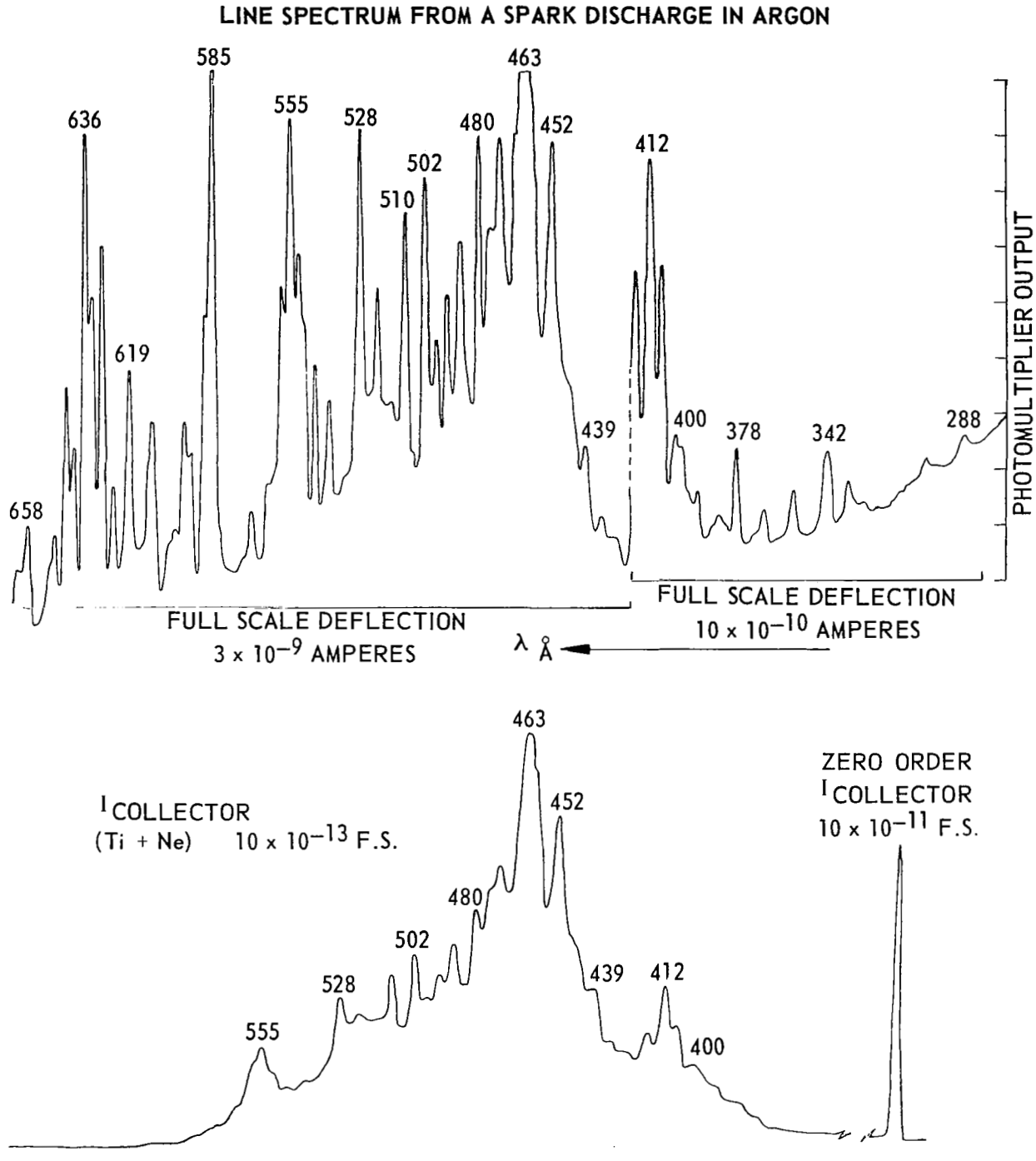

SPECTRAL RESPONSE OF THE SELECTIVE DETECTOR USING Ti FILM AND Ne GAS

FIGURE 58

LINE SPECTRUM FROM A SPARK DISCHARGE IN ARGON

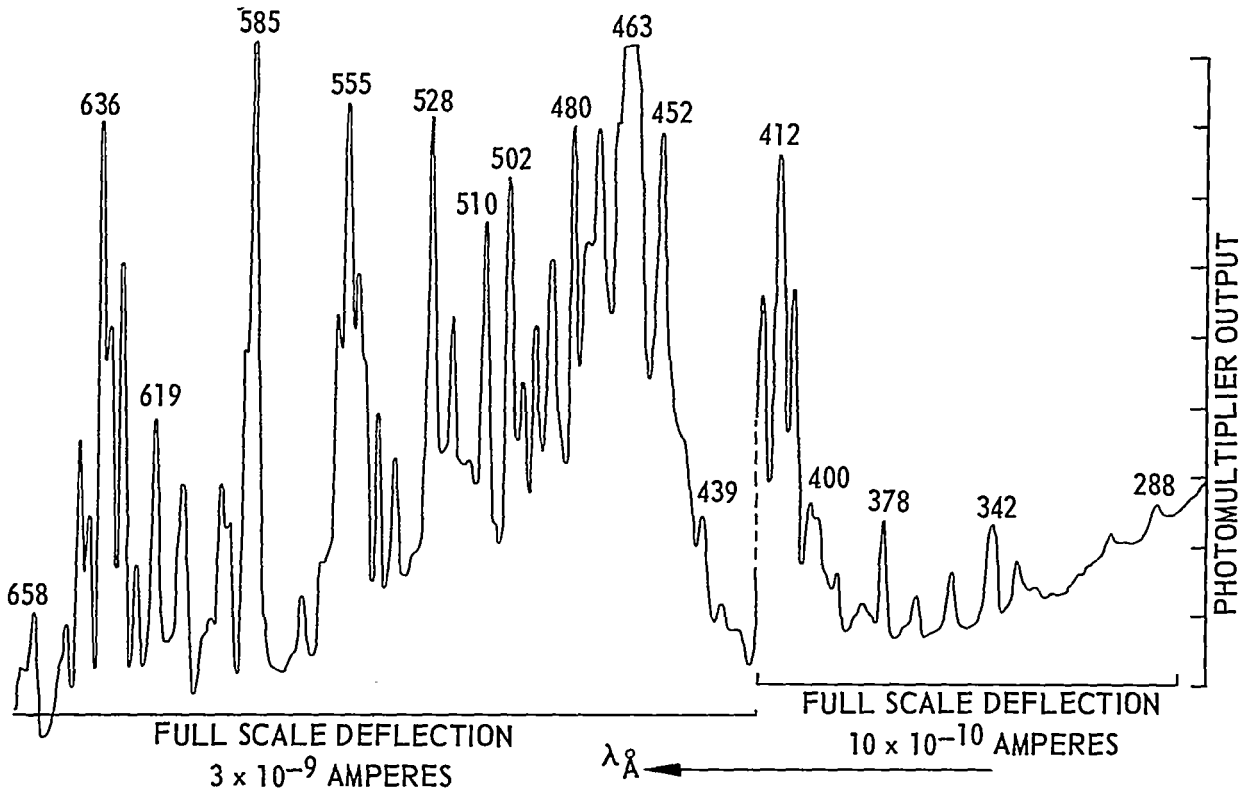

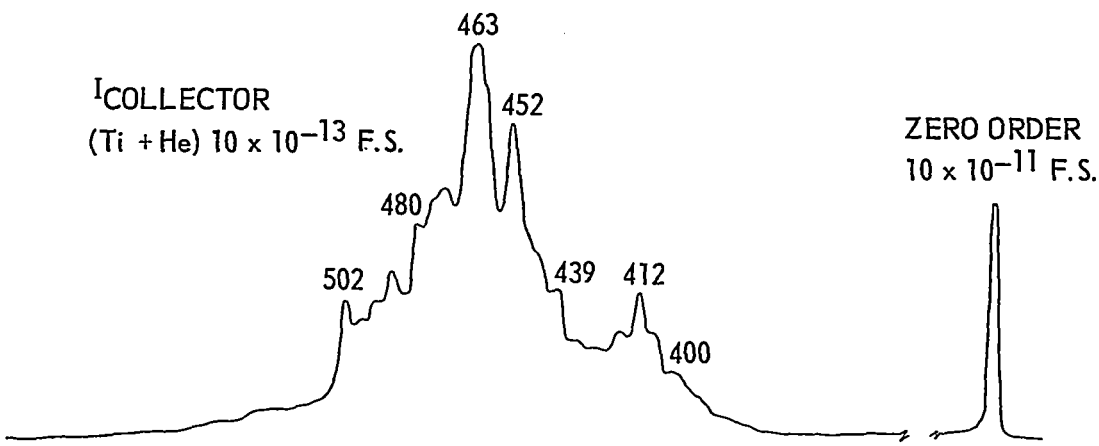

SPECTRAL RESPONSE OF THE SELECTIVE DETECTOR USING Ti FILM AND He GAS

FIGURE 59

defined as the number of electrons produced per incident photon, is known from previous measurements, a rough estimate of the photon flux entering the chamber is known. We also observe the collector current due to positive ions produced by photoionization. The photoionization efficiency, defined as the ratio of ions produced to the number of photons absorbed, is unity for all rare gases at photon energies greater than the ionization threshold. Therefore, the number of photons absorbed is equal to the number of ions produced which is obtained by dividing the charge on one ion into the total ion current provided all the ions created are collected. Hence a ratio of photoelectric current at the cathode without any gas in the chamber to the ion current at the collector with complete absorption should be equal to the photoelectric yield of the cathode. The ratio was calculated when the bismuth film was used with argon in the chamber and was found to be 12.57%, within the experimental error limit, the same as reported by weissler.[11] It is, therefore, concluded that all the ions produced in the chamber are collected at the collector and that all the photons entering the chamber are absorbed before reaching the photocathode. The adequacy of the gas pressure required to make complete absorption has been demonstrated by the constancy of the output signal in the overlapping spectral region using different gases.

Knowing the transmittance of the thin film - mosaic glass combination, it is thus possible to calculate the total photon flux in a specified wavelength interval by observing the collector signal corresponding to that radiation.

Photoelectric Measurements

From past experience, it was thought worthwhile to measure photoelectric emission from unbacked thin films since these films are an integral part of the selective detectors developed during this program. An experimental chamber made out of stainless steel was designed. On one of the flanges, a ¼" rod carried the sample holder which could be moved into and out of the radiation beam. The film holder was electrically

insulated from the rest of the chamber so that the photoemission current could be monitored when a collector was placed at a positive potential surrounding the sample. Two hemispherical collectors, 5 inches in diameter, were supported from the same flange as the sample holder but electrically insulated from it and from each other. A series of holes, ½ inch in diameter, were drilled in these hemispheres in the plane of incidence, and a spherical mesh screen gird of 90% optical transparency and 4 inches in diameter was supported on the inside of the hemispherical collector by levite insulators. This photoelectric cell was thus capable of making spectral reflectance measurements as a function of angle and photoelectric yield measurements separately, both in the forward direction, opposite the incident beam, and in the backward direction which is in the direction of the incident beam. The optical alignment was achieved using the zero order spectrum and a ground glass plate. For monitoring the radiation, an EMR electron multiplier tube type 641W-20 having a Ni photocathode was installed inside the chamber. In order to calibrate it, the following procedure was adopted. First, to measure the input signal to the multiplier tube, a Stancor P6462 filament transformer was connected to the filament and adjusting the input voltage in the vicinity of 1 volt, a current was measured at the Ni photocathode by means of a micro-microammeter, as shown in Figure 60(a). After this signal was registered, the complete electron multiplier was connected as shown in Figure 60(b) so that the amplified signal at the collector could be measured as the total voltage was varied. Simultaneously, the dark current at the collector was also measured as a function of voltage with the filament switched off.

The gain measurements thus made agreed with those provided by the manufacturer and are, therefore, omitted from this report.

The first use of the spherical photoelectric cell was made in the measurement of the photoelectric yield of an alloy of copper and tungsten called elkonite 10W3. It consists of 57% of tungsten and 43% of copper and has been used successfully as an electrode material in the capillary spark discharge light source. The sample surface was prepared by a

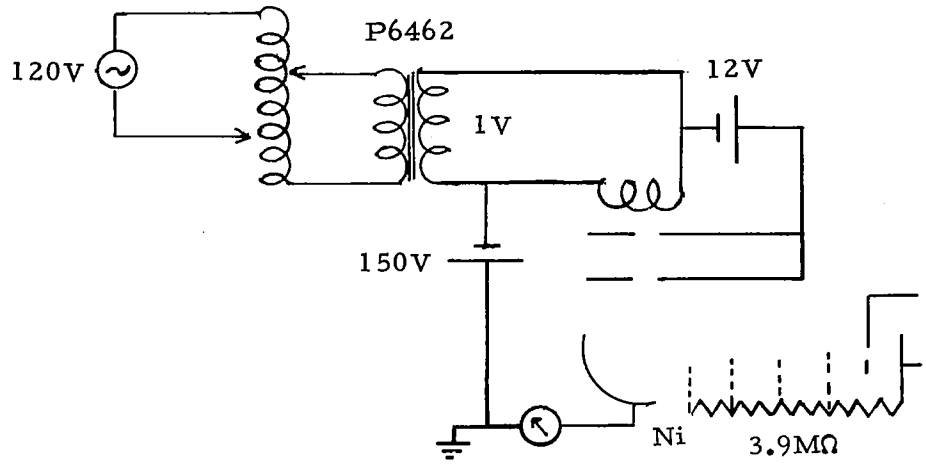

(a)

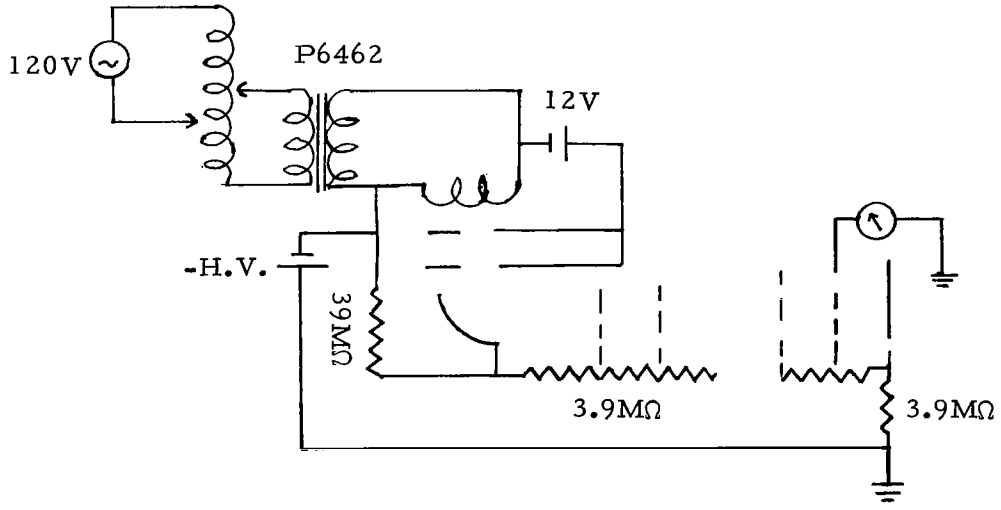

(b)

Figure 60. Circuit for Electron Multiplier Gain Measurement.

conventional milling technique without the use of any lubricant and was polished with Armor silicon carbide paper and emery cloth. After buffing the surface with jewellers rouge, Onesco #15, it was rinsed with reagent grade acetone and cleaned, using the ultrasonic technique, before installation in the photocell.

The electron current leaving the sample was measured by connecting the micro-microammeter to the sample while the screen and collectors were kept at +45 volts. Figure 61, shows the photoelectric yield in arbitrary units, calculated by dividing the electron current by the photomultiplier output for each wavelength, as a function of wavelength. We find that the yield attains a maximum value near 600Å and drops off on either side of the maximum.

Photo Diode Studies

The ultraviolet photodiode UV 100 is a silicon dioxide passivated silicon P-N junction device. It was mounted on a T05 transistor header with mechanical protection provided by a cylindrical shield which was open at one end. It was located in the exit slit assembly and replaced the radiation thermocouple. The electrical connections were made in such a manner that the meter registered the signal due to the internal photovoltaic effect only. We used the pulse-burst mode operation of the light source in conjunction with the Brower synchronous amplifier and were able to monitor signals in the 100 nv region when exposed to the radiation in the 100 - 1000Å region. No signals were observed above 700Å but clear signals were registered on the chart recorder between 400 and 700Å. Further work could not be continued because of noise problems in the amplifier due to RF generated in the light source.

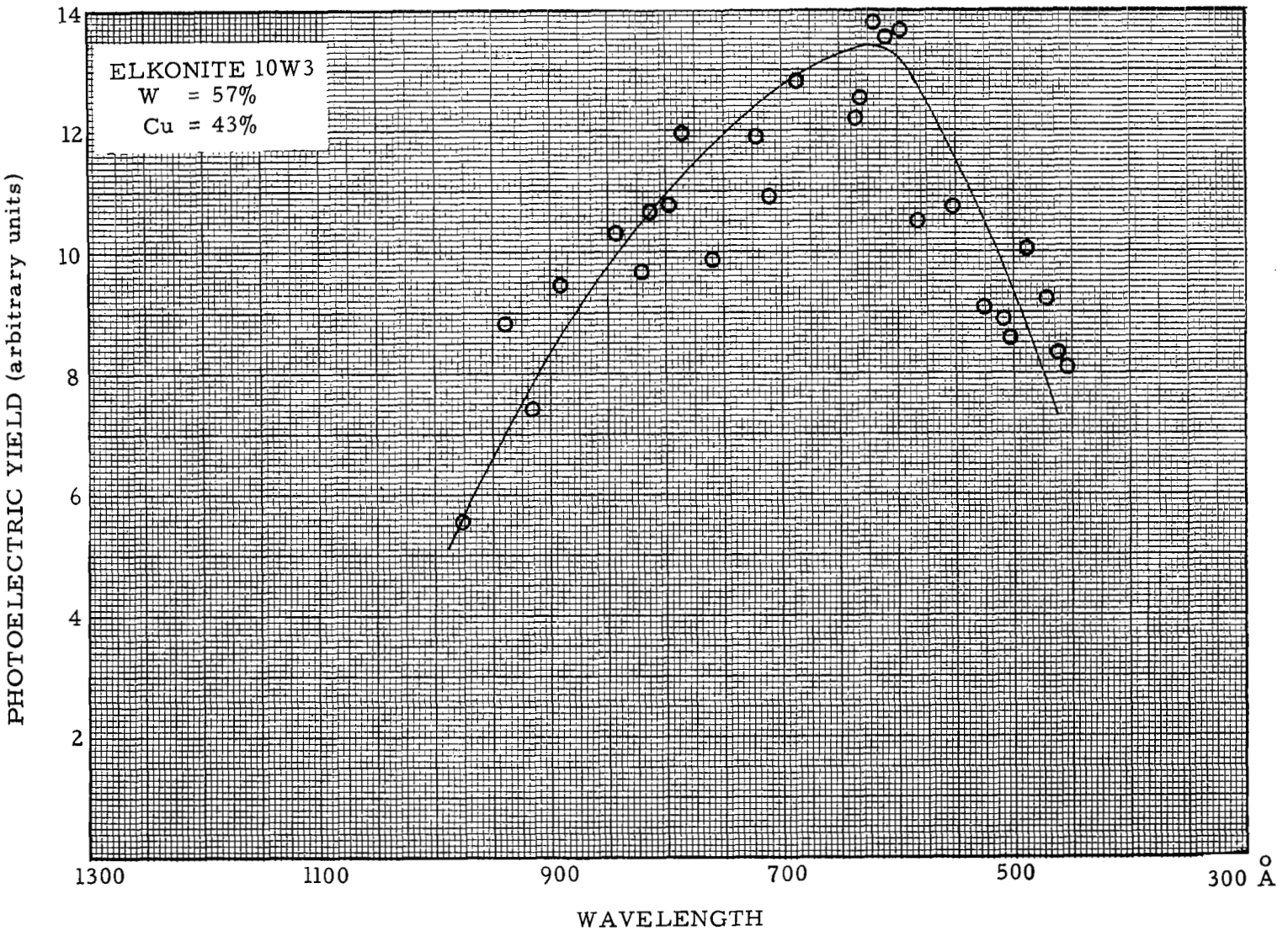

Figure 61. Photoelectric Yield of ELKONITE 10W3

SECTION VII

CONCLUSIONS

The results reported in Section VI of this report have conclusively shown that thin films can be used as filters as well as windows for the rare gas ion chambers to result in selective detectors for the wavelength region between 100 and 1000Å. We have seen that a Ti film, which is transparent in the wavelength region between 680Å and 325Å with a peak transmission near 400Å, when attached to an ion chamber filled separately with A, Ne, and He results in detectors sensitive over the wavelength region 680 - 325Å, 580 - 325Å, and 504 - 325Å respectively. Similarly a Bi film, which is transparent in the wavelength region from 850Å to 510Å, when attached to the ion chamber filled separately with Kr, A, and Ne results in detectors sensitive over the wavelength region 850 - 510Å, 787 - 510Å, and 580 - 510Å respectively. Because of the thickness of the Bi film used, the upper limit both for Kr and A, as seen in Figures 44 and 45, seems to be 686Å. This indicates that the Bi film used was not able to transmit the weak radiation between 686Å and 850Å. However, an indium film, which is transparent in the wavelength region from 1100Å to 740Å, when attached to the ion chamber filled with Xe, Kr, and A results in detectors sensitive over the wavelength region 1022 - 740Å, 888 - 740Å, and 787 - 740Å respectively.

Considering the last case where the detector is sensitive over a wavelength interval of less than 50Å, we can calculate the sensitivity. The minimum detectable signal, say near 750Å, is 1×10^{-14} amp which is roughly the limit of our electrometer. This corresponds to a photon flux of approximately 10^5 inside the detector. Assuming that the transmittance of a thin film-mosaic glass combination is 5%, then the photon

flux impinging on the detector is 2×10^6. This represents the minimum photon flux which a selective detector developed so far is capable of detecting. Hence there is no problem of detecting an extended source of 1 KR (10^9 photons cm^{-2} sec^{-1} $\mathring{A}^{-1}$) at 500$\mathring{A}$ when the proper thin film and gas combination is used. The monitoring of photons is done in real time and the response time for this detector with associated electronics is dependent on the electronics only. Based on this study, it is suggested that further work for the development of selective detectors should be pursued with solid state diodes which were barely explored during this program.

SECTION VIII

REFERENCES

1. H. Friedman, IRE Transaction on Military Electronics, Vol. MIL-4, No. 1, p. 18, Jan. (1960); Acton, Chubb, Kreplin, and Meekins, J. Geophys. Res. 68, 3335 (1963); Kreplin, Chubb, and Friedman, J. Geophys. Res. 67, 2231 (1962).
2. M. Nicolet, Proc. Colloquium on "Les Spectres des Astres dans L' Ultraviolet Lointain," Mem. Roy. Soc. Sci., Liege, p. 319 (1961).
3. H. E. Hinteregger and K. Watanabe, J. Geophys. Res. 67, 3373 (1962); Hall, Schweizer, and Hinteregger, J. Geophys. Res. 70, 105 (1965).
4. C. W. Allen, Space Sci. Rev. 4, 91 (1965).
5. L. Goldberg, Proc. Colloquium on "Les Spectres des Astres dans L' Ultraviolet Lointain," Mem. Roy. Soc. Sci., Liege, p. 30 (1961); J. Quant. Spectros. Radiat. Transfer, 3, 519 (1963).
6. Baum, Johnson, Oberly, Rochwood, Strain, and Tousey, Phys. Rev. 70, 781 (1946).
7. R. Tousey, Space Sci. Rev. 2, 1 (1963).
8. W. A. Rense, Space Sci. Rev. 5, 234 (1966).
9. V. Schumann, Wien. Akad. Anzeiger 23, 230 (1892).
10. J. A. R. Samson, J. Opt. Soc. Am. 54, 6 (1964).
11. G. L. Weissler, Handbuch der physik (Spring Verlag, Berlin, 1956), Vol. XXI.
12. B. Vodar, J. Quant. Spectros. Radiat. Transfer, 2, 393 (1962).

13. Huffman, Tanaka, and Larrabee, Appl. Opt., 2, 617 (1963); 4, 1581 (1965); Huffman, Larrabee, and Chambers, ibid, 4, 1145 (1965); Jap. J. Appl. Phys., 4, 494 (1965).

14. Huffman, Tanaka, and Larrabee, J. Chem. Phys. 39, 910 (1963).

15. Huffman, Tanaka, and Larrabee, J. Chem. Phys. 39, 902 (1963).

16. Huffman, Tanaka, and Larrabee, J. Chem. Phys. 40, 2261 (1964).

17. Huffman, Tanaka, and Larrabee, Dis. Faraday Soc. No. 37, p. 159, (1964).

18. Huffman, Larrabee, and Tanaka, J. Chem. Phys. 45, 3205 (1966).

19. Huffman, Tanaka, and Larrabee, Appl. Opt. 2, 947 (1963).

20. G. R. Cook and P. H. Metzger, VI Int. Conf. Phenomenes. d' Ionization dans Les Gaz (Paris: S.E.R.M.A. Vol. 1, p. 149 (1963)).

21. G. R. Cook and P. H. Metzger, J. Opt. Soc. Am. 57, 968 (1964).

22. Cook, Metzger, and Ogawa, Canad. J. Phys. 43, 1706 (1965).

23. G. R. Cook and P. H. Metzger, J. Chem. Phys. 41, 321 (1964).

24. Metzger, Cook, and Ogawa, Canad. J. Phys. 45, 203 (1967).

25. P. H. Metzger and G. R. Cook, J. Chem. Phys. 41, 642 (1964).

26. Watanabe, Nakayama, and Mottl, J. Quant. Spectros. Rad. Transfer, 2, 369 (1962).

27. J. A. R. Samson, J. Opt. Soc. Am. 54, 420 (1964).

28. J. A. R. Samson, J. Opt. Soc. Am. 54, 842 (1964).

29. J. A. R. Samson, J. Opt. Soc. Am. 54, 876 (1964).

30. J. A. R. Samson, Phys. Rev. 132, 2122 (1963).

31. J. A. R. Samson, J. Opt. Soc. Am. 55, 935 (1965).

32. J. A. R. Samson and R. B. Cairns, J. Geophys. Res., 69, 4583 (1964).

33. J. A. R. Samson and R. B. Cairns, J. Opt. Soc. Am. 55, 1035 (1965).

34. R. B. Cairns and J. A. R. Samson, J. Opt. Soc. Am. 56, 526 (1966).

35. R. B. Cairns and J. A. R. Samson, Phys. Rev. 139, A1403 (1965).

36. Rustgi, Fisher, and Fuller, J. Opt. Soc. Am. 54, 745 (1964).

37. O. P. Rustgi, J. Opt. Soc. Am. 54, 464 (1964).

38. D. L. Ederer and D. H. Tomboulian, Phys. Rev. 133, A1525 (1964).

39. D. L. Ederer, Phys. Rev. Letters, 13, 760 (1964).

40. Lowry, Tomboulian, and Ederer, Phys. Rev. 137, A1054 (1965).

41. R. P. Madden and K. Codling, Phys. Rev. Letters, 10, 516 (1963).

42. R. P. Madden and K. Codling, J. Opt. Soc. Am. 54, 268 (1964).

43. K. Codling and R. P. Madden, Phys. Rev. Letters, 12, 106 (1964).

44. Weissler, Samson, Ogawa, and Cook, J. Opt. Soc. Am. 49, 338 (1959).

45. R. I. Schoen, J. Chem. Phys. 37, 2032 (1962).

46. Schoen, Judge, and Weissler, Proc. Fifth Conf. Ionization Phenomenon in Gases (Edited by H. Maecker); Vol. 1, p. 25, North Holland Publishing, Amsterdam (1962).

47. Tanaka, Huffman, and Larrabee, J. Quant. Spectros. Rad. Transfer 2, 451 (1962).

48. D. Pines, Rev. of Mod. Phys. 28, 184 (1956).

49. G. B. Sabine, Phys. Rev. 55, 1064 (1939).

50. Walker, Rustgi, and Weissler, J. Opt. Soc. Am. 49, 471 (1959).

51. Rustgi, Walker, and Weissler, J. Opt. Soc. Am. 51, 1357 (1961).

52. Cox, Waylonis, and Hunter, J. Opt. Soc. Am. 49, 807 (1959).

53. G. Hass and R. Tousey, J. Opt. Soc. Am. 49, 593 (1959).

54. Robin-Kandare, Damany, and Tertian, J. Phys. Rad. 20, 504 (1959).

55. Berning, Hass, and Madden, J. Opt. Soc. Am. 50, 586 (1960).

56. Angel, Hunter, and Tousey, J. Opt. Soc. Am. 51, 913 (1961).

57. W. R. Hunter, Optica Acta. 9, 255 (1962).

58. R. P. Madden, Physics of Thin Films, edited by G. Hass, Vol. I, p. 123 (1963).

59. W. R. Hunter, J. Opt. Soc. Am. 54, 208 (1964); J. de Phys. 25, 154 (1964).

60. Rustgi, Nodvik, and Weissler, Phys. Rev. 122, 1131 (1961).

61. Ehrenreich, Philipp and Segall, Phys. Rev. 132, 1918 (1963); Ehrenreich and Philipp, Phys. Rev. 128, 1622 (1962).

62. O. P. Rustgi, J. Opt. Soc. Am. 55, 630 (1965).

63. W. C. Walker, Phys. Chem. Solids, 24, 1667 (1963).

64. J.A.R. Samson, J. P. Padur, and A. Sharma, J. Opt. Soc. Am. 57, 966 (1967).

65. N. N. Axelrod and M. P. Givens, Phys. Rev. 130, 2105 (1960).

66. H. Kroger and D. H. Tomboulian, Phys. Rev. 130, 152 (1963).

67. J. A. R. Samson, J. Opt. Soc. Am. 57 , 966 (1967).

68. Tomboulian, Bedo, and Neupert, Phys. Chem. Solids 3, 282 (1957).

69. W. R. Hunter and R. Tousey, J. de Phys. 25, 148 (1964); W. R. Hunter, Appl. Optics, 4, 891 (1965).

70. H. E. Hinteregger and K. Watanabe, J. Opt. Soc. Am. 43, 604 (1952).

71. Walker, Wainfan, and Weissler, J. Appl. Phys. 26, 1366 (1955).

72. L. Heroux and H. E. Hinteregger, Appl. Optics, 1, 701 (1962).

73. J. A. R. Samson, Rev. Sci. Instrum. 36, 19 (1965).

74. S. W. Duckett and P. H. Metzger, Phys. Rev. 137, A953 (1965).

75. R. G. Newburgh, Phys. Rev. 132, 1570 (1963).

76. A. P. Lukirskii, M. A. Rumsh and L. A. Smirnov, Opt. and Spectros. (USSR) 9, 265 (1960).

77. R. B. Cairns and J. A. R Samson, J. Opt. Soc. Am. 57, 433 (1967).

78. Johnson, Watanabe, and Tousey, J. Opt. Soc. Am. 41, 702 (1951).

79. R. Lincke and T. D. Wilkerson, Rev. Sci. Instrum. 33, 911 (1962).

80. L. Dunkelman, J. Quant. Spectros. Rad. Transfer 2, 533 (1962).

81. H. E. Hinteregger, J. Quant. Spectros. Rad. Transfer 2, 561 (1962).

82. G. W. Goodrich and W. G. Wiley, Rev. Sci. Instrum. 32, 846 (1961).

83. G. W. Goodrich and W. G. Wiley, Proc. Image Intensifier Sympos. Fort Belvoir, Va. (Oct. 1961).

84. T. A. Chubb and H. Friedman, Rev. Sci. Instrum. 26, 493 (1955).

85. K. Watanabe, H. Sakai, and K. Griswold, Photon Ionization Counter for VUV, Scientific Report No. 3, Univ. of Hawii (1958).

86. A. K. Stober, NASA Technical Note TND-1180 NASA, March (1962).

87. D. L. Judge, A. L. Morse, S. Furmanski, and G. L. Weissler, Proceedings of the 6th International Conference on "Ionization Phenomenon," Paris, July 1963; to be published, Vol. 2 (1964).

88. F. E. Carpenter and J. A. Curcio, Rev. Sci. Instr., 21, 675 (1950).

89. D. Conlon and W. P. Doyle, J. Sci. Instr. 42, 286 (1965).

90. K. Codling, R. P. Madden, W. R. Hunter, and D. W. Angel, J. Opt. Soc. Am. 56, 189 (1966).

91. Judge, Morse, and Weissler, Photo-Ionization and Photoionization-induced Ion-Molecule Reactions, Final Report AFCRL-63-877, Contract AF 19(604)-6119 (August 1963, unpublished).

92. Judge and Weissler, Fluorescence Spectra of the Molecular Ions O_2^+, N_2^+, and CO^+ Excited by Vacuum Ultraviolet Radiation, Technical Report USC-VacUV-105, Contract Nonr 228 (27) (August 1965).

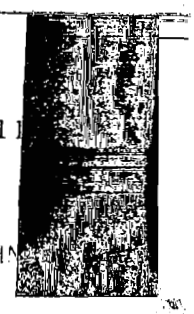

"The aeronautical and space activities of the United States shall be conducted so as to contribute . . . to the expansion of human knowledge of phenomena in the atmosphere and space. The Administration shall provide for the widest practicable and appropriate dissemination of information concerning its activities and the results thereof."

—NATIONAL AERONAUTICS AND SPACE ACT OF 1958

NASA SCIENTIFIC AND TECHNICAL PUBLICATIONS

TECHNICAL REPORTS: Scientific and technical information considered important, complete, and a lasting contribution to existing knowledge.

TECHNICAL NOTES: Information less broad in scope but nevertheless of importance as a contribution to existing knowledge.

TECHNICAL MEMORANDUMS: Information receiving limited distribution because of preliminary data, security classification, or other reasons.

CONTRACTOR REPORTS: Scientific and technical information generated under a NASA contract or grant and considered an important contribution to existing knowledge.

TECHNICAL TRANSLATIONS: Information published in a foreign language considered to merit NASA distribution in English.

SPECIAL PUBLICATIONS: Information derived from or of value to NASA activities. Publications include conference proceedings, monographs, data compilations, handbooks, sourcebooks, and special bibliographies.

TECHNOLOGY UTILIZATION PUBLICATIONS: Information on technology used by NASA that may be of particular interest in commercial and other non-aerospace applications. Publications include Tech Briefs, Technology Utilization Reports and Notes, and Technology Surveys.

Details on the availability of these publications may be obtained from:

SCIENTIFIC AND TECHNICAL INFORMATION DIVISION

NATIONAL AERONAUTICS AND SPACE ADMINISTRATION

Washington, D.C. 20546